2002

Varible amplitude fatigue resistance of welded stainless steel bulkhead attachments

Brenda M. (Marie) Brownell
Lehigh University

Brownell, Brenda M.

Variable Amplitude Fatigue Resistance of Welded Stainless Steel Bulkhead Attachments

June 2002

Variable Amplitude Fatigue Resistance of Welded Stainless Steel Bulkhead Attachments

by

Brenda M. Brownell

A Thesis
Presented to the Graduate and Research Committee
of Lehigh University
in Candidacy for Degree of
Master of Science

in

Civil Engineering

Lehigh University

May 2, 2002

This thesis is accepted and approved in partial fulfillment of the requirements for the Master of Science.

April 29, 2002
Date

Thesis Advisor

Chairperson of Department

Acknowledgements

Financial support for this research was provided by the U.S. Office of Naval Research, Grant #N00014-99-0887, and by the Pennsylvania Infrastructure Technology Alliance (PITA) (Project No.: IIS – 021). Support from all sponsors is greatly appreciated. The reported research was conducted at the Advanced Technology for Large Structural Systems (ATLSS) Engineering Research Center at Lehigh University in Bethlehem, Pennsylvania.

Thanks are given to the technical staff of the ATLSS Center at Lehigh University, especially to Dr. Ben T. Yen, Dr. John W. Fisher, Brian Metrovich, John Hoffner, Roger Moyer, Todd Anthony, and Russ Longenbach.

Finally, thanks are given to F. David Crudele, for without his support and understanding the completion of this research would not have been possible.

Table of Contents

List of Tables

List of Figures

Nomenclature

a	Crack length
A	Constant regarding crack growth rate
a_d	Crack depth
a_f	Half crack length at the end of each stress application
$a_{f\text{-step\#1}}$	Half crack length at the end of step #1
a_i	Half crack length at the beginning of each stress application
$a_{i\text{-step\#1}}$	Half crack length at the beginning of a step #1
b	Weibull shape parameter
B	Constant regarding crack growth rate
C	y-intercept
CAFL	Constant amplitude fatigue limit
$CAFL_{initial}$	Initial constant amplitude fatigue limit
$CAFL_{new}$	New constant amplitude fatigue limit
d	Constant regarding power fit
da/dN	Crack growth rate
e	Stress concentration factor decay coefficient
F_e	Crack shape correction factor
F_g	Stress gradient correction factor
F_s	Front free surface correction factor
F_w	Back free surface correction factor
g	Major semidiameter of crack
h	Minor semidiameter of crack
e	Constant regarding power fit
F_y	Yield stress
GMAW	Gas Metal Arc Welding
GTAW	Gas Tungsten Arc Welding
m	Slope – Linear regression
MIG	refers to GMAW
n	Slope – crack growth equation
n_i	Number of cycles at stress range $_i$
N_{spec}	Number of cycles in one spectrum
n_{trunc}	Number of cycles in one truncated spectrum
N	Number of cycles to failure
N_a	Number of cycles above the CAFL
N_i	Number of cycles to cause failure at stress range $_i$

$N_{non\text{-}trunc}$	Number of cycles to failure with non-truncated spectrum
p	Probability density
q	Stress gradient correction factor decay exponent
RMC	Root Mean Cubed
RMS	Root Mean Squared
R^2	R squared value
σ	Standard Deviation
S_r	Stress range
S_{ravg}	Average stress range
S_{re}	Equivalent stress range
S_{ri}	Stress Range $_i$
S_{rmax}	Maximum stress range
S_{rmin}	Minimum stress range
t_f	Flange thickness
TIG	refers to GTAW
w	Half crack width
W	Width
x	Range of stress ranges
α	Parameter defining a Rayleigh curve
β	Geometry factor
β_I	Initial Geometry factor
ΔK	Stress intensity range
ΔK_{th}	Stress intensity range threshold
$\Delta\sigma$	Stress range
μ	Mean
θ	Weibull scale parameter

ABSTRACT

Twelve I-Section beams with fillet welded simulated bulkhead attachments were tested under random variable amplitude stresses in tension and in reversal (tension and compression). The beams were made of AL-6XN superaustenitic stainless steel; and the basic stress range histogram was from measurements on a ship. The tension only test specimens had longer fatigue life than corresponding constant amplitude fatigue tests when the variable amplitude stress were converted to an equivalent stress range by the root-mean-cube procedure. The results from the few reversal specimens showed relatively large amount of scatter. All tests provided longer life than predicted by the AASHTO fatigue strength (S-N) curve.

The test specimens also had longer life than the analytical values developed on the concept of decreasing fatigue limit. The analytical S-N curves predict longer life than the AASHTO curves, particularly below the constant amplitude fatigue limit.

More studies on long-life fatigue near and below the fatigue limit are recommended.

1. INTRODUCTION

1.1 Problem Statement

For the past thirty some years many engineers have been using design live load stress range, S_r, to check fatigue susceptibility of bridges, ships, industrial buildings and facilities, or any other welded structures that are subjected to repeated loading. The primary references are the fatigue strength curves of American Association of State and Highway Officials (AASHTO) (1). These fatigue strength curves are based on extensive fatigue tests of beams under constant amplitude stresses even though almost all structural details will see variable amplitude stresses in the field. There are many factors that differentiate the phenomena of variable amplitude fatigue failure from those of constant amplitude testing. The most important parameter is the stress spectrum. Questions are raised about the collection of representative stress spectrum. For example, should a stress history of a bridge's busiest day be used, or just a normal day? Should the spectrum imitate a stress history of a ship crossing the ocean, or one in a high sea state? How should these be translated into the spectrum for a fatigue test in the laboratory? It becomes clear that the evaluation of variable amplitude fatigue strength is very complex and needs to be investigated more thoroughly to determine if the design of a structure subjected to variable amplitude fatigue can be based on constant amplitude fatigue strength curves.

1.2 Objectives

The objectives of this study are the following:

A. To conduct variable amplitude fatigue tests of structural components that have the same details and material as those used in previous constant amplitude fatigue tests.

B. To examine the correlation between the results from constant and variable amplitude fatigue tests.

C. To develop a model for the evaluation of variable amplitude fatigue using constant amplitude fatigue strength curves.

Simulated bulkhead attachments on beams of AL-6XN non-magnetic superaustenitic stainless steel, for a Navy project, are the specimens for the study.

2. BACKGROUND INFORMATION

2.1 Fatigue of Metal

Fatigue of metal may be defined as the repeated application of stress causing the initiation and propagation of insignificant cracks or flaws into cracks of significant size. A small crack caused by an initial flaw will grow slightly with each application of stress. One good explanation of the crack growth mechanism is provided by Broek (2).

> *"Growth occurs at the crack front, which is initially sharp. Even at relatively low loads, there will be a high concentration of stresses at the crack front causing plastic deformations (slip on atomic planes) in this area. Continued slip results in a blunted crack tip, and the crack grows a minute amount during the process. Upon unloading, not necessarily to zero, the crack tip again becomes sharp. This process is repeated during each loading cycle causing crack growth."*

Both constant amplitude loading and variable amplitude loading on steel structures cause crack growth as described above.

2.2 Constant Amplitude Fatigue

As it implies, constant amplitude fatigue is the repeated loading over one stress range. Results of studies show that constant amplitude fatigue strengths of

welded structural steel details can be represented by S-N curves (3). These S-N curves are described by the following equation.

$$N = A\,\Delta\sigma^{-n} \qquad (2.2.1)$$

N is the number of cycles to failure for a given stress range, $\Delta\sigma$. Equation (2.2.1) can also be derived by integrating Paris's crack growth equation (4,5).

$$dN/da = B\,\Delta K^{n} \qquad (2.2.2)$$

For a category of structural detail only two parameters in Equation (2.2.1) are needed to define the governing S-N curve, A and n. A is a constant pertaining to the detail type and n is a material constant.

Alternatively Equation (2.2.1) can be written as

$$\log N = \log A - n \log \Delta\sigma \qquad (2.2.3)$$

Equation (2.2.3) defines a straight line on a log-log plot of stress range versus number of cycles.

For design and evaluation of structural steel members, the parameter n is commonly taken as 3.0 and A is dependent on the detail category (Table 2.2.1). With this information S-N curves can be plotted for detail categories (Figure 2.2.1). It has been shown experimentally that using the same values of n and A

determined for structural carbon steel with stainless steel provides a conservative result (6).

Another important concept regarding fatigue of steel structures is the constant amplitude fatigue limit, CAFL. Each design category has a unique CAFL (Table 2.2.1). CAFL is directly related to the crack growth threshold (7). Application of a stress cycle below the CAFL will not contribute to fatigue damage or fatigue crack growth. This becomes very important in the consideration of variable amplitude fatigue when the magnitudes of stress cycles are both above and below the CAFL.

2.3 Variable Amplitude Fatigue

Variable amplitude fatigue is the repeated loading of a structural detail by stress cycles with different stress ranges. When there is more than one stress range the fatigue damage due to each stress cycle is different. The cumulative damage of all cycles must be considered. The theory most commonly used in structural engineering is Miner's Rule (8). Miner's Rule is a linear theory by which the total damage due to fatigue is hypothesized as the linear sum of the damage fraction at each stress range.

$$\Sigma\, n_i/N_i = 1 \qquad (2.3.1)$$

Where, n_i = number of cycles at stress range $_i$

N_i = number of cycles to cause failure at stress range $_i$

When $\sum n_i/N_i$ is less than one, the structural detail has not reached its fatigue life or failure. Because the failure cycle N_i is related to the magnitude of stress range S_{ri} by the S-N curves, an equivalent or effective constant amplitude stress range (S_{re}) can be calculated for a given variable amplitude stress spectrum (9).

$$S_{re} = [\Sigma (n_i/N_i S_{ri}^n)]^{1/n} \qquad (2.3.2)$$

A variable amplitude stress spectrum is a statistical presentation of stress history at a structural detail. When a stress history becomes more complicated it is difficult to determine the actual number of cycles at different stress ranges. It has been shown that the best cycle counting procedure when applying linear damage theory is the rainflow counting method (10).

3. REVIEW OF PREVIOUS STUDIES

3.1 Variable Amplitude Fatigue Studies for Carbon Steels

There are only a small number of experimental studies on variable amplitude fatigue of structural details. Some of these are reviewed briefly here.

NCHRP Report #188 contains findings from an extensive laboratory investigation of fatigue effects in welded steel beams subjected to variable amplitude loading similar to that seen in bridges (9). A family of Rayleigh distributions was used as stress spectra (11). The Rayleigh spectrum was found to adequately replicate fifty-one sets of strain gage data taken from six sources. All bridges were on Interstate or US routes in semi-rural or metropolitan locations.

For testing of the beams, the input spectrums were divided into five hundred individual stress ranges that were placed in a random sequence as would be expected on most actual bridges.

Fatigue data came from 108 tests on A514 steel with cover plates, 45 tests on A36 steel with cover plates, 30 tests on A514 welded beams, and 36 tests on A36 welded beams. Three types of cover plates were tested, "A", "B", and "C". Type "A" cover plates had the longitudinal edges of the cover plate first welded to the flange, and then the flange to the web. This was not normal practice. Type "B" cover plates had the longitudinal edge of the cover plate welded to the flange after the beam was fabricated. Type "C" cover plates are similar to they "B" in the

assembly process, but there was also a fillet weld across the ends of the cover plates. Submerged-arc welding was used for all welds.

The root mean square (RMS) approach and Equation (2.3.2) with n = 3.0 (RMC) were taken for calculating the effective stress range. The latter provides better correlation. The results are summarized in Figures 3.1.1 – 3.1.3. All "A" cover plates fell above AASHTO Category E except for one test. "B" & "C" cover plates fell above and below AASHTO Category E. The welded beams fell mostly above AASHTO Category B. It was concluded that Miner's Rule was satisfactory to relate variable and constant amplitude data. The report also included suggestions on estimating the remaining life of existing bridges and the design life of new bridges.

In 1979, Albrecht and Friedland reported results of their study on the effect of CAFL on variable amplitude fatigue of stiffeners (12). Forty-one small welded specimens were tested under repeated random load blocks corresponding to a skewed stress range histogram. There were low cycles in the load blocks and the equivalent stress ranges were computed by Equation 2.3.2 (RMC). The test data showed that above the CAFL equivalent stress range provided good correlation with results of 38 constant amplitude tests. When the equivalent stress range was below the CAFL, the test specimens had much longer life than indicated by the extension of the S-N curve. By assuming that stress ranges in the load spectrum below the CAFL do not contribute to crack growth, a S-N curve below the CAFL was developed and a variable amplitude fatigue limit was estimated.

NCHRP Report 267 presented results of testing welded attachments (gusset plates and cover plates) on beams under random variable amplitude load spectra of Rayleigh type distributions, and on small fillet welded cruciform type specimens (13). The equivalent stress ranges at the welded attachments of category E and E' were low, well below the respective CAFL. The results indicate that even a small number of cycles above the CAFL in a spectrum will cause fatigue crack growth. It was concluded the AASHTO fatigue strength categories for constant amplitude loading can be used to predict fatigue life of structural details subjected to variable amplitude loading by using the RMC equivalent stress range above and below the CAFL. More studies in the long life region, and a thorough examination of all data were recommended.

NCHRP Report 354 provided further confirmation of the findings from NCHRP Report 267 (14). Cover plates, web attachments simulating gusset plates and transverse stiffeners on welded plate girders were subjected to variable amplitude loads. The procedure of truncating lower stress ranges in a spectrum to shorten test time was introduced. Only a few cycles of stress ranges above the CAFL resulted in fatigue cracking. The adequacy of AASHTO fatigue strength curves for the prediction of fatigue life with equivalent stress range below the CAFL was again determined. However, it was found that for category C, the test data all fell well beyond the extension of the fatigue strength curve below the CAFL.

In 1999 H. Agerskov and J. A. Nielsen of University of Denmark carried out variable amplitude fatigue tests on small plate specimens with transverse

attachments (15). Stress spectrums for these tests correspond to one week of traffic loading determined from two strain gages. The gages were placed on the bottom of a trapezoidal longitudinal stiffener located under the deck plate of the orthotropic steel deck on the Farϕ Bridge in Denmark. The stiffener chosen was located under the most heavily loaded lane of the bridge. Root-mean-square and root-mean-cubed (Miner's Rule) values were determined from rainflow counting on the loading histories.

Fatigue tests included 27 tests using the spectrum from strain gage #1 (mostly in tension), and 35 tests using the spectrum from strain gage #5 (reversal). Yield stress was approximately 400 – 409 Mpa (58-59.3 ksi). Each test specimen had two transverse secondary plates welded to the main plate by full penetration butt welds. The main plate was 40mm wide and 8mm thick. The secondary plates were 40mm wide and 5mm thick.

Test results are summarized in Figures 3.1.4 and 3.1.5 using the root-mean-cubed effective stress range. Data for reversal and tension specimens fall mostly above AASHTO Category B, with a few below. For this test series it was found that fatigue life, in general, was shorter with variable amplitude loading than with constant amplitude loading at the same equivalent stress range level, for load histories almost equally in tension and compression (gage #5). While when the load history was mostly in tension (gage #1) the fatigue life, in general, was similar for variable amplitude loading and constant amplitude loading at the same equivalent stress range. The authors concluded that the distribution of load history in tension and compression has a significant influence on the validity of

results obtained by Miner's Rule, possibly predicting unconservative results of fatigue life.

3.2 Constant Amplitude Fatigue Studies for Stainless Steel

Extensive laboratory investigation of fatigue effect in welded superaustenitic stainless steel subjected to constant amplitude loading has been performed (6). Three different details were investigated; longitudinal fillet-welded joints, groove welds in flanges and webs, and fillet-welded bulkhead attachments. The material used was nonmagnetic superaustenitic stainless steel alloy designated AL-6XN. The minimum specified yield strength was 344 Mpa (50 ksi). The weld metal used for all details was IN625. GMAW was the process used for all welds.

All of the test specimens were nominally 3.2 meters long. The flanges were 152mm wide and 13mm thick, while the web was 305mm high and 9.5 mm thick. All tests were conducted under four point bending with a 1.2 meter long constant moment region where the test details were located.

Fatigue data was obtained from 12 bulkhead attachments tested in reversal and six tested in tension only. The reversal specimens were tested at stress ranges of 165 Mpa (24 ksi), 110 Mpa (16 ksi), and 55 Mpa (8 ksi). The tension specimens were tested at stress ranges of 110 Mpa (16 ksi) and 55 Mpa (8 ksi). The cycles at first detection of cracks along with failure data were given. Test results are summarized in Figures 3.2.1 and 3.2.2. The reversal specimens, in general, had longer fatigue lives than the tension specimens. Failure of all

specimens fell well above AASHTO Category E, and mostly above AASHTO Category D. It was recommended to use AASHTO Category E for the bulkhead attachments.

3.3 Variable Amplitude Fatigue Studies for Stainless Steels.

In the United Kingdom in 1999 variable amplitude fatigue tests were performed on duplex and austenitic stainless steels (16). The loading spectrum used was a Gaussian probability density curve (11). This spectrum was chosen as a reasonable representation of a wide range of service load spectra. The spectrum was divided into 500,000 load cycles and applied in random order. Equivalent stress range was calculated using Miner's Rule, where n was the slope of the constant amplitude tests performed in this study.

Fatigue tests included six plate specimens of both austenitic and duplex stainless steel. The ultimate strength of the austenitic steel was 582 Mpa (84.4 ksi), while the ultimate strength of the duplex steel was 797 Mpa (115.6 ksi). These tests were performed on plates with two transverse attachments. The plate was 150mm wide and 10mm thick. The transverse attachments were 10mm thick. The austenitic steel was welded using MIG process, while the duplex steel was welded using TIG process. AWS type ER 308L filler metal was used to weld the austenitic steel, while ER 2209 was used to weld the duplex steel.

Test results are summarized in Figures 3.3.1 and 3.3.2. Data for the austenitic steel fell mostly above AASHTO Category B with one below. All data for the

duplex steel fell above AASHTO Category B. The authors concluded that using Miner's Rule to compare the variable amplitude with the constant amplitude curve would have been conservative for all the austenitic steel. With the duplex steel the scatter is such that some individual tests were unconservative. Therefore it may be unconservative to use Miner's Rule for duplex stainless steel. However, the results reported in this paper lead to the opposite conclusion.

3.4 Discussion

Among the studies reviewed, Schilling et al (9) compared test results from constant amplitude and variable amplitude stress on similar beam specimens of structural carbon steel. It was concluded that Equation (2.3.2) derived from Miner's Rule was satisfactory. Albrecht and Friedland compared test results from constant and variable amplitude stresses on similar small specimens of ASTM A588 steel (12). The results confirmed that above the CAFL the RMC equivalent stress range works well. It was found that below the CAFL modification to equivalent stress range needs to be made. Examination of the effect of CAFL on variable amplitude stress fatigue is part of the goal of this study.

NCHRP Reports 267 and 354 both concluded that only a few cycles of stress ranges above the CAFL will cause fatigue crack growth (13,14). Yet, test results showed the conservative nature of using the extension of AASHTO strength curves below the CAFL. This situation is to be examined in this study.

Agerskov and Nielsen (15) and Maddox et al (16) tested small plate specimens with transverse attachments of carbon and stainless steels, respectively. These specimens would not have the same pattern of distribution and magnitude of residual stresses as contained in those beam specimens of the S-N curves of AASHTO (17,18). Direct comparison of results from tests on similar small plate specimens under constant and variable amplitude stresses could provide information for checking the validity of Equation (2.3.2).

In order to be able to achieve the objectives of this study test specimens identical to some of those used in the study of AL-6XN stainless steel (6) were chosen for testing.

4. DESCRIPTION OF TESTS

4.1 Test Specimens

All test specimens were I shaped beams and nominally 3.2 meters long. The flanges were 152mm wide and 13mm thick, while the web was 305mm high and 9.5mm thick. Each beam contained two welded simulated bulkhead attachments as seen in Figure 4.1.1 (6). The attachments were made of the same material as the beam, AL-6XN. The two attachments were fillet welded to one of the flanges (Figure 4.1.2). This allowed for a total of four possible crack initiation sites per beam. "Smart paint" was applied to nine test specimens on two of the four welds. Cracking was expected to originate from the toe of the transverse fillet weld at the outside face of the flanges of each attachment.

Fabrication of the first three test specimens (Stage I) was done by Bath Iron Works/Electric Boat Corp., at the Quanset Point, RI facility. The material used was nonmagnetic superaustenitic stainless steel alloy AL-6XN. The AL-6XN alloy conforms to ASTM B688, UNS N08367 for the fabrication of test specimens. Standard shipyard quality workmanship was specified conforming to MIL-STD-1089. The weld joint design conformed to MIL-STD-22D. The weld metal was IN625. The welding process for simulated bulkhead attachments was GMAW. The attachments were fabricated as subassemblies, welded complete,

and welded to the beams after completion of all other beam welding operations. The minimum specified yield strength of the steel was 344 Mpa (50 ksi).

Fabrication of the other nine test specimens (Stage II) was done by Metro Machines in Erie, Pa. The same materials were used and the quality of the workmanship was of similar nature. A different filler metal was used, IN622. Information regarding chemical composition, yield strength, tensile strength, and other material properties are listed in Tables 4.1.1 and 4.1.2.

4.2 Test Matrix

The intent of this test program was to develop a correlation between variable amplitude fatigue tests and constant amplitude fatigue tests on welded AL-6XN superaustenitic stainless steel. By assuming that an equivalent constant amplitude stress range, S_{re}, is computed according to Equation (2.3.2), twelve specimens were used in this variable amplitude program of four cells (Table 4.2.1). The test matrix had three specimens in each cell. Specimens with equivalent stress ranges of 55 Mpa (8 ksi) (Tension), 110 Mpa (16 ksi) (Tension), and 110 Mpa (16 ksi) (Reversal) were chosen to match the constant amplitude tests previously done on the same type of test specimens (6). An additional cell of three test specimens was chosen at an equivalent stress range of 82.5 Mpa (12 ksi) (Tension) to provide more information for defining the S-N curve for variable amplitude loading.

4.3 Stress Spectra

A stress range histogram from measurements on a ship was provided for this study (19). This is shown in Figure 4.3.1. The histogram has an equivalent stress range of 53.8 Mpa (7.8 ksi). For variable amplitude fatigue testing, a random load spectrum was to be determined from the histogram. This random spectrum was to be repeated throughout the test. When choosing the size of the spectrum it was necessary to make sure that the size used was not too small; otherwise it would not simulate random loading. It has been shown from a previous study that as little as 100 stress cycles could be used to determine a spectrum without distorting data (9).

For the first set of three tests with a target equivalent stress range of 55 Mpa (8 ksi) the original histogram was used as the basis for the random spectrum. Due to the resolution of the control system for running the test it was necessary to adopt a random spectrum with the equivalent stress range of 53.8 Mpa (7.8 ksi), slightly less than the target equivalent stress range. There are 583 cycles in the spectrum (Figure 4.3.2). Figure 4.3.3 shows a small portion of the load input spectrum used for the 55 Mpa (8 ksi) test specimens. More details will be presented later with respect to input and output loads during testing.

The second set of three tests would target an equivalent stress range of 82.5 Mpa (12 ksi). The basic stress range histogram was first scaled by 1.46 (Figure

4.3.4), then truncated below 16.5 Mpa (2.5 ksi) (Figure 4.3.5). It was decided to truncate the spectrum due to the excessive length of time it took to run the first set of three tests. Since the value of 16.5 Mpa (2.4 ksi) was well below the conservative CAFL value of 31 Mpa (4.5 ksi) the truncated stress cycles were assumed not to have an effect on results. It has been shown by constant amplitude tests that the CAFL for this exact detail is in-between 41.4 Mpa (6 ksi) and 48.3 Mpa (7 ksi) (20). Figure 4.3.5 was used as the input histogram for the second set of tests targeting an equivalent stress range of 82.5 Mpa (12 ksi). This spectrum had 498 stress cycles and an equivalent stress range of 80.6 Mpa (11.7 ksi). Figure 4.3.6 shows the corresponding random load spectrum and Figure 4.3.7 shows a small portion of the load input used for the 82.5 Mpa (12 ksi) test specimens.

The third and fourth set of three tests would target an equivalent stress range of 110 Mpa (16 ksi), one set of three in tension only, while the other set of three in complete reversal. The basic stress range histogram was first scaled by 1.9 (Figure 4.3.8). The scaled histogram was then truncated below 16.5 Mpa (2.5 ksi) for the same reasons given above. It can be seen from Figure 4.3.8 that there was a small percentage of stress ranges greater than 250 Mpa (36.3 ksi), the largest being 310 Mpa (45 ksi). It was decided to truncate these larger stress ranges due to the capability of the actuators in achieving very high stress range cycles, and due to the stability of the test specimens. The resulting histogram is shown as Figure 4.3.9; it was used as the input histogram of the third and fourth set of three tests targeting 110 Mpa (16 ksi). This histogram had 518 stress cycles and an

equivalent stress range of 108.9 Mpa (15.8 ksi). Figure 4.3.10 is the corresponding random load spectrum while Figure 4.3.11 shows a small portion of the load input used for the 110 Mpa (16 ksi) tension test specimens.

For the reversal load specimens it was difficult to achieve a random spectrum when the actuators must push and pull through the zero load position. Adjustments to the load spectrum needed to be made. Figures 4.3.12 and 4.3.13 respectively show the load spectrum and a small portion of the load input used for the 110 Mpa (16 ksi) reversal test specimens. Approximately five stress ranges of similar magnitudes were placed together to achieve reversal type loading and an equivalent stress range of 111.7 Mpa (16.2 ksi). The test spectrum contained a total of 518 stress cycles with 3 groups of 4 similar cycles, 92 groups of five similar cycles, 4 groups of 6 similar cycles, 2 groups of 7 similar cycles, and 1 group of 8 similar cycles. Different group sizes were utilized to achieve the target equivalent stress range.

4.4 Test Setup

All twelve beam specimens were tested on a 3.05m span under four point loading. The bulkhead attachments were located in the 1.2 meter long constant moment region (Figure 4.4.1). Loading was applied from below the specimens through a spreader beam. Specimens were subjected either to tension loading only or to reversal loading. Tension loading applied tension stress to one (the top) flange, while reversal loading applied equal tension and compression to both

flanges. All tests were conducted at Lehigh's ATLSS Laboratory. All tests were conducted using a test frame that had the capability to test two beams simultaneously. Hydraulic actuators with digital computer control systems were positively attached to the spreader beams to enable the application of both tension and compression loads. The spreader beams and the pin and roller end supports were clamped to the test specimen (Figure 4.4.2). One actuator was used per beam. The maximum dynamic capacity of the actuators was 490 kN. The computer control system enabled the actuators to operate at frequencies close to 2 Hz.

The digital control system was programmed to have the hydraulic actuators apply loads in a specified random sequence that correlated with each histogram. It was possible to run the same sequence or spectrum on two specimens simultaneously or to run each beam separately with its own specific spectrum. When the specimens were run simultaneously with the same spectrum slightly different equivalent stress ranges were experienced. This was because each actuator had slightly different gain settings to enable dynamic control of the system.

The digital control system contained limit settings to turn off the pressure to the actuators if the displacements or the loads exceeded specified values. Mechanical limit switches were also used. A mechanical limit switch was placed on each end of the test specimen (Figure 4.4.3) to ensure that the end rotations were not excessive, and in the event that one of the end fixtures would come loose. Two more mechanical limit switches were placed around the spreader

beam to ensure that the test specimen would not experience excessive positive or negative vertical deflections (Figure 4.4.4). All of the mechanical limit switches were wired through the I/O board enabling the pressure to be turned off in the event that one of the switches was tripped. Both types of limit switches were used simultaneously for redundancy.

Each test specimen had three strain gages attached to the flange with the attachments (Figure 4.4.5). The strain gages used were type CEA-06-250UN-350 made by Micro-Measurements Division in Raleigh, NC. One gage was placed at the centerline of the beam, approximately 10.2cm (4in) from the inside face of the attachments. One gage was placed approximately 10.2cm (4in) from the outside face of each attachment. The strain gages were attached to a PC 9000 Logger data acquisition system. Strains were monitored regularly to ensure the output spectrum agreed with the desired target spectrum.

The data acquisition system was also used to keep track of the cycle counts for each test specimen. A digital counter was attached to the data acquisition system and was programmed to count once every time a specified strain gage crossed the single high point of the spectrum. Therefore each number on the counter indicated one full completion of the spectrum. A digital counter was also attached to the control system and was programmed to count once at the end of each completed spectrum. Both counters were used to have redundancy and ensure proper cycle counting. To calculate the total number of cycles, multiply the number on the counter by the number of cycles in one spectrum.

5. TEST RESULTS AND EVALUATION

5.1 Monitoring Load Spectra

Variable amplitude loading poses a condition of monitoring that constant amplitude does not have. With a constant amplitude fatigue test the output load can be easily adjusted so that the proper load can be achieved repeatedly. With a variable amplitude test it becomes impossible to achieve each intended load precisely, especially larger loads, because of the varying dynamic response of the specimen to the input loads. Specifying different time steps according to the magnitude of the load steps reduced this problem. For higher loads a longer time step was used, which allowed the actuators to approach these higher loads. In general a time step of 0.2 seconds was used for load ranges less than 178 kN, 0.3 seconds for load ranges between 178 kN and 267 kN, and 0.4 seconds for load ranges larger than 267 kN. Strain gage data acquired during testing was used to monitor how accurately the loading system was operating.

Load history data was processed for one specimen from each cell of the test matrix. Figures 5.1.1 and 5.1.2 show partial load histories for a test specimen with a target equivalent stress range of 55 Mpa (8 ksi). The entire load spectrum contained 583 load cycles. In Figure 5.1.1 the maximum spectrum input load of 264.8 kN was at 144 seconds. The output at the same time was recorded as 250.9 kN, showing a difference of 13.9 kN. The control system had a tendency to

undershoot the increasing load values, but overshoot the minimum target load of 22.1 kN. Figure 5.1.3 shows a comparison of input and output stress range histograms. It can be seen that below the S_{re} the percentage of stress ranges on the output histogram were slightly less than the percentage of stress ranges on the input histogram, while above the S_{re} the opposite was true. The output S_{re} was 56.5 Mpa (8.2 ksi), which was slightly above the target S_{re} of 55 Mpa (8 ksi). Overall the representation of the input spectrum by the output spectrum for the 55 Mpa (8 ksi) tests was considered very accurate.

Figures 5.1.4 and 5.1.5 show partial load histories for a test specimen with a target equivalent stress range of 82.5 Mpa (12 ksi). The entire load spectrum contained 498 load cycles. In Figure 5.1.4 the maximum input load of 368.1 kN occurred at 149 seconds. The output at the same time was recorded as 343.4 kN, showing a difference of 24.7 kN. Once again the control system tended to undershoot the increasing load values, but overshoot the minimum target load of 22.1 kN. Figure 5.1.6 compares the input and output stress range histograms. Similarly to the 55 Mpa (8 ksi) specimen, below the S_{re} the percentage of stress ranges on the output histogram were slightly less than the percentage of stress ranges on the input histogram, while above the S_{re} the opposite was true. The output S_{re} was 82.1 Mpa (11.9 ksi), which was slightly lower than the target S_{re} of 82.5 Mpa (12 ksi). Overall the representation of the target spectrum for the 82.5 Mpa (12 ksi) tests was regarded as very satisfactory.

Figures 5.1.7 and 5.1.8 show partial load histories for a tension test specimen with a target equivalent stress range of 110 Mpa (16 ksi). The entire

load spectrum contained 518 load cycles. In Figure 5.1.7 the maximum input load of 415.4 kN appears at 106 seconds. The output at the same time was recorded as 373.2 kN, showing a difference of 42.2 kN. In Figure 5.1.9 the maximum input stress range was 221 Mpa (32.1 ksi), which corresponds to 352 kN. Since the control system tended to undershoot larger load values, the maximum load input for the 110 Mpa (16 ksi) tension specimen was programmed at a larger load of 415.4 kN in order to achieve a value closer to 352 kN. Once again the control system tended to overshoot the minimum target load of 22.1 kN. Figure 5.1.9 compares the input and output stress range histograms. Below the S_{re} the percentage of stress ranges on the output histogram were well below the percentage of stress ranges on the input histogram, while above the S_{re} the opposite can be seen. Even though the input and output stress range histograms look rather different, a similar S_{re} was experienced. The output S_{re} was 115.1 Mpa (16.7 ksi), which was slightly higher than the target S_{re} of 110 Mpa (16 ksi). Overall the simulation of the targeted spectrum for the 110 Mpa (16 ksi) tension tests was reasonable.

Figures 5.1.10 and 5.1.11 show partial load histories for a reversal test specimen with a target equivalent stress range of 110 Mpa (16 ksi). The entire load spectrum contained 518 load cycles. In Figure 5.1.10 the maximum input load of 229.7 kN and minimum load of –227.2kN is at 33.6 seconds. The output at the same time was recorded as 211.2 kN and –212.5 kN, showing a difference of 18.5 kN and 14.7 kN, respectively. The control system was able to provide very accurate values at most loads, but it tended to undershoot the larger load

values. Figure 5.1.12 compares the input and output stress range histograms. The input and output stress range histograms look very similar. The output S_{re} was 108.9 Mpa (15.8 ksi), which was slightly lower than the target S_{re} of 110 Mpa (16 ksi). Overall the simulation of the targeted spectrum for the 110 Mpa (16 ksi) reversal tests was regarded as satisfactory.

5.2 Test Results

A. S-N Data

Twelve beams with bulkhead attachments were tested under variable amplitude loading conditions, shown in the test matrix (Table 4.2.1). Each beam had two attachments thus, for all beams there were 48 anticipated crack locations. A total of 34 cracks of various degrees of severity were experienced. Each beam was tested until one crack propagated through the thickness of the flange (Figures 5.2.1 and 5.2.2) or, as with one beam, until 15 million cycles had occurred with only minimal crack growth. Failure was defined as the cycle count at which the fatigue crack propagated through the flange thickness. In all of the beams tested, cracks were detected at the toe of the welds in at least two of the four possible crack locations. Table 5.2.1 shows test results. The number of cycles at first detection and the number of cycles to failure are reported. Attachment location and use of "smart paint" was also included. The stress range versus cycles (S-N) results are presented in Figures 5.2.3 and 5.2.4, superimposed on S-N curves of welded steel details (1).

The use of "smart paint" was exploratory. The paint with special incapsulated paint pigment was expected to enhance the detection of cracks when developed. There were two cases on separate beams where the smart paint on a sharp or abrupt weld toe may have caused early release of paint pigment and premature indication of a crack (Figure 5.2.3). Each of these two cracks appeared in the smart paint much earlier than the other cracks on the same beam, and did not grow for at least another million cycles. In most cases the use of smart paint allowed for earlier detection than when a magnifying glass alone was used (Figure 5.2.4).

Figure 5.2.5 shows the S-N fatigue data for crack growth through the flange thickness under variable amplitude stresses in all tension and reversal. All tension tests fell above the AASHTO category D fatigue curve, while two of the reversal tests fell on or below AASHTO category D. All ten data points from tension and reversal tests fell above AASHTO category E, the fatigue strength category recommended for bulkhead attachments (6).

Figure 5.2.6 compares the results of variable amplitude tests to those from constant amplitude tests previously done (6). Figures 5.2.7 and 5.2.8 compare the tension only and reversal tests, respectively. All of the variable amplitude tension tests had longer lives than the constant amplitude tension tests (Figure 5.2.7). The targeted 110 Mpa (16 ksi) variable amplitude tension tests with an output S_{re} of 115.1 Mpa (16.7 ksi) and higher percentage of higher stress range above S_{re} showed lives that were about 20% longer than the 110 Mpa (16 ksi) constant amplitude tests. While the 55 Mpa (8 ksi) variable amplitude tension tests

showed lives that were more than 200% longer than the 55 Mpa (8 ksi) constant amplitude tests.

The results of variable amplitude reversal tests were much more scattered (Figure 5.2.8). At 110 Mpa (16 ksi) one variable amplitude reversal test had life similar to those from constant amplitude reversal tests, while the other two variable amplitude reversal tests had much shorter lives. This discrepancy could be due to the sequence of the loading spectrum. As indicated in section 4.3 and shown in Figures 4.3.12 and 4.3.13, the spectrum for the reversal loading is not completely random. Five stress ranges of similar magnitudes were placed together to achieve the targeted equivalent stress range. This grouping of similar magnitude stress ranges with its unknown effects on crack growth may have contributed to the shorter life. Also, a slag inclusion measuring approximately 1mm deep was found in specimen VB10 (Figure 5.2.9). More experimental studies are needed in order to examine the effects of "grouped" spectrums and, more importantly, variable amplitude reversal stresses.

B. Regression Lines

Test results were analyzed by using the $\log_{10}$ function applied to equivalent stress range, S_{re}, and the number of cycles to failure, N. Linear regression was used to transform the data into a straight-line equation

$$\text{Log}(N) = m\,\text{Log}(S_{re}) + C \qquad (5.2.1)$$

where m is the slope and C is the intercept on the axis of Log N. Analysis was done using the method of least squares, which minimizes the sum of the squares of the log (S_{re}) deviations from the data points.

Two separate linear regression routines were performed, one with only the results of tension tests and the other with the results from both tension and reversal tests included. The test data and the linear regression lines are superimposed on AASHTO fatigue strength curves in Figures 5.2.10. Both regression lines have a slope much flatter than the value of –3.0 for current fatigue resistance curves. Values for slopes were –4.14 for tension only tests and –4.65 for tension and reversal tests. Both tension only and tension and reversal linear regression lines crossed the AASHTO category E curve at very high stress ranges of 330 Mpa (47.9 ksi) and 280 Mpa (40.6 ksi), respectively.

It should be noted that the S_{re} values in Figure 5.2.10 are computed using Equation (2.3.2) with n = 3.0, corresponding to the slope of –3.0 for the fatigue strength curves of AASHTO. If the slope of regression lines for the AL-6XN specimens were different from –3.0, a different value for n would have to be used. The effects on the location of the data points in Figure 5.2.10, however, are not expected to be great.

Regardless of the difference between the slopes of the regression lines, the data points for all through flange thickness failure fall well above the fatigue strength curve of AASHTO category E, (Figure 5.2.10). This Indicates that the variable amplitude fatigue strength for the detail of simulated bulkhead attachments can be conservatively described by the category E resistance curve.

5.3 Results and Stress Range Histograms

Only one of the four sets of test specimens at the target S_{re} of 55 Mpa (8ksi) was tested using the full histogram of Figure 4.3.1. Because of the excessive amount of time it took to complete this set of tests and it was believed that very low stress ranges do not contribute to crack growth, truncating of such stress ranges was adopted. It has been shown by constant amplitude tests that the CAFL for this exact detail is somewhere between 41.4 Mpa (6 ksi) and 48.3 Mpa (7 ksi) (20). Consequently, three out of four histograms used in testing were truncated below 16.5 Mpa (2.5 ksi). Table 5.3.1 shows the number of stress cycles per histogram when truncated and which of these were used. If the assumption is true that very low stress ranges do not contribute to crack growth in variable amplitude fatigue testing, then the corresponding data evaluated from the truncated and non-truncated histograms should provide identical regression lines.

In order to compare the number of cycles to failure and the equivalent stress range for each set of tests, they must be transformed to corresponding values of the non-truncated histogram. Truncating the scaled stress range histograms below 16.5 Mpa (2.5 ksi) will increase the S_{re} by approximately 2 Mpa (0.3 ksi) and 7 Mpa (1 ksi) for the targeted values of 82.5 Mpa (12 ksi) and 110 Mpa (16 ksi), respectively (Figures 4.3.5 and 4.3.8 versus Figures 4.3.6 and 4.3.9). However, there was discrepancy of input and output stresses in testing which resulted in

about the same amount of shifting of S_{re} in the opposite direction for tension only tests at these two targeted values (Figures 5.1.6 and 5.1.9). Because of this situation and the condition that there was no available method to transform the S_{re}, the equivalent stress ranges from the output stresses were used.

The transformation of number of cycles to failure, $N_{non\text{-}trun}$, was calculated using Equations 5.3.1 and 5.3.2. In the equations, N is the final number of cycles

$$Z = \frac{N}{n_{trunc}} . \qquad (5.3.1)$$

$$N_{non\text{-}trunc} = Z \times 583 \qquad (5.3.2)$$

to failure experienced in testing, n_{trunc} is the number of cycles per truncated spectrum (Table 5.3.1), and Z indicates the number of repetitions of the load spectrum corresponding to the truncated histogram.

Results with all truncated histograms transformed to reflect non-truncated histograms are shown in Table 5.3.2. The data of transformed stress range and life cycle to failure are shown in Figures 5.3.1 and 5.3.2 with those data from truncated histograms. All of the non-truncated data points fall to the right of the truncated data points. This indicates that truncating the very low stress ranges of a histogram for fatigue life estimate could be considered conservative.

Two linear regression analyses were performed on the non-truncated data of Figure 5.3.1. One of the analyses included tension only tests, (Figure 5.3.3); the other included tension and reversal tests (Figure 5.3.4). Both regression lines give a slope much flatter than the value of –3.0 for the current fatigue resistance

curves. The value of slope for the tension only tests in Figure 5.3.3 is –4.05. This is slightly different from –4.14, the value in Figure 5.2.10 for the truncated case. The slope for the tension and reversal tests in Figure 5.3.3 is –4.58, comparable to –4.65 in Figure 5.2.10 for truncated data. The condition of almost identical correspondent regression lines confirms the validity of truncating very low stress ranges in a histogram in order to shorten the time of conducting variable amplitude fatigue tests.

5.4 Fatigue Striations

A. Striations from Variable Amplitude Fatigue

Several crack surfaces were inspected using a Scanning Electron Microscope, SEM, to detect unusual defects and to obtain fatigue striations. Crack surfaces inspected included failure cracks from beams VB5 (at 82.5 Mpa tension), VB7 (at 110 Mpa tension), and VB12 (at 110 Mpa reversal).

Figure 5.2.9, presented earlier, shows the example of crack surfaces. Figures 5.4.1 and 5.4.2 show fatigue striations from beam VB12, a 110 Mpa (16 ksi) reversal specimen. Fatigue striations for variable loading are easily seen due to the varying width of bands, each with five striation marks. These bands correspond to the loading spectrum, which consists of a sequence of approximately 100 different groups of five similar load ranges (Figures 4.3.12 & 4.3.13).

Figure 5.4.3 shows striations from beam VB7, a 110 Mpa (16 ksi) tension specimen. This loading spectrum did not have five similar loads grouped together. The load spectrum was of a more random nature (Figures 4.3.10 & 4.3.11). The varying width of the striation marks identifies the loads of variable amplitude. It is very easy to distinguish the larger load cycles from the smaller load cycles.

Figure 5.4.4 shows striations from beam VB5, an 82.5 Mpa (12 ksi) tension specimen. The widths of the striations appear to be uniform as from constant amplitude loading. This is caused by the condition that at a relatively low equivalent stress range there were only a small number of load cycles within the spectrum large enough to cause a visible striation. In a repeated application of random load spectrum with a low equivalent stress range, the striations give the illusion of constant amplitude loading.

Since the grouping of five striations in Figures 5.4.1 and 5.4.2 is directly corresponding to the grouping of five similar load ranges in the load spectrum, it is possible to match the groups of five for further examination of crack growth. Figures 5.4.5 and 5.4.6 show the SEM micrograph and the accompanying portion of the load history that possibly caused the striations. Bands A, B1, B2, C, and D match the fatigue striations in Figure 5.4.5 with appropriate loads in Figure 5.4.6. Bands A and C in Figure 5.4.5 have very wide width, most likely generated by two of the load groups with high magnitudes in the spectrum. Bands D, B2, and B1 had lower load magnitudes and narrower width of the bands. Between bands A and B1, and B2 and C, no striations are seen. This corresponds to the condition

that the loads between bands, A and B1, and B2 and C, were all less than 75 kN, which induced a stress range of 47.0 Mpa (6.8 ksi), about the value of CAFL. These low magnitude loads very possibly did not generate crack growth.

Figures 5.4.7 and 5.4.8 show the SEM micrograph and the accompanying portion of the load history that possibly caused the striations. Striation bands A, B, C, D, and E in Figure 5.4.7 roughly matches with the respective loads in Figure 5.4.8. Bands B and D had the highest load ranges and the widest width; bands A and E had lower loads and narrower band width. However, the loads between bands A and B, at 95 kN and 59.7 Mpa (8.7 ksi), being higher than the CAFL, do not appear to have caused fatigue striations. Yet the smaller loads between bands B and C seem to have generated crack growth. Regardless of these two uncertainties, the sequence of bands in the figures is the best possible fit within the entire load spectrum of approximately 100 load groups.

B. Stresses at Cracks

Crack tip stress analysis was performed through the determination of an average crack growth rate (da/dN) from the SEM micrographs and the use of ΔK - da/dN relationship of AL-6XN material. From the micrographs of Figures 5.4.5 and 5.4.7, the widths of the striation bands were measured and then divided by five to determine the average crack growth rate of each group of five cycles. These data are listed in the first column of Table 5.4.1. The crack growth rate

characteristics of ΔK-da/dN, Figure 5.4.9, were obtained from tests conducted on small specimens of the same material used for the beams in this study (21).

Crack growth rates from the SEM micrographs were fairly large when compared to the values in Figure 5.4.9. The smallest da/dN from the SEM micrograph was 34×10^{-8} m/cycle, while the largest on Figure 5.4.9 was 24×10^{-8} m/cycle. For the purpose of extrapolation of ΔK- da/dN relationship in Figure 5.4.9, a power fit was used giving the following result with an R squared value of 0.9989.

$$\frac{da}{dN} = 4\times10^{-12}\Delta K_{th}^{\ 3.18} \qquad (5.4.1)$$

The ΔK values calculated for each da/dN measured from the SEM micrograph are listed in the second column of Table 5.4.1. A crack tip stress range was then calculated using the following formula where F_s, F_w, F_e, and F_g are correction factors (22).

$$\Delta K = F_s \times F_w \times F_e \times F_g \times \Delta\sigma \sqrt{\pi a} \qquad (5.4.2)$$

$$F_s = 1.211 - 0.186 \sqrt{a_d/a} \qquad (5.4.3)$$

$$F_w = \sqrt{\sec\left(\frac{\pi a_d}{2w}\right)} \qquad (5.4.4)$$

$$F_e = \left(\int_0^{2\pi}\left(1-k^2\sin^2\theta\right)^{1/2}d\theta\right)^{-1},\ k^2 = \frac{a^2 - a_d^{\ 2}}{a^2}, \qquad (5.4.5)$$

$$F_g = \frac{1+2\frac{g}{h}}{1+\frac{1}{e}\left(\frac{a_d}{t_f}\right)^q} \qquad (5.4.6)$$

These calculated stress ranges were then compared with the actual output stress ranges determined from the appropriate load histories (Table 5.4.1).

Comparisons of stresses are also shown graphically in Figures 5.4.10 and 5.4.11. In Figure 5.4.10 the stresses are arranged by loading order, showing the agreement between measured and calculated values. In Figure 5.4.11 the stresses are presented in ascending order of magnitude, which allows for comparison of results from two separate SEM micrographs and loading histories. It can be seen that differences are minimal in calculated stresses and applied stresses at the crack tip. As shown in the last column of Table 5.4.1, the average differences are 13.3 % and 5.8 % for the two samples. This relatively good result is in spite of the situation that the crack growth data of Figure 5.4.9 were from small specimens and that the actual states of stress at the cracks in the full size beam specimens were not know because of residual stresses. It is believed that the fairly large crack growth rate of Figure 5.4.5 and 5.4.7 renders the effect of stress ratios minimal (7).

6. VARIABLE AMPLITUDE FATIGUE ANALYTICAL MODEL

6.1 Concept of Decreasing Fatigue Limit

For constant amplitude fatigue loads the number of cycles to failure, N, can be determined using Equation (6.1.1) which is derived from Equation (6.1.2) and (6.1.3) (4). In these equations, a_i and a_f are the initial and final length of crack, B is the material property of crack growth, β is the characteristic of crack size and shape (see Equation 5.4.2), and $\Delta\sigma$ is the nominal stress range.

$$N = \int_{a_i}^{a_f} \frac{da}{B(\beta \Delta\sigma \sqrt{\pi a})^3} \qquad (6.1.1)$$

$$\frac{dN}{da} = B \Delta K^n \qquad (6.1.2)$$

$$\Delta K = \beta \Delta\sigma \sqrt{\pi a} \qquad (6.1.3)$$

For variable amplitude fatigue loads, the prediction of fatigue life is through the use of the equivalent constant amplitude stress range, S_{re}, as defined by Equation (2.3.2). This equivalent stress substitutes $\Delta\sigma$ in Equation (6.1.1) for the calculation. While the AASHTO fatigue strength curves represent quite well the experimental data (17,18), results such as Figure 5.3.3 indicate the inadequacy of using these strength curves for variable stresses when the equivalent stress is near or below the constant amplitude fatigue limit, CAFL.

Since any actual load spectrum will produce many stress ranges both above and below the CAFL, and only stress ranges above the CAFL contribute to crack growth, the sequence of load application will have influence on the fatigue life of the structure. The adoption of CAFL for variable amplitude fatigue needs to be examined. If the threshold of stress intensity factory of a material, ΔK_{th}, is correspondent with the CAFL, Equation (6.1.3) can be transformed into Equation (6.1.4).

$$\Delta K_{th} = \beta \, CAFL \, \sqrt{\pi a} \qquad (6.1.4)$$

Hypothetically, because both ΔK_{th} and CAFL are threshold values, the crack size, a, in the equation is a "critical" value. When the crack size increases and ΔK_{th} remains as a constant, the fatigue limit (CAFL) will decrease allowing more stress ranges to contribute to crack growth. This concept of decrease in fatigue limit renders the calculation of fatigue life of variable amplitude loading difficult and complicated.

Fortunately for structures such as bridges and ships, there is quite some degree of repetition in loading pattern within certain lengths of time and the stress range histogram is applicable throughout the life. This permits the assumption that the fatigue limit is a fixed value in the duration of a repetitious loading period. Equation 6.1.1 is to be evaluated many times until the crack length grows to failure.

The decrease of fatigue limit with increasing crack length will cause a change in slope of the S-N curve below the CAFL.

6.2 Analytical Procedure

The analytical procedure was used to obtain analytical results for comparison with experimental data of fatigue failure of AL–6XN superaustenitic stainless steel beams. The same procedure can be used to compile analytical results for fatigue strengths of any other metal by substituting the proper crack growth properties for that material.

(1) Initially a histogram of stress ranges needs to be chosen as the loading spectrum. This spectrum will be repeated until the crack length grows to a predetermined final value, which constitutes failure. Spectrums used in this study will be described in the next section.

(2) Estimation of the initial crack length, $a_{i\text{-}step\#1}$, corresponding to the crack growth stress intensity threshold, ΔK_{th}, and CAFL.

$$a_{i\text{-}step\#1} = \left(\frac{\Delta K_{th}}{\beta_i CAFL}\right)^2 \left(\frac{1}{\pi}\right) \qquad (6.2.1)$$

Equation 6.2.1 is derived from Equation (6.2.2) by substituting $\Delta\sigma$ = CAFL and $a = a_{i\text{-}step\#1}$. When the stress range $\Delta\sigma$ is higher than the fatigue limit CAFL, the crack will grow.

$$\Delta K_{th} = \beta\, \Delta\sigma\, \sqrt{\pi a} \qquad (6.2.2)$$

(3) Selection of size of stress range blocks in the loading spectrum for crack growth calculation. Smaller blocks provide more accurate results, but

require more computation. Stress range blocks of 6.9 Mpa (1 ksi) were used in this study.

(4) Determination of the number of stress cycles above the CAFL, N_a, in each of the blocks and the average stress range, S_{ravg}. Only the stress ranges above the CAFL will contribute to crack growth. For example, if there are 46 stress cycles in a stress block between 6.9 Mpa (1 ksi) and 13.8 Mpa (2 ksi) and 40 of the stress cycles are above CAFL. N_a equals 40 stress cycles and S_{ravg} is equal to 10.4 Mpa (1.5 ksi).

(5) Calculation of crack length, a_f, at the end of application of a stress block.

$$a_f = \left(\frac{N_a B \beta^3 S_{ravg}{}^3 \pi^{3/2}}{-2} + \frac{1}{\sqrt{a_i}} \right)^{-2} \qquad (6.2.3)$$

Equation 6.2.3 is derived from equation 6.1.1 by substituting $N = N_a$ and $\Delta\sigma = S_{ravg}$ and solving for a_f.

(6) Repeat Item (5) for all stress range blocks in the spectrum. Once a_f has been calculated for the whole spectrum, set $a_f = a_{f\text{-step\#1}}$.

(7) Determination of new fatigue limit, $CAFL_{step\#1}$. Since ΔK_{th} is a constant of material property, Equation (6.1.4) can be transformed into Equation (6.2.4) for calculating the new, decreased fatigue limit $CAFL_{step\#1}$ which would cause more subsequent stress ranges to contribute to crack growth.

$$CAFL_{step\#1} = \frac{\Delta K_{th}}{\beta\sqrt{\pi a_{f-step\#1}}} \qquad (6.2.4)$$

This is the end of Step #1.

(8) Let $a_{f\text{-}step\#1} = a_{i\text{-}step\#2}$, and repeat the algorithm from (4) to (7). Repeat these steps until a_f reaches the predetermined final crack size. In the analytical work of this study 1.3 cm (0.5 inch) was chosen as final crack size because it was the thickness of the flange of the AL-6XN stainless steel beams being tested. Crack growth through the thickness of the flange was the failure criterion.

(9) Total cycles to failure, N, are calculated as the number of steps times the number of stress ranges in the load spectrum.

6.3 Defining Stress Spectra

In order to explore the validity of the concept, four different variable amplitude stress range histograms or distributions were adopted as stress spectra. The first spectrum was used in the experimental tests (Figure 4.3.2). The original histogram had an equivalent stress range, S_{re}, of 53.8 Mpa (7.8 ksi) and a maximum stress range, S_{rmax}, of 151.7 Mpa (22 ksi). To achieve varying values of S_{re}, all of the stress ranges in the histogram were scaled proportionally. The analytical model was run using scale factors between 0.38 and 2.4 resulting in S_{re} values between 20.2 Mpa (2.9 ksi) and 131.0 Mpa (19 ksi).

The second spectrum chosen for analysis was a family of Rayleigh distributions (11).

$$p = \frac{x}{\alpha^2} \exp\left(-0.5\left(\frac{x}{\alpha}\right)^2\right), \quad \alpha > 0 \qquad (6.3.1)$$

In Equation (6.3.1), p is the probability density, α is the parameter defining the curve shape, and x is the stress range, S_r (Figure 6.3.1). The Rayleigh distribution has been shown to accurately describe variable amplitude stress cycles due to traffic patterns on a bridge (9). Ten values of α were chosen between 6.9 Mpa (1 ksi) and 69 Mpa (10 ksi). The values of S_{re} and S_{rmax} were calculated for each α value. It was found that both S_{re} and S_{rmax} vary linearly with α (Figure 6.3.2).

$$S_{re} = 1.4837\,\alpha + 0.7884 \qquad (6.3.2)$$

$$S_{rmax} = 2.823\,\alpha + 9.0554 \qquad (6.3.3)$$

The analytical model of this study was run using the Rayleigh distribution with α between 14.5 Mpa (2.1 ksi) and 89.6 Mpa (13 ksi), and S_{re} between 22.3 Mpa (3.2 ksi) and 133.8 Mpa (19.4).

The third spectrum chosen was a normal distribution with a constant standard deviation equal to 13.8 Mpa (2 ksi) (11).

$$p = \frac{1}{\sigma\sqrt{2\pi}} \exp\left(-0.5\left(\frac{x-\mu}{\sigma}\right)^2\right), \mu > 0 \qquad (6.3.4)$$

In Equation (6.3.4), μ is the mean which is the parameter defining the scale of the curve, σ is the standard deviation which defines the shape of the curve, and x is stress range, S_r (Figure 6.3.3). Figure 6.3.4 shows the normal distribution with a low mean value and some stress ranges extending into the negative region. The distributions with μ > 34.5 Mpa (5 ksi) do not include negative values of stress

ranges. Since the total area under the probability density curve must equal one, the normal distributions with $\mu < 34.5$ Mpa (5 ksi) were scaled up so that the total area under each curve was equal to one (Figure 6.3.4). This causes a slight increase in S_{re} and S_{rmax} when $\mu < 34.5$ Mpa (5 ksi).

For this study ten values of μ were chosen between 6.9 Mpa (1 ksi) and 69 Mpa (10 ksi). The values of S_{re} and S_{rmax} were calculated for each μ value. Again it was found that both S_{re} and S_{rmax} vary linearly with μ, but with a break at $\mu =$ 34.5 Mpa (5 ksi) (Figure 6.3.5).

For $\mu < 34.5$ Mpa,

$$S_{re} = 0.73\,\mu + 13.824 \qquad (6.3.5)$$

$$S_{rmax} = 0.94\,\mu + 39.99 \qquad (6.3.6)$$

and for $\mu \geq 34.5$ Mpa,

$$S_{re} = 0.93\,\mu + 6.44 \qquad (6.3.7)$$

$$S_{rmax} = \mu + 37.92 \qquad (6.3.8)$$

Analysis was run using normal distributions having μ between 6.9 Mpa (1 ksi) and 152.2 Mpa (22.1), and S_{re} between 8.5 Mpa (1.2 ksi) and 148.0 Mpa (21.5 ksi).

The effect of having a constant mean value and varying standard deviation was also investigated. The analytical model was run using five normal distributions with constant $\mu = 93.1$ Mpa (13.5 ksi) and σ varying from 6.9 Mpa (1 ksi) to 34.5 Mpa (5 ksi). All five spectrums were analyzed for each AASHTO

category B, C, D, and E. As the standard deviation of each spectrum increased so did S_{re} and N. The results are shown in Figures 6.3.6 to 6.3.9. It can be seen that except in one case the value of σ used did not have an effect on the results of the computed fatigue life, as the points fell expectedly parallel to the AASHTO fatigue curves in these figures. The number of cycles to failure was more dependent on S_{re} than on the shape of the spectrum. The only exception to the good agreement is in Category B (Figure 6.3.6) with a small standard deviation of 6.9 Mpa (1 ksi). A larger N value occurred because S_{rmax} was equal to 113.8 Mpa (16.5 ksi), which is only slightly larger than CAFL of 110 Mpa (16 ksi). Therefore a majority of the stress cycles did not contribute to crack growth in the beginning requiring a noticeable amount of extra cycles before failure. Since the situation did not occur using a standard deviation of 13.8 Mpa (2 ksi), this was the value that was chosen for the rest of the analytical work with the normal distribution.

The fourth spectrum chosen was a Weibull distribution (11). In the following equation p is the probability density, b is the parameter defining the curve shape, θ is the parameter defining the curve scale, and x is the stress range.

$$p = \frac{b}{x}\left(\frac{x}{\theta}\right)^{b} \exp\left(-\left(\frac{x}{\theta}\right)^{b}\right) \qquad (6.3.9)$$

Since this is a two parameter function several values of each parameter were chosen to show that how S_{re} varied with each parameter. Changing the shape parameter b while holding the scale parameter θ constant caused only a slight change in S_{re} (Figure 6.3.10). Changing the scale parameter θ while holding the

shape parameter constant caused significant changes in S_{re} (Figure 6.3.11). The analytical model was run using the Weibull distribution having b, θ, and S_{re} between 2 and 4, 13.8 Mpa (2 ksi) and 89.6 Mpa (13 ksi), and 22.9 Mpa (3.3 ksi) and 95.1 Mpa (13.8 ksi), respectively.

6.4 Values of Constants for Analysis

Table 6.4.1 contains the values of the constants that were used to compute fatigue life using the analytical model defined above. Crack growth stress intensity threshold, ΔK_{th}, the S-N curve slope and intercept (n and A of Eq. 2.2.3), and other crack growth properties of AL-6XN superaustenitic stainless steel are not well known at this time. ΔK_{th} was estimated by referring to the value for ferrite-pearlite carbon steel and the data in Figure 5.4.9. A value of 2.5 ksi$\sqrt{in}$ was chosen conservatively. Converting to SI units, ΔK_{th} = 2.75 Mpa$\sqrt{m}$. The crack growth rate constant (B of Eq. 2.3.2), was taken as the same value as for ferrite-pearlite steel (7). This was due to the results obtained from constant amplitude tests performed with AL-6XN superaustenitic stainless steel (6). The stainless steel performed at the same level or better than carbon steel so using this value was conservative.

6.5 Results of Analysis

A. Computed Fatigue Life and Strength Curves

The results of computed fatigue life under variable amplitude stresses are compared with the corresponding fatigue data and the constant amplitude fatigue strength curves of AASHTO in Figures 6.5.1 to 6.5.4. Equivalent stress ranges of the stress spectra were used to produce the points in the figures. The analytical results are also listed in Tables 6.5.1 – 6.5.8.

The computed fatigue lives from all stress spectra agree well with the constant amplitude fatigue strength curves above the CAFL for all categories. Below the CAFL, a computed life is longer than that indicated by the AASHTO curves. The difference is more for higher strength categories with a higher CAFL. Obviously, for higher fatigue strength categories, more stress cycles in a stress spectrum do not contribute to the growth of crack until the crack becomes relatively large.

The computed results below the CAFL were examined by using the $\log_{10}$ function applied to both S_{re} and N. Linear regression was used to transform the data into a straight-line equation with the following format.

$$\text{Log}(N) = m\,\text{Log}(S_{re}) + C \qquad (6.5.1)$$

The slope is m and C is the intercept with the Log (N) axis. Analysis was done using the method of least squares, which minimizes the sum of the squares of Log (N) deviations from the data points. The regression lines are shown in Figures 6.5.5 to 6.5.8 and the values of m and D are given in Table 6.5.9.

For each fatigue category, B through E, five separate linear regression routines were performed below the CAFL. One for each of the four spectra by itself and one including all data points below the CAFL. In Figures 6.5.5 to 6.5.8, all regression lines are close to each other. (The only exception in Figure 6.5.5 will be discussed later.) The slope of theses lines are flatter than that of the AASHTO strength curves. This result indicates that for common variable amplitude load spectra on structural details, the fatigue life is longer that that described by the AASHTO lines.

To check the results of Figures 6.5.5 to 6.5.8 a power fit was also calculated for each category below the CAFL (Table 6.5.10). Data was fit to the following equation, where e and d are constants.

$$S_{re} = e\,N^{d} \qquad (6.5.2)$$

R^2 values were very close to one, showing an accurate fit. Linear regression and power fit results were plotted together for AASHTO Category B (Figure 6.5.9). Category B had the most diversion of results from the stress range spectra (Figure 6.5.5). There is no noticeable difference between the S-N lines from linear regression and power fit in Figure 6.5.9. The slope of the power fit line is –4.04.

The change of slope of the S-N lines above and below the CAFL was examined further by comparing the stress range versus load cycle regression lines in Figures 6.5.10 to 6.5.13. For all cases, Categories B through E, the slope above the CAFL is about –3.0, the value of AASHTO strength curves. The average value of the slope below the CAFL is –4.0.

B. Effects of Stress Spectrum

Linear regression analysis was performed on the analytical results from each family of stress spectrum individually as well as from all of the data as a whole. The Rayleigh spectrum, Navy spectrum, and Weibull spectrum gave similar results independent of fatigue strength category. The normal distribution gave similar results to the Rayleigh, Navy, and Weibull spectrums in Categories D and E (Figures 6.5.7 and 6.5.8), but provided smaller, flatter slopes in Categories B and C (Figures 6.5.5 and 6.5.6).

The main reason for this difference is the shape of the stress spectrum. While Rayleigh, Navy, and Weibull distributions are representative of stress range histograms of structures and are skewed to one side, the normal distribution generally does not describe structural behavior and is symmetrical with respect to the mean value, μ (Figure 6.3.3). When μ is less than 34.5 Mpa (5 ksi), the distribution was modified to a skewed shape for the analytical study (Figure 6.3.4). The lower the mean value, the more the skew, and the closer the analytical results to that of the other three distribution functions. For Categories B and C, the effects of the symmetrical normal distribution are dominant and provided higher fatigue life (Figures 6.5.5 and 6.5.6). In spite of this deviation, the regression line from all data in these figures is very close to those from Rayleigh, Navy, and Weibull distribution. This situation assures the validity of the overall regression line to provide S-N relationship below the CAFL.

C. Effects of Number of Cycles in Histogram

In a real life application it is sometimes difficult to obtain representative stress range frequency diagram or histogram for a structure within a manageable short length of time. The number of cycles in the stress spectrum for each step of the analytical model of fatigue life prediction, N_{spec}, could be large compared to the number of cycles to failure, N. Obviously, the smaller the ratio of N_{spec}/N is, the more accurate the results will be because the reference fatigue limit in each step is allowed to decrease more often. One the other hand if the stress spectrum covers a wide range, larger number of stress range blocks must be used in the analysis. Whether the values of N_{spec} used in the study was adequate needed to be examined.

Nine different Weibull spectra were analyzed with respect to four AASHTO Categories to determine how the size of the spectrum affected the results (Table 6.5.11). Each spectrum was analyzed using either two or three spectrum sizes, 5830 cycles, 58300 cycles, or 583000 cycles. The size of the spectrum analyzed was dependent on the AASHTO Category, the spectrum itself, and the capabilities of the computer program.

To examine the accuracy of results, the ratio of N_{spec}/N (in percent) and the percentage of difference in number of cycles to failure between two spectrum sizes are listed in Tables 6.5.12 for each analysis. In most cases the reference spectrum size was the smallest with 5830 cycles. It was found that as long as N_{spec}/N was less than 6%, the difference between the number of cycles to failure

would be at most 3.5% (Table 6.5.12). In several cases N_{spec}/N was greater than 6% and still the difference was less than 3.5% (Table 6.5.12).

Analytical results of fatigue life compiled for this study used small sizes of N_{spec}. These results were used to define the variable amplitude fatigue curves for Categories B, C, D, and E (Figures 6.5.10 to 6.5.13). These fatigue curves are compared with experimental results next.

7. COMPARISON OF EXPERIMENTAL AND ANALYTICAL RESULTS

7.1 Comparison with Results from AL-6XN Stainless Steel Beams

Experimental variable amplitude tests were conducted on simulated bulkhead attachments on AL-6XN stainless steel beams. The test results showed that the fatigue resistance of this structural detail is above the category E and even the category D fatigue strength curves of AASHTO (Figure 5.2.5). Figure 7.1.1 shows the same experimental data plotted with the category E AASHTO curve and the analytical variable amplitude fatigue curve developed for category E. All of the experimental data except those from reversal tests fall well above the analytical fit for category E, which itself falls above the AASHTO Category E resistance curve.

The linear regression results for the experimental data including tension and reversal tests are also plotted in Figure 7.1.2. The slopes of the experimental and analytical results are very different. The analytical curve above the CÁFL has a slope equal to the AASHTO fatigue resistance curve, while the regression line of the test data has a much flatter slope. It is obvious that more data from variable amplitude tests in tension and in reversal loads are needed for a better correlation of the analytical and experimental results.

The variable amplitude experimental data are also plotted with the analytical curve developed for category D (Figure 7.1.3). Again, all of the experimental

tension data falls above the analytical curve, while the reversal data did not. The analytical curve for category D appears to be a better representation than the category E curve for the experimental data. This is consistent with the results from constant amplitude tests of AL-6XN beams with simulated bulkhead attachments (6).

7.2 Comparison with Results from Carbon Steel Beams

While there is insufficient experimental data on AL-6XN stainless steel beams for a thorough comparison with the analytical fatigue strength curves, a comparison with test data from structural carbon steel may provide some meaningful information of correlation. This is particularly so because the derivation of the analytical curves was based on the AASHTO fatigue strength categories as well as on a fatigue crack growth threshold for structural steels.

The variable amplitude fatigue test data of Figure 3.1.2 (9) is plotted in Figure 7.1.4 with the AASHTO fatigue strength curves and the analytical fatigue curve for category E. The experimental data fell both above and below the analytical fatigue curve as well as the AASHTO strength curve for category E. Below the CAFL the fatigue test data of A514 steel from the previous study essentially follow the AASHTO category E curve with no indication of increasing fatigue life, as it is expected from the concept of decreasing fatigue limit.

There are some factors that may have affected the results of comparison. Among which are the differences between end-welded and not end-welded cover

plates (B and C in Figure 7.4.1), and the definition of failure of test beams. Also the difference among the crack growth characteristics of A514 steel and of ferrite-pearlite carbon steel in the low stress range region of S-N curves could have profound influences. Obviously, more study on these contributing factors needs to be made. Examination of other existing test data (12,13,14) must be added and more fatigue testing under variable amplitude loading must be conducted before more definite comparisons can be drawn.

Regardless of these needed studies the result that AASHTO category E fatigue strength curve can be used for all the simulated bulkhead attachments and cover plates is well established.

8. SUMMARY AND CONCLUSIONS

8.1 Summary of Findings

1. An equivalent constant amplitude stress range was calculated for the stress range histogram from a navy ship structure. This histogram and the effective stress range were expanded as input for testing of AL-6XN superaustenitic stainless steel beams with simulated bulkhead attachments. It was found that for variable amplitude fatigue testing, the stress variation in test beams differed slightly from the intended input values. The output equivalent stress range, however, were close to the targeted values for tension tests. For variable amplitude stresses in reversal, the derivation was too large so grouping of stress ranges has to be made.

2. All variable amplitude tension tests of AL-6XN simulated bulkhead specimens had longer lives than the constant amplitude tension tests. Specimens subjected to a variable amplitude tension spectrum with a low S_{re}, with respect to the CAFL, experienced much longer lives when compared to constant amplitude tests with similar S_r. On the other hand, specimens subjected to a variable amplitude tension spectrum with a high S_{re}, with respect to the CAFL, experienced only slightly longer lives than

the constant amplitude tests with similar S_r. All test data, tension and reversal, variable and constant amplitude, fall above the AASHTO category E fatigue strength curve.

3. In order to achieve high equivalent stress ranges for testing without having to take a long time for testing, some very low stress ranges in the histogram were truncated. Results of analysis confirmed the validity of this procedure.

4. Variable amplitude loads produced striations in crack surfaces. Some striations from reversal tests correlated well with the applied loads through visual determination of crack advance (da/dN) and the use of crack growth rate characteristics (da/dN - ΔK).

5. The concept of decreasing fatigue limit was applied to a number of stress range spectra to develop S-N curves below the CAFL. The slope of the analytical curves were flatter than that of the AASHTO strength curves, with a value of –4.0 for category B, and an average value of –4.0 for categories B to E.

6. The test data of the AL-6XN simulated bulkhead specimens have relatively longer fatigue lives than the predicted by the analytical S-N curve for AASHTO category E. Some test data from previous studies on

carbon steel beams compared fairly well with the analytical curve, but more studies need to be made before this new slope of S-N curve below the CAFL can be utilized

8.2 Conclusions

All of the results of studies done on the AL-6XN superaustenitic stainless steel simulated bulkhead attachments including variable amplitude fatigue tests, constant amplitude fatigue tests (6), and the analytical work with the concept of decreasing fatigue limit indicate the AASHTO category E fatigue strength curve as a lower bound. Until further studies are done to improve the accuracy, it is recommended that for simplified variable amplitude fatigue analysis using equivalent stress range, S_{re}, the AASHTO category E resistance curve should be used for AL-6XN simulated bulkhead attachments.

8.3 Future Work

1. As shown by the test data of AL-6XN specimens, there was a relatively large amount of scatter with the results from variable amplitude specimens. More variable amplitude tests at several different equivalent stress ranges are needed for more comparison with existing limited data

from variable amplitude tests and data with from constant amplitude fatigue tests.

2. An investigation into different types of reversal loading sequence in a spectrum should be considered. The complete reversal loading sequence used in this study had stress blocks of five similar stress ranges centered about zero and randomly placed within the spectrum in order to achieve that targeted equivalent stress range. Loading sequences with varying block sizes should be used, if possible, to determine the effect of different loading sequences.

3. Examinations of the influence of different load spectra, including truncating of spectra need to be made. Tests should be performed with a non-truncated spectrum and with several truncations at varying levels of stress range to determine how much the smaller stress ranges can be truncated for analysis and testing.

4. Additional work on the concept of decreasing fatigue limit should be carried out. Analytically the effects of loading sequence and load spectra should be examined with the appropriate fatigue crack growth threshold, ΔK_{th}. Experimentally a statistically significant number of

variable amplitude fatigue tests pertaining to several details should be conducted.

9. REFERENCES

1. AASHTO, "LRFD Bridge Design Specifications," First Edition American Association of State Highway and Transportation Officials, Washington D.C., (1994)

2. Broek, D., *The Practical Use of Fracture Mechanics,* Kluwer Academic Publishers, Dordrecht, The Netherlands, (1989)

3. Keating, P.B., Fisher J.W., "Evaluation of Fatigue tests and Design Criteria on Welded Details," NCHRP Report 286, (1986)

4. Paris, P. and Erdogan, F., "A Critical Analysis of Crack Propagation Laws," Trans. ASME (Series D), 85, 528-534, (1963)

5. Fisher, J.W., Kulak, G., and Smith, I., "A Fatigue Primer for Structural Engineers," ATLSS Report No, 97-11, (1997)

6. Fisher, J.W., Yen, B.T., Cheng, X., Kaufmann, E.J., Metrovich, B., Ma, Z., "Fatigue Resistance of Large Welded AL-6XN Stainless Steel Components with Fillet, Groove, and Attachment Welds," ATLSS Report No. 01-04, (2001)

7. Barsom, J.M., Rolfe, S.T., "Fracture & Fatigue Control in Structures – Application of Fracture Mechanics," 3rd edition, (1996)

8. Miner, M.A., "Cumulative Damage in Fatigue," Journal of Applied Mechanics, 12, no. 3, 159-164, (1945)

9. Schilling, C.G., Klippstein, K.H., Barsom, J.M., Blake, G.T., "Fatigue of Welded Steel Bridge Members Under Variable-Amplitude Loading," NCHRP Report 188, (1978)

10. Clarke, S.N., Goodpasture, D.W., Bennett R.M., Deatherage, J.H., Burdette, E.G., "Effect of Cycle-Counting Methods on Effective Stress Range and Number of Cycles for Fatigue Prone Details," Transportation Research Record 1740, Paper 00-0622 , National Research Council, Washington, D.C., pp. 49-60, (2000)

11. Ang, A.H-S., Tang, W.H., "Probabliltiy Concepts in Engineering Planning and Design," John Wiley & Sons, Inc., New York, (1975)

12. Albrecht, P., and Friedland, I. M., "Fatigue Limit Effects on Variable Amplitude Fatigue of Stiffeners," Journal of Structural Engineering, ASCE, Vol. 105, (1979)

13. Fisher, J.W., Mertz, D.R., and Zhong, A., "Steel Bridge Members Under Variable Long Life Fatigue Loading," NCHRP Report 267, (1979)

14. Fisher, J.W., Nussbaumer, A.C., Keating, P.B., and Yen, B.T., "Resistance of Welded Details under Variable Amplitude Long-Life Fatigue Testing," NCHRP Report 354, (1990)

15. Agerskov, H., Nielsen, J.A., "Fatigue in Steel Highway Bridges Under Random Loading," Journal of Structural Engineering, 125 (2), 152-162, (1999)

16. Maddox, S.J., Branco, M.C., Sonsino, C.M., Manteghi, S., Kueppers, M., Infante, V., "Fatigue Data For Welded Stainless Steels," International Institute of Welding, United Kingdom Delegation, IIW Document No. XIII-1798-99

17. Fisher, J.W., Albrecht, P.A., Yen, B.T., Klingerman, D.F., McNamee, B.M., "Fatigue Strength of Steel Beams with Welded Stiffeners and Attachments," NCHRP Report 147, (1974)

18. Fisher, J.W., Frank, K.H., Hirt, M.A., McNamee, B.M., "Effect of Weldments on the Fatigue Strength of Steel Beams," NCHRP Report 102, (1970)

19. Nussbaumer, A.C., "Propagation of Long Fatigue Cracks in Multi-cellular Box Beams," PhD dissertation, Lehigh University, Bethlehem, Pennsylvania, (1993)

20. Metrovich, B., "Fatigue Strength and Behavior of Welded AL-6XN Stainless Steel," PhD dissertation, Lehigh University, Bethlehem, Pennsylvania, (in Progress)

21. Quarterly Report on Navy Stainless Steel ADH Projects

22. Zettlemoyer, N., Fisher, J.W., "Stress Gradient and Crack Shape effects on Stress Intensity at Welded Details," Welding Journal Research Supplement, (1978)

Detail Category	Crack Growth Constant, A $(Mpa)^3$	Constant Amplitude Fatigue Limit (Mpa)
A	8.20E+12	165.0
B	3.93E+12	110.0
B'	2.00E+12	82.7
C	1.41E+12	69.0
C'	1.44E+12	82.7
D	7.21E+11	48.3
E	3.61E+11	31.0
E'	1.28E+11	19.9

Note: 1 ksi = 6.895 Mpa

Table 2.2.1 - Constants to Be Used With Figure 2.2.1

Heat Number	Thickness	C	Mn	P	S	Si	Ni	Cr	Mo	Co	Cu	N	Fe
Specified Range		0.03 max	2.00 max	0.04 max	0.03 max	1.00 max	23.5-25.50	20-22.00	6.00-7.00	_	0.75 max	0.18-0.25	_
879346	9.9 mm	0.018	0.44	0.021	4E-04	0.4	24.45	21.07	6.32	0.14	0.18	0.22	46.74
885547	12.7 mm	0.018	0.35	0.022	4E-04	0.45	24.61	21.14	6.31	0.18	0.26	0.23	46.43
4292204	9.9 mm	0.014	0.27	0.023	3E-04	0.41	23.89	20.44	6.27	0.15	0.08	0.22	48.23
4292268	12.7 mm	0.017	0.4	0.023	2E-04	0.41	23.99	20.39	6.22	0.12	0.17	0.23	48.03

Table 4.1.1(a) - AL-6XN Chemical Component (weight %) for Stage I Beams

Heat Number	Thickness	C	Mn	P	S	Si	Ni	Cr	Mo	Co	Cu	N	Fe
Specified Range		0.03 max	2.00 max	0.04 max	0.03 max	1.00 max	23.5-25.50	20-22.00	6.00-7.00	_	0.75 max	0.18-0.25	_
3200526HL4	9.9 mm	0.041	0.29	0.02	3E-04	0.33	23.97	20.64	6.24	0.2	0.13	0.227	47.83
891594	12.7 mm	0.024	0.31	0.024	5E-04	0.39	23.9	20.41	6.22	0.12	0.22	0.22	48.06

Table 4.1.1(b) - AL-6XN Chemical Component (weight %) for Stage II Beams

Heat Number	Thickness	0.2 %Yield Strength (ksi)	Ult. Tensile Strength (ksi)	UTS/YS	Elongation (%)	Reduction in Area (%)	Hardness (BHN)
879346	9.9 mm	48.1	107.1	2.23	56.9	73.8	183
885547	12.7 mm	53.5	111	2.07	58	73	179
4292204	9.9 mm	53.0	106	2.00	55	69	170
4292268	12.7 mm	57.1	110	1.93	48	68	187

Table 4.1.2(a) - AL-6XN Mechanical Properties (Transverse Direction) for Stage I Beams

Heat Number	Thickness	0.2 %Yield Strength (ksi)	Ult. Tensile Strength (ksi)	UTS/YS	Elongation (%)	Reduction in Area (%)	Hardness (BHN)
3200526HL4	9.9 mm	48.8	104	2.13	55	73	163
891594	12.7 mm	50.0	107	2.14	57	78	170

Table 4.1.2(b) - AL-6XN Mechanical Properties (Transverse Direction) for Stage II Beams

	Equivalent Stress Range of Spectrum		
Spectum Desctription	55 Mpa 8 ksi	82.5 Mpa 12 ksi	110 Mpa 16 ksi
Tension S_{min} - 14 Mpa (2 ksi)	3	3	3
Reversal Centered at Zero	-	-	3

Table 4.2.1 - Simulated Bulkhead Attachment Test Matrix

Variable Amplitude Fatigue Tension Tests							
Beam No.	$S_{r\,min}$ (Mpa)	$S_{r\,max}$ (Mpa)	S_{re} (Mpa)	Cycles when crack first detected	Cycles when through flange	Attachment Location	Use of Smart Paint
VB1	2.1	152.4	53.8		Damaged		
VB2	2.1	152.4	53.1	12,145,639**	Test Stopped	Exterior	no
				12,810,842***	at 15,000,000	Interior	no
VB3	2.1	152.4	56.5	8,056,477	-	Interior	no
				11,413,391	14,962,695	Interior	no
				13,027,718	-	Exterior	no
VB4	16.5	215.1	77.9	1,233,546	-	Exterior	yes
				2,686,212	-	Interior	yes
				3,481,020	5,018,346	Interior	no
VB5	16.5	215.1	82.1	387,444*	-	Exterior	yes*
				1,139,922	-	Interior	yes
				1,716,606	4,008,900	Interior	no
				1,716,606	-	Exterior	no
VB6	16.5	215.1	79.3	823,692*	-	Interior	yes*
				1,540,812	-	Exterior	no
				2,622,468	-	Exterior	yes
				3,148,356	6,435,156	Interior	no
VB7	18.6	218.6	115.8	163,170	1,053,612	Interior	yes
				193,214	-	Exterior	yes
				353,794	-	Exterior	no
VB8	18.6	218.6	115.1	186,480	867,132	Interior	yes
				232,582	-	Exterior	yes
				343,952	-	Exterior	no
VB9	18.6	218.6	116.5	95,830	-	Exterior	yes
				95,830	770,784	Interior	yes
				252,784	-	Interior	no

Note: Minimum stress for all tension tests was 13.8 Mpa.

* Denotes possible early detection due to sharpness of weld toe and use of "smart" paint.

** This crack was shallow and 2.2 cm long when the test was stopped. It had grown 2.2 cm in length after 3.5 million cycles.

*** This crack was very shallow and 0.64 cm long when the test was stopped. The crack had not grown in length since detection.

Table 5.2.1(a) - Results for Variable Amplitude Tension Tests

Variable Amplitude Fatigue Reversal Tests							
Beam No.	$S_{r\,min}$ (Mpa)	$S_{r\,max}$ (Mpa)	S_{re} (Mpa)	Cycles when crack first detected	Cycles when through flange	Attachment Location	Use of Smart Paint
VB10	21.4	286.8	108.9	157,472	450,142	Interior	no
				450,142	-	Exterior	yes
VB11	21.4	286.8	107.6	450,142	-	Exterior	no
				578,606	1,127,168	Interior	no
				717,948	-	Exterior	yes
				856,664	-	Interior	yes
VB12	21.4	286.8	112.4	139,342	516,645	Interior	yes
				275,058	-	Exterior	yes
				275,058	-	Exterior	no

Note: Mean stress for all reversal tests was zero Mpa.

Table 5.2.1(b) - Results for Variable Amplitude Reversal Tests

Beam No.	$S_{r\,min}$ (Mpa)	$S_{r\,max}$ (Mpa)	S_{re} (Mpa)	Cycles when crack first detected	Cycles when through flange	Attachment Location	Use of Smart Paint
VB1	2.1	152.4	53.8		Damaged		
VB2	2.1	152.4	53.1	12,145,639	Test Stopped	Exterior	no
				12,810,842	at 15,000,000	Interior	no
VB3	2.1	152.4	56.5	8,056,477	-	Interior	no
				11,413,391	14,962,695	Interior	no
				13,027,718	-	Exterior	no
VB4	16.5	215.1	77.9	1,233,546	-	Exterior	yes
				2,686,212	-	Interior	yes
				3,481,020	5,874,891	Interior	no
VB5	16.5	215.1	82.1	453,574	-	Exterior	yes
				1,334,487	-	Interior	yes
				2,009,601	4,693,150	Interior	no
				2,009,601	-	Exterior	no
VB6	16.5	215.1	79.3	964,282	-	Interior	yes
				1,803,802	-	Exterior	no
				3,070,078	-	Exterior	yes
				3,685,726	7,533,526	Interior	no
VB7	18.6	218.6	115.8	191,020	1,233,445	Interior	yes
				226,192	-	Exterior	yes
				414,181	-	Exterior	no
VB8	18.6	218.6	115.1	209,880	975,942	Interior	yes
				261,767	-	Exterior	yes
				387,112	-	Exterior	no
VB9	18.6	218.6	116.5	107,855	-	Exterior	yes
				107,855	867,504	Interior	yes
				284,504	-	Interior	no
VB10	21.4	286.8	108.9	177,232	506,627	Interior	no
				506,627	-	Exterior	yes
VB11	21.4	286.8	107.6	506,627	-	Exterior	no
				651,211	1,268,608	Interior	no
				808,038	-	Exterior	yes
				964,160	-	Interior	yes
VB12	21.4	286.8	112.4	156,827	581,475	Interior	yes
				309,573	-	Exterior	yes
				309,573	-	Exterior	no

Table 5.3.2 - Results for Variable Amplitude Tests without Truncating

	Number of Cycles per Histogram	
S_{re} (Mpa)	Truncated, n_{trunc}	Not Truncated
55	465	583*
82.5	498*	583
110	518*	583

* Histogram Used for Testing

Table 5.3.1 - Number of Cycles per Histogram used for Testing

Data from Figures 5.4.5 & 5.4.6					
da/dN (m/cycle x 10^{-8})		ΔK (Mpa sqrt m)	Crack Tip Stress – Δσ (Mpa)	Applied Stress Δσ (Mpa)	% Difference - Δσ
Measured from SEM Micrograph		From Figure 5.4.9	From $\Delta K = Fs*Fw*Fe*Fg*\Delta\sigma\,(\pi a)^{1/2}$	Measured from Actual Test	
A	150	56.8	244.7	263.4	7.1
B1	50	40.2	173.1	129.6	33.6
B2	70	44.7	192.5	164.8	16.8
C	130	54.3	233.9	242.0	3.4
D	80	46.6	200.7	190.3	5.5
				average =	13.3

Data from Figures 5.4.7 & 5.4.8					
da/dN (m/cycle x 10^{-8})		ΔK (Mpa sqrt m)	Crack Tip Stress – Δσ (Mpa)	Applied Stress Δσ (Mpa)	% Difference - Δσ
Measured from SEM Micrograph		From Figure 5.4.9	From $\Delta K = Fs*Fw*Fe*Fg*\Delta\sigma\,(\pi a)^{1/2}$	Measured from Actual Test	
A	54	41.2	177.4	166.9	6.3
B	100	50.0	215.3	220.0	2.1
C	34	35.6	153.3	134.5	14.0
D	80	46.6	200.7	194.4	3.2
E	40	37.5	161.4	166.9	3.3
				average =	5.8

	mm	m
Location of Figure 5.4.5, a =	9.5	0.0095
Location of Figure 5.4.7, a =	9.5	0.0095

From Figure 5.4.9
$da/dN = 4x10^{-12}\,\Delta K^{3.18}$

Correction Factors	
Fs =	1.118
Fw =	1
Fe =	0.932
Fg =	1.29

Table 5.4.1 - Comparison of Stress Ranges at Cracks

Category	CAFL - Mpa
B	110
C	69
D	48.3
E	31

Parameter	Value
n	3
W	15.24 cm
β_i	1
ΔK_{th}	2.75 Mpa M $^{1/2}$
B	3.6 E -10

Table 6.4.1 - Crack Growth Parameters for Superaustenitic Stainless Steel

Specturm	S_{rmax} (Mpa)	S_{rmin} (Mpa)	S_{re} (Mpa)	Cycles to Failure
Rayleigh	223.17	4.83	113.32	2.26E+06
Rayleigh	242.63	4.83	123.55	1.77E+06
Rayleigh	262.09	6.21	133.78	1.56E+06
Navy	353.44	4.70	119.97	1.98E+06
Navy	385.57	5.13	131.01	1.63E+06
Normal	162.03	86.19	122.25	1.62E+06
Normal	189.61	113.77	147.98	898,000

Table 6.5.1 - Data for Category B, Above CAFL

Specturm	S_{rmax} (Mpa)	S_{rmin} (Mpa)	S_{re} (Mpa)	Cycles to Failure
Rayleigh	112.22	2.07	55.01	5.247E+07
Rayleigh	118.06	2.07	58.08	3.521E+07
Rayleigh	125.84	2.07	62.17	2.338E+07
Rayleigh	145.31	2.07	72.40	1.096E+07
Rayleigh	164.77	3.45	82.63	6.47E+06
Rayleigh	184.24	3.45	92.86	4.37E+06
Rayleigh	203.70	3.45	103.09	3.09E+06
Navy	136.56	1.82	46.47	8.745E+07
Navy	144.59	1.92	49.16	6.413E+07
Navy	152.62	2.03	51.99	4.069E+07
Navy	160.65	2.14	54.61	3.504E+07
Navy	176.72	2.35	60.12	2.105E+07
Navy	192.78	2.56	65.57	1.405E+07
Navy	224.91	2.99	76.47	7.46E+06
Navy	257.05	3.42	87.57	4.80E+06
Navy	289.18	3.85	98.60	3.49E+06
Navy	321.31	4.27	106.73	2.53E+06
Normal	113.77	37.92	77.21	3.230E+07
Normal	120.66	44.82	83.64	1.218E+07
Normal	127.56	51.71	90.08	6.41E+06
Normal	131.01	55.85	93.30	4.95E+06
Normal	134.45	58.61	96.51	4.11E+06
Normal	141.35	65.50	102.95	3.01E+06
Weibull	120.66	2.07	59.02	3.556E+07
Weibull	134.45	2.07	66.40	1.714E+07
Weibull	146.86	2.07	73.50	1.079E+07
Weibull	166.17	2.07	84.33	6.24E+06
Weibull	137.21	22.75	86.88	6.59E+06
Weibull	153.76	13.10	88.67	5.54E+06
Weibull	185.48	3.45	95.08	4.07E+06

Table 6.5.2 - Data for Category B, Below CAFL

Specturm	S_{rmax} (Mpa)	S_{rmin} (Mpa)	S_{re} (Mpa)	Cycles to Failure
Rayleigh	164.77	3.45	82.63	3.17E+06
Rayleigh	203.70	3.45	103.09	1.66E+06
Rayleigh	242.63	4.83	123.55	985,000
Navy	160.65	2.14	54.61	1.096E+07
Navy	321.31	4.27	106.73	1.39E+06
Normal	106.87	31.03	70.78	5.17E+06
Normal	131.01	55.85	93.30	2.02E+06
Weibull	146.86	2.07	73.50	4.72E+06
Weibull	166.17	2.07	84.33	3.09E+06
Weibull	137.21	22.75	86.88	2.79E+06
Weibull	153.76	13.10	88.67	2.61E+06
Weibull	185.48	3.45	95.08	2.12E+06

Table 6.5.3 - Data for Category C, Above CAFL

Specturm	S_{rmax} (Mpa)	S_{rmin} (Mpa)	S_{re} (Mpa)	Cycles to Failure
Rayleigh	77.18	0.69	36.59	8.687E+07
Rayleigh	86.91	0.69	41.71	3.790E+07
Rayleigh	106.38	2.07	51.94	1.463E+07
Rayleigh	125.84	2.07	62.17	7.93E+06
Navy	112.46	1.50	38.27	4.722E+07
Navy	120.49	1.60	41.03	3.323E+07
Navy	128.52	1.71	43.71	2.524E+07
Navy	136.56	1.82	46.47	1.971E+07
Navy	144.59	1.92	49.16	1.592E+07
Navy	152.62	2.03	51.99	1.300E+07
Navy	176.72	2.35	60.12	7.87E+06
Navy	192.78	2.56	65.57	5.95E+06
Normal	79.29	3.45	45.04	4.431E+07
Normal	86.19	10.34	51.48	2.029E+07
Normal	93.08	17.24	57.91	1.143E+07
Normal	99.98	24.13	64.34	7.40E+06
Weibull	79.29	2.07	37.16	7.754E+07
Weibull	93.08	0.69	44.54	2.915E+07
Weibull	75.16	10.34	46.68	4.886E+07
Weibull	86.19	4.83	47.85	2.606E+07
Weibull	106.87	2.07	51.92	1.551E+07
Weibull	120.66	2.07	59.02	9.74E+06
Weibull	95.84	14.48	59.99	9.68E+06
Weibull	106.87	7.58	61.30	8.75E+06
Weibull	134.45	0.00	66.40	6.59E+06

Table 6.5.4 - Data for Category C, Below CAFL

Specturm	S_{rmax} (Mpa)	S_{rmin} (Mpa)	S_{re} (Mpa)	Cycles to Failure
Rayleigh	106.38	2.07	51.94	7.93E+06
Rayleigh	125.84	2.07	62.17	4.59E+06
Rayleigh	164.77	3.45	82.63	1.94E+06
Rayleigh	203.70	3.45	103.09	1.03E+06
Rayleigh	242.63	4.83	123.55	612,000
Navy	144.59	1.92	49.16	8.63E+06
Navy	152.62	2.03	51.99	7.29E+06
Navy	160.65	2.14	54.61	6.24E+06
Navy	176.72	2.35	60.12	4.58E+06
Navy	192.78	2.56	65.57	3.53E+06
Navy	321.31	4.27	106.73	863,000
Normal	86.19	10.34	51.48	8.40E+06
Normal	93.08	17.24	57.91	5.77E+06
Normal	99.98	24.13	64.34	4.12E+06
Normal	106.87	31.03	70.78	3.07E+06
Normal	131.01	55.85	93.30	1.26E+06
Weibull	106.87	2.07	51.92	8.34E+06
Weibull	120.66	2.07	59.02	5.60E+06
Weibull	95.84	14.48	59.99	5.19E+06
Weibull	106.87	7.58	61.30	4.90E+06
Weibull	134.45	0.00	66.40	3.87E+06
Weibull	146.86	2.07	73.50	2.86E+06
Weibull	166.17	2.07	84.33	1.88E+06
Weibull	137.21	22.75	86.88	1.72E+06
Weibull	153.76	13.10	88.67	1.61E+06
Weibull	185.48	3.45	95.08	1.31E+06

Table 6.5.5 - Data for Category D, Above CAFL

Specturm	S_{rmax} (Mpa)	S_{rmin} (Mpa)	S_{re} (Mpa)	Cycles to Failure
Rayleigh	59.66	0.69	27.39	9.969E+07
Rayleigh	61.61	0.69	28.41	8.279E+07
Rayleigh	63.56	0.69	29.43	6.705E+07
Rayleigh	65.50	0.69	30.46	5.888E+07
Rayleigh	67.45	0.69	31.48	5.130E+07
Rayleigh	77.18	0.69	36.59	2.740E+07
Rayleigh	86.91	0.69	41.71	1.644E+07
Navy	88.36	1.18	30.06	8.045E+07
Navy	96.39	1.28	32.82	3.620E+07
Navy	112.46	1.50	38.27	2.017E+07
Navy	120.49	1.60	41.03	1.568E+07
Navy	128.52	1.71	43.71	1.265E+07
Navy	136.56	1.82	46.47	1.032E+07
Normal	59.43	0.69	28.80	9.969E+07
Normal	65.92	0.69	33.97	4.250E+07
Normal	72.40	0.69	38.61	2.245E+07
Normal	79.29	3.45	45.04	1.329E+07
Weibull	64.12	0.69	30.13	6.938E+07
Weibull	54.47	6.21	30.89	7.404E+07
Weibull	72.40	0.69	33.72	4.023E+07
Weibull	62.74	3.45	34.20	4.489E+07
Weibull	79.29	2.07	37.16	2.682E+07
Weibull	93.08	0.69	44.54	1.364E+07
Weibull	75.16	10.34	46.68	1.183E+07

Specturm	S_{rmax} (Mpa)	S_{rmin} (Mpa)	S_{re} (Mpa)	Cycles to Failure
Rayleigh	67.45	0.69	31.48	1.895E+07
Rayleigh	77.18	0.69	36.59	1.160E+07
Rayleigh	86.91	0.69	41.71	7.46E+06
Rayleigh	106.38	2.07	51.94	3.78E+06
Rayleigh	125.84	2.07	62.17	2.24E+06
Rayleigh	164.77	3.45	82.63	962,000
Rayleigh	203.70	3.45	103.09	513,000
Rayleigh	242.63	4.83	123.55	303,000
Navy	96.39	1.28	32.82	1.492E+07
Navy	112.46	1.50	38.27	9.09E+06
Navy	120.49	1.60	41.03	7.23E+06
Navy	128.52	1.71	43.71	5.95E+06
Navy	136.56	1.82	46.47	4.89E+06
Navy	144.59	1.92	49.16	4.13E+06
Navy	152.62	2.03	51.99	3.50E+06
Navy	160.65	2.14	54.61	3.03E+06
Navy	176.72	2.35	60.12	2.25E+06
Navy	192.78	2.56	65.57	1.74E+06
Navy	321.31	4.27	106.73	431,000
Normal	65.92	0.69	33.97	1.557E+07
Normal	72.40	0.69	38.61	9.33E+06
Normal	79.29	3.45	45.04	6.00E+06
Normal	86.19	10.34	51.48	3.99E+06
Normal	93.08	17.24	57.91	2.80E+06
Normal	99.98	24.13	64.34	2.04E+06
Normal	106.87	31.03	70.78	1.53E+06
Normal	131.01	55.85	93.30	630,000
Weibull	72.40	0.69	33.72	1.568E+07
Weibull	62.74	3.45	34.20	1.469E+07
Weibull	79.29	2.07	37.16	1.125E+07
Weibull	93.08	0.69	44.54	6.35E+06
Weibull	75.16	10.34	46.68	5.40E+06
Weibull	86.19	4.83	47.85	5.04E+06
Weibull	106.87	2.07	51.92	3.98E+06
Weibull	120.66	2.07	59.02	2.71E+06
Weibull	95.84	14.48	59.99	2.55E+06
Weibull	106.87	7.58	61.30	2.40E+06
Weibull	134.45	0.00	66.40	1.92E+06
Weibull	146.86	2.07	73.50	1.41E+06
Weibull	166.17	2.07	84.33	933,000
Weibull	137.21	22.75	86.88	857,000
Weibull	153.76	13.10	88.67	799,000
Weibull	185.48	3.45	95.08	653,000

Table 6.5.7 - Data for Category E, Above CAFL

Specturm	S_{rmax} (Mpa)	S_{rmin} (Mpa)	S_{re} (Mpa)	Cycles to Failure
Rayleigh	49.93	0.69	22.27	7.288E+07
Rayleigh	51.88	0.69	23.29	5.830E+07
Rayleigh	53.82	0.69	24.32	4.839E+07
Rayleigh	55.77	0.69	25.34	4.198E+07
Rayleigh	57.72	0.69	26.36	3.638E+07
Rayleigh	59.66	0.69	27.39	3.014E+07
Rayleigh	61.61	0.69	28.41	2.676E+07
Rayleigh	63.56	0.69	29.43	2.303E+07
Rayleigh	65.50	0.69	30.46	2.087E+07
Navy	59.44	0.79	20.20	9.270E+07
Navy	72.29	0.96	24.55	4.058E+07
Navy	80.33	1.07	27.30	2.752E+07
Navy	88.36	1.18	30.06	2.000E+07
Normal	46.47	0.69	18.46	9.853E+07
Normal	51.66	0.69	22.59	6.879E+07
Normal	52.95	0.69	23.63	5.830E+07
Normal	54.57	0.69	24.92	4.956E+07
Normal	56.84	0.69	26.73	3.790E+07
Normal	59.43	0.69	28.80	2.892E+07
Weibull	50.33	0.69	22.89	6.879E+07
Weibull	64.12	0.69	30.13	2.390E+07
Weibull	54.47	6.21	30.89	1.597E+07

Table 6.5.8 - Data for Category E, Below CAFL

Category	Specturm	Location	# of Data	m = Slope	C = Intercept
B	Rayleigh	Below CAFL	7	-4.45	15.38
B	Navy	Below CAFL	10	-4.17	14.79
B	Normal	Below CAFL	6	-8.27	23.03
B	Weibull	Below CAFL	7	-4.32	15.14
B	All	Below CAFL	30	-4.04	14.64
B	All	Above CAFL	7	-3.16	12.86
C	Rayleigh	Below CAFL	4	-4.46	14.86
C	Navy	Below CAFL	8	-3.79	13.63
C	Normal	Below CAFL	4	-5.02	15.93
C	Weibull	Below CAFL	9	-4.43	14.86
C	All	Below CAFL	25	-4.11	14.26
C	All	Above CAFL	12	-3.03	12.30
D	Rayleigh	Below CAFL	7	-4.23	14.05
D	Navy	Below CAFL	6	-4.46	14.41
D	Normal	Below CAFL	4	-4.55	14.61
D	Weibull	Below CAFL	8	-4.18	14.04
D	All	Below CAFL	25	-4.24	14.10
D	All	Above CAFL	26	-2.97	11.98
E	Rayleigh	Below CAFL	9	-3.98	13.21
E	Navy	Below CAFL	6	-3.88	13.02
E	Normal	Below CAFL	4	-2.76	12.27
E	Weibull	Below CAFL	3	-4.45	13.89
E	All	Below CAFL	22	-3.64	12.73
E	All	Above CAFL	43	-3.01	11.75

Table 6.5.9 - Linear Regression Results. Log (N) = m * Log (S_{re}) + C

Category	Specturm	Location	# of Data	e	d	R^2
B	Rayleigh	Below CAFL	7	2734.8	-0.222	0.986
B	Navy	Below CAFL	10	3371.5	-0.237	0.987
B	Normal	Below CAFL	6	571.6	-0.1170	0.966
B	Weibull	Below CAFL	7	3017.9	-0.228	0.983
B	All	Below CAFL	30	3074.4	-0.229	0.924
C	Rayleigh	Below CAFL	4	2032.2	-0.221	0.986
C	Navy	Below CAFL	8	3873.7	-0.263	0.995
C	Normal	Below CAFL	4	1454.1	-0.198	0.994
C	Weibull	Below CAFL	9	1816.3	-0.212	0.941
C	All	Below CAFL	25	2153.9	-0.224	0.921
D	Rayleigh	Below CAFL	7	2082.6	-0.236	0.997
D	Navy	Below CAFL	6	1485.2	-0.216	0.964
D	Normal	Below CAFL	4	1571.9	-0.218	0.991
D	Weibull	Below CAFL	8	2176.4	-0.236	0.988
D	All	Below CAFL	25	1904.7	-0.230	0.976
E	Rayleigh	Below CAFL	9	2067.7	-0.251	0.997
E	Navy	Below CAFL	4	2234.6	-0.257	0.997
E	Normal	Below CAFL	6	11713.9	-0.348	0.963
E	Weibull	Below CAFL	3	1145.9	-0.216	0.962
E	All	Below CAFL	22	2461.9	-0.261	0.951

Table 6.5.10 - Power Fit Results. $S_{re} = e*N^d$

Category	S_{rmax} (Mpa)	S_{re} (Mpa)	Spectrum Size	Cycles to Failure
B	134.45	66.40	58300	1.71E+07
			583000	1.75E+07
B	185.45	95.08	5830	4.07E+06
			58300	4.08E+06
			583000	4.08E+06
B	153.76	88.67	58300	5.54E+06
			583000	5.83E+06
B	137.21	86.88	58300	6.59E+06
			583000	7.00E+06
C	106.87	51.92	58300	1.551E+07
			583000	1.574E+07
C	86.19	47.85	58300	2.606E+07
			583000	2.682E+07
C	75.16	46.68	58300	4.89E+07
			583000	4.96E+07
C	134.45	66.40	58300	6.59E+06
			583000	7.00E+06
C	106.87	61.30	58300	8.75E+06
			583000	9.33E+06
C	95.84	59.99	58300	9.68E+06
			583000	9.91E+06
C	185.48	95.08	5830	2.12E+06
			58300	2.16E+06
C	153.7585	88.6697	5830	2.61E+06
			58300	2.62E+06
			583000	2.92E+06
C	137.21	86.88	5830	2.79E+06
			58300	2.80E+06
			583000	2.92E+06

Table 6.5.11 - Analytical Results Using Varying Number of Cycles in Spectrum

Category	S_{rmax} (Mpa)	S_{re} (Mpa)	Spectrum Size	Cycles to Failure
D	106.87	51.92	58300	8.34E+06
			583000	8.75E+06
D	86.19	47.85	58300	1.084E+07
			583000	1.108E+07
D	75.16	46.68	58300	1.18E+07
			583000	1.22E+07
D	134.45	66.40	5830	3.87E+06
			58300	3.91E+06
			583000	4.08E+06
D	106.87	61.30	5830	4.90E+06
			58300	4.96E+06
			583000	5.25E+06
D	95.84	59.99	5830	5.19E+06
			58300	5.19E+06
			583000	5.25E+06
D	185.48	95.08	5830	1.31E+06
			58300	1.34E+06
D	153.76	88.67	5830	1.61E+06
			58300	1.63E+06
D	137.21	86.88	5830	1.72E+06
			58300	1.75E+06
			583000	1.75E+06
E	106.87	51.92	5830	3.98E+06
			58300	4.02E+06
			583000	4.08E+06
E	86.19	47.85	5830	5.04E+06
			58300	5.07E+06
			583000	5.25E+06
E	75.16	46.68	5830	5.40E+06
			58300	5.42E+06
			583000	5.83E+06
E	134.45	66.40	5830	1.90E+06
			58300	1.92E+06
			583000	2.33E+06
E	106.87	61.30	5830	2.40E+06
			58300	2.45E+06
			583000	2.92E+06
E	95.84	59.99	5830	2.55E+06
			58300	2.57E+06
			583000	2.92E+06
E	185.48	95.08	5830	6.53E+05
			58300	7.00E+05
E	153.76	88.67	5830	7.99E+05
			58300	8.16E+05
E	137.21	86.88	5830	8.57E+05
			58300	8.75E+05

Table 6.5.11 (Contiued) - Analytical Results Using Varying Number of Cycles in Spectrum

Category	S_{rmax} Mpa	S_{re} Mpa	Number of Cycle in Spectrum	Cycles to Failure	% Difference in Cycles to Failure	% of N_{spec} / N
E	86.19	47.85	5830	5.40E+06	0	0.11
D	106.87	61.30	5830	5.19E+06	0	0.11
E	106.87	51.92	5830	5.04E+06	0	0.12
D	134.45	66.40	5830	4.90E+06	0	0.12
C	75.16	46.68	58300	4.89E+07	0	0.12
B	134.45	66.40	5830	4.07E+06	0	0.14
E	137.21	86.88	5830	3.98E+06	0	0.15
D	75.16	46.68	5830	3.87E+06	0	0.15
C	153.76	88.67	5830	2.79E+06	0	0.21
C	185.48	95.08	5830	2.61E+06	0	0.22
C	86.19	47.85	58300	2.606E+07	0	0.22
E	106.87	61.30	5830	2.55E+06	0	0.23
E	134.45	66.40	5830	2.40E+06	0	0.24
C	185.48	95.08	5830	2.12E+06	0	0.28
E	75.16	46.68	5830	1.90E+06	0	0.31
D	153.76	88.67	5830	1.72E+06	0	0.34
B	134.45	66.40	58300	1.71E+07	0	0.34
D	153.76	88.67	5830	1.61E+06	0	0.36
C	106.87	51.92	58300	1.551E+07	0	0.38
D	185.48	95.08	5830	1.31E+06	0	0.45
D	75.16	46.68	58300	1.18E+07	0	0.49
D	86.19	47.85	58300	1.084E+07	0	0.54
C	95.84	59.99	58300	9.68E+06	0	0.60
C	106.87	61.30	58300	8.75E+06	0	0.67
E	137.21	86.88	5830	8.57E+05	0	0.68
D	106.87	51.92	58300	8.34E+06	0	0.70

Table 6.5.12 - % of N_{spec} / N in Acending Order

Category	S_{rmax} Mpa	S_{re} Mpa	Number of Cycle in Spectrum	Cycles to Failure	% Difference in Cycles to Failure	% of N_{spec} / N
E	153.76	88.67	5830	7.99E+05	0	0.73
B	137.21	86.88	58300	6.59E+06	0	0.88
C	134.45	66.40	58300	6.59E+06	0	0.88
E	185.48	95.08	5830	6.53E+05	0	0.89
B	153.76	88.67	58300	5.54E+06	0	1.05
E	75.16	46.68	58300	5.42E+06	0.37	1.08
D	95.84	59.99	58300	5.19E+06	0.00	1.12
E	86.19	47.85	58300	5.07E+06	0.60	1.15
D	106.87	61.30	58300	4.96E+06	1.22	1.18
C	75.16	46.68	583000	4.96E+07	1.43	1.18
B	185.45	95.08	58300	4.08E+06	0.25	1.43
E	106.87	51.92	58300	4.02E+06	1.01	1.45
D	134.45	66.40	58300	3.91E+06	1.03	1.49
C	137.21	86.88	58300	2.80E+06	0.36	2.08
C	86.19	47.85	583000	2.682E+07	2.92	2.17
C	153.76	88.67	58300	2.62E+06	0.38	2.23
E	95.84	59.99	58300	2.57E+06	0.78	2.27
E	106.87	61.30	58300	2.45E+06	2.08	2.38
C	185.48	95.08	58300	2.16E+06	1.89	2.70
E	134.45	66.40	58300	1.92E+06	1.05	3.04
D	137.21	86.88	58300	1.75E+06	1.74	3.33
B	134.45	66.40	583000	1.75E+07	2.04	3.33
D	153.76	88.67	58300	1.63E+06	1.24	3.58
C	106.87	51.92	583000	1.574E+07	1.48	3.70
D	185.48	95.08	58300	1.34E+06	2.29	4.35
D	75.16	46.68	583000	1.22E+07	3.47	4.76

Table 6.5.12 (Continued) - % of N_{spec} / N in Acending Order

Category	S_{rmax} Mpa	S_{re} Mpa	Number of Cycle in Spectrum	Cycles to Failure	% Difference in Cycles to Failure	% of N_{spec} / N
D	86.19	47.85	583000	1.108E+07	2.21	5.26
C	95.84	59.99	583000	9.91E+06	2.38	5.88
C	106.87	61.30	583000	9.33E+06	6.63	6.25
D	106.87	51.92	583000	8.75E+06	4.92	6.66
E	137.21	86.88	58300	8.75E+05	2.10	6.66
E	153.76	88.67	58300	8.16E+05	2.13	7.14
B	137.21	86.88	583000	7.00E+06	6.22	8.33
C	134.45	66.40	583000	7.00E+06	6.22	8.33
E	185.48	95.08	58300	7.00E+05	7.20	8.33
B	153.76	88.67	583000	5.83E+06	5.23	10.00
E	75.16	46.68	583000	5.83E+06	7.96	10.00
D	106.87	61.30	583000	5.25E+06	7.14	11.10
D	95.84	59.99	583000	5.25E+06	1.16	11.10
E	86.19	47.85	583000	5.25E+06	4.17	11.10
B	185.45	95.08	583000	4.08E+06	0.25	14.29
D	134.45	66.40	583000	4.08E+06	5.43	14.29
E	106.87	51.92	583000	4.08E+06	2.51	14.29
C	153.76	88.67	583000	2.92E+06	11.88	19.97
C	137.21	86.88	583000	2.92E+06	4.66	19.97
E	106.87	61.30	583000	2.92E+06	21.67	19.97
E	95.84	59.99	583000	2.92E+06	14.51	19.97
E	134.45	66.40	583000	2.33E+06	22.63	25.02
D	137.21	86.88	583000	1.75E+06	1.74	33.31

- Values above double lines have % difference in cycles to failure less than 3.5%, while N_{spec} / N was less than 6%.
- Highlighted values have % difference in cycles to failure less than 3.5%, while Nspec / N was greater than 6%.

Table 6.5.12 (Continued) - % of N_{spec} / N in Acending Order

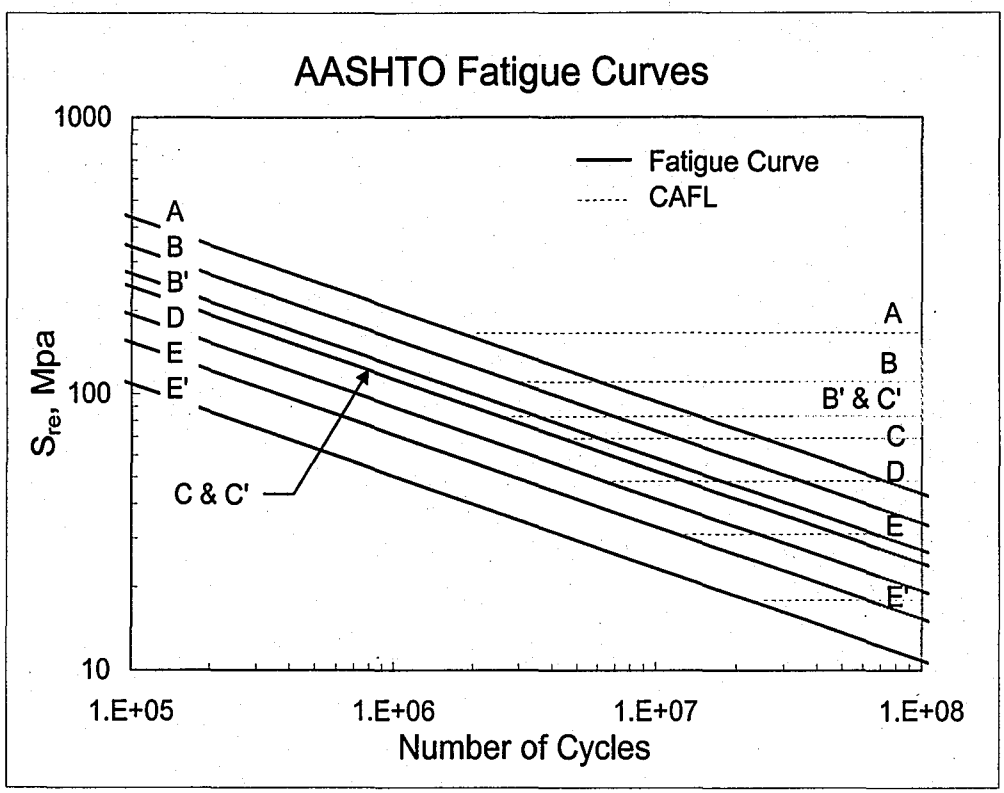

Figure 2.2.1 - Fatigue Life, AASHTO Specification

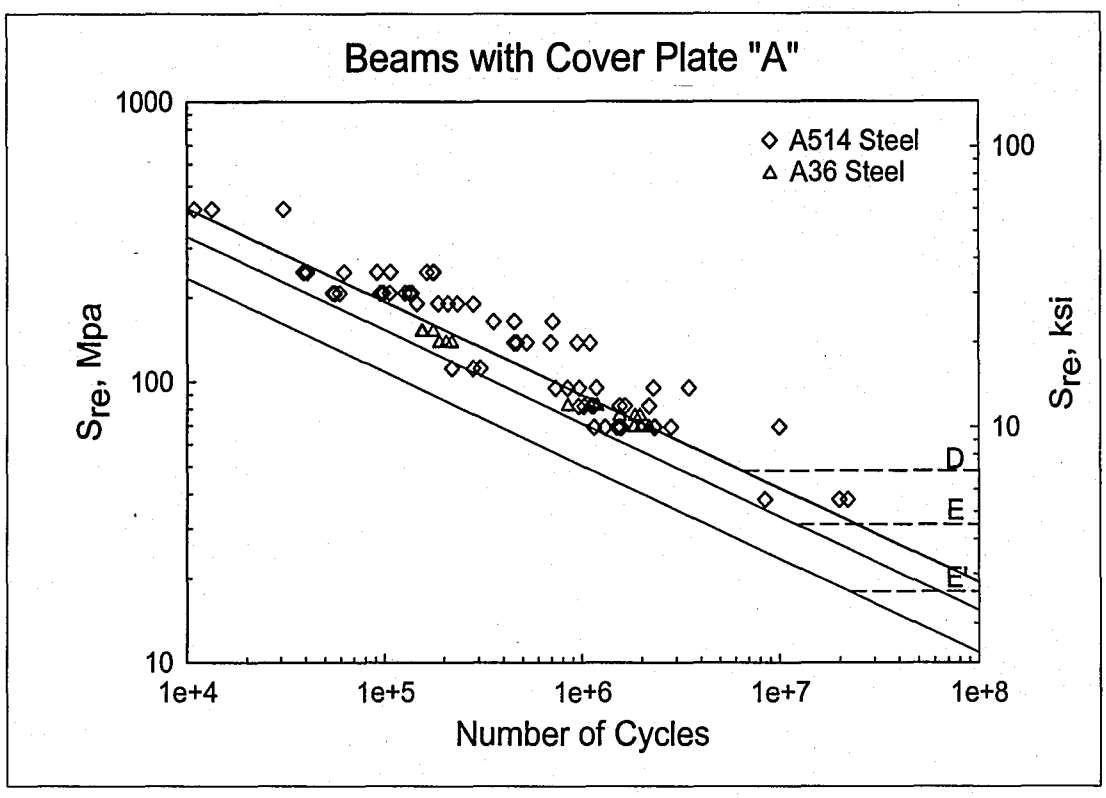

Figure 3.1.1 - Variable Amplitude Fatigue Test Data
from NCHRP Report #188

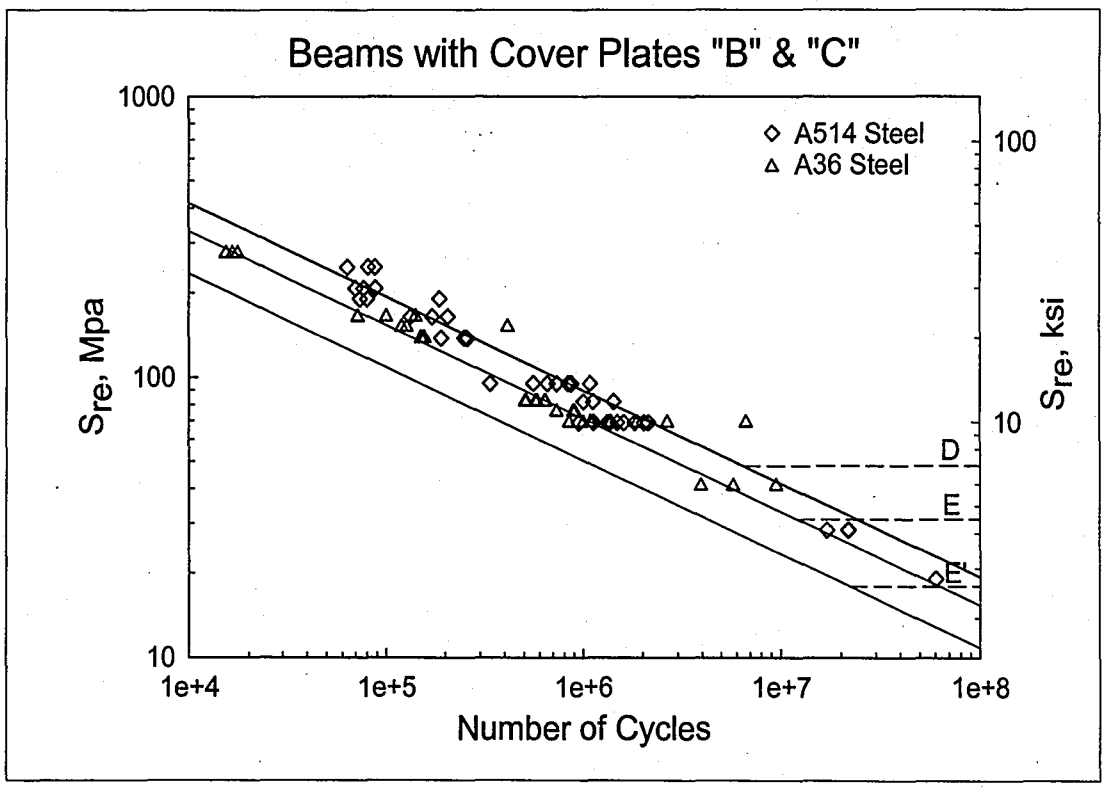

Figure 3.1.2 - Variable Amplitude Fatigue Test Data
from NCHRP Report #188

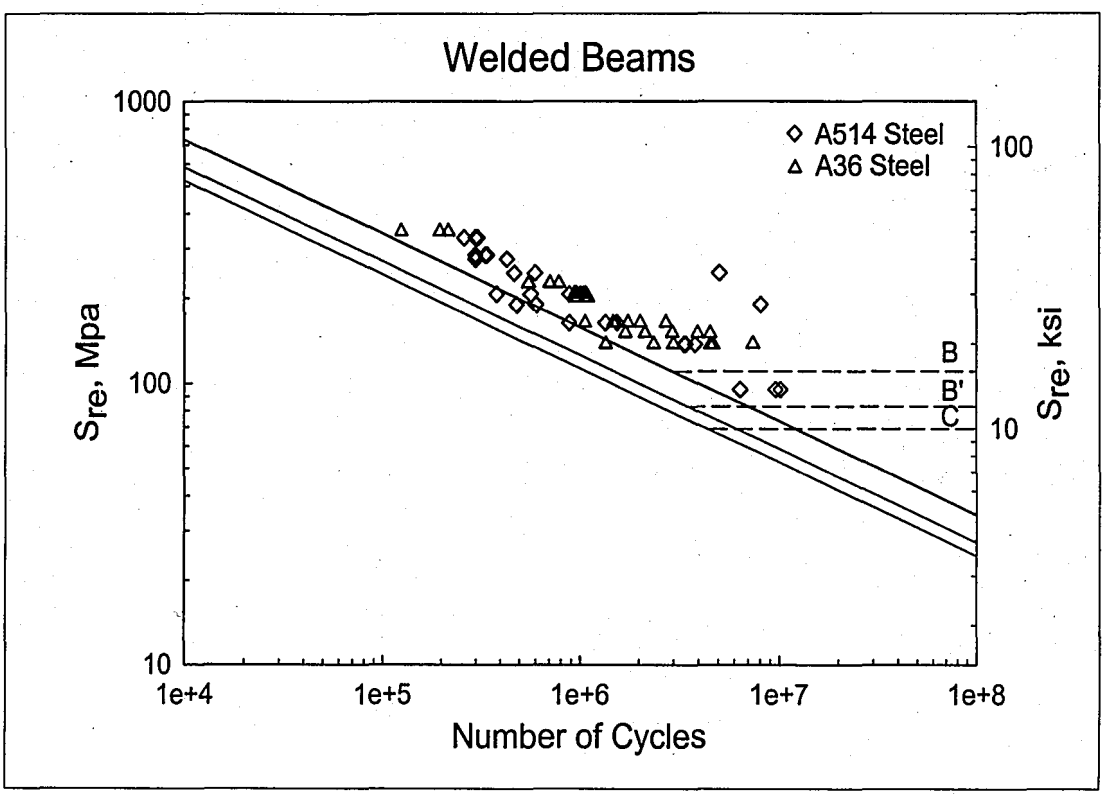

Figure 3.1.3 - Variable Amplitude Fatigue Test Data
from NCHRP Report #188

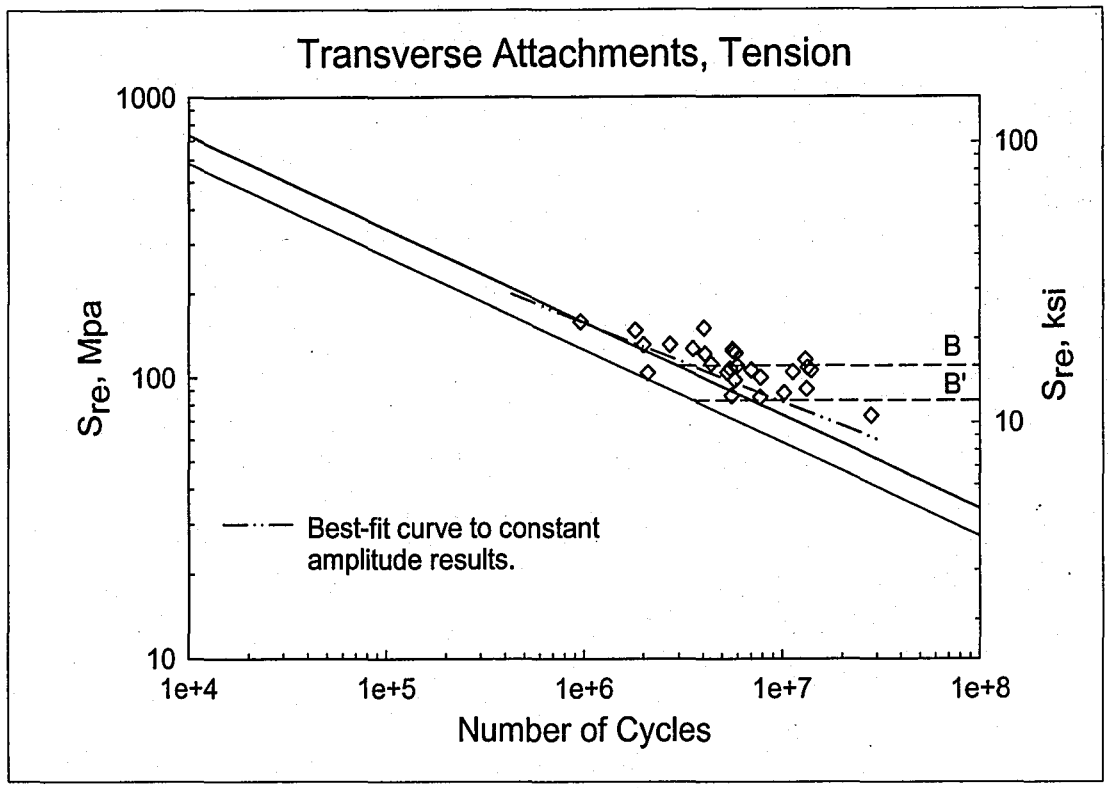

Figure 3.1.4 - Variable Amplitude Fatigue Test Data from Agersov & Nielson

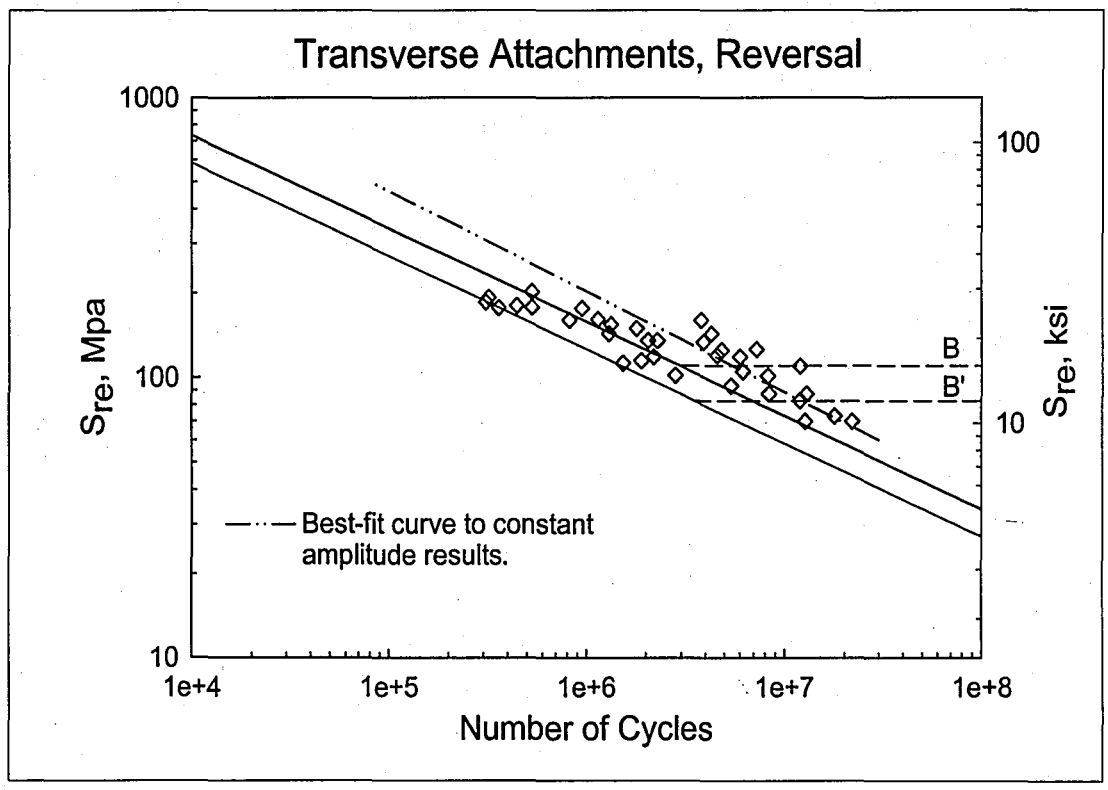

Figure 3.1.5 - Variable Amplitude Fatigue Data from Agersov & Nielson

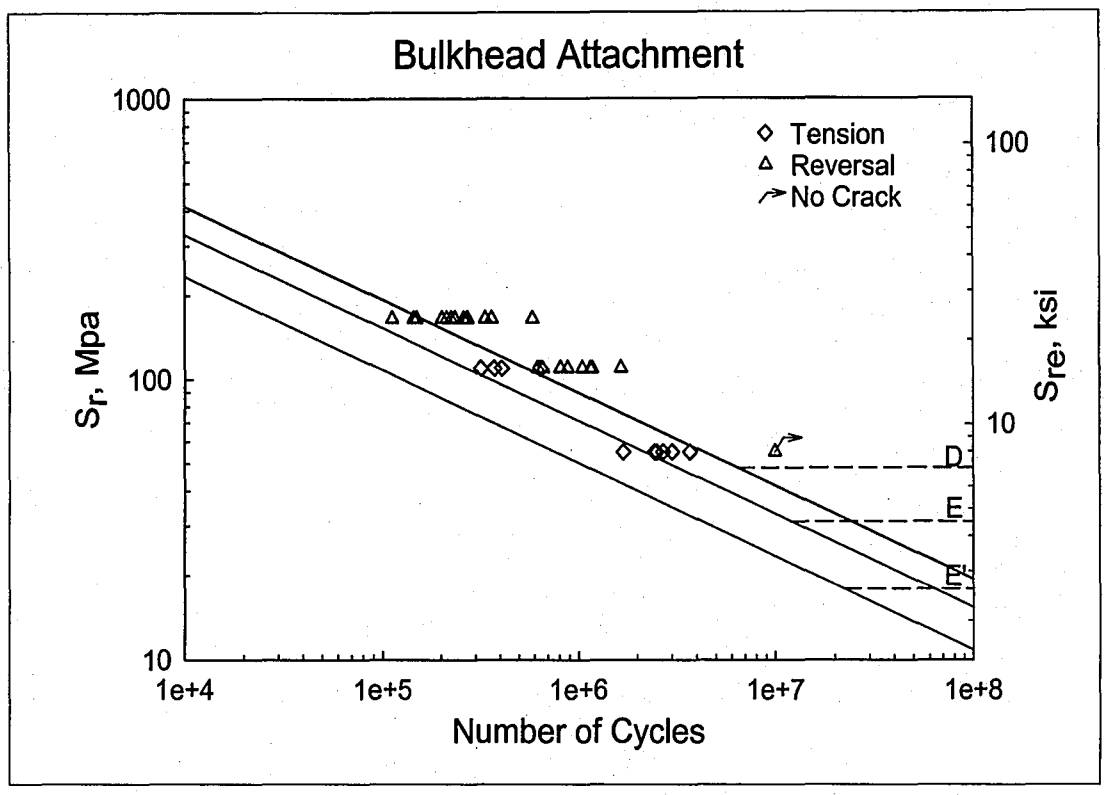

Figure 3.2.1 - Constant Amplitude Fatigue Data for AL-6XN Stainless Steel, First Observation of Cracking

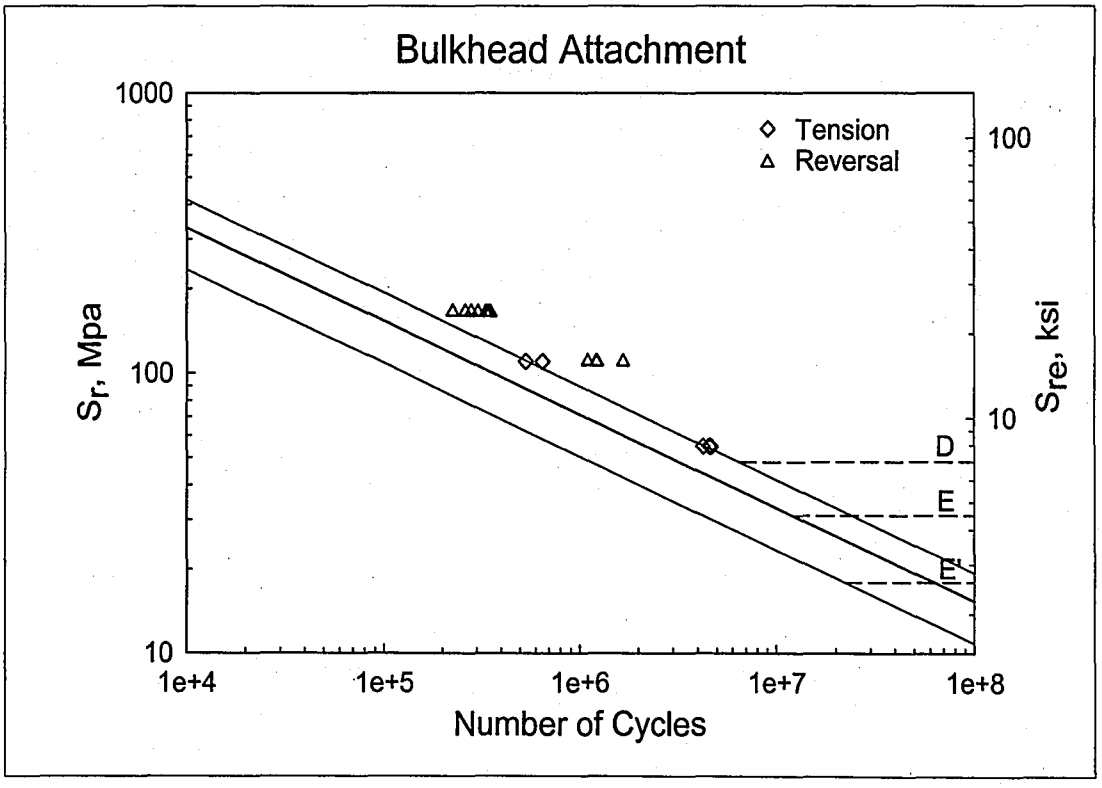

Figure 3.2.2 - Constant Amplitude Fatigue Data for AL-6XN Stainless Steel, Through-Flange Cracking

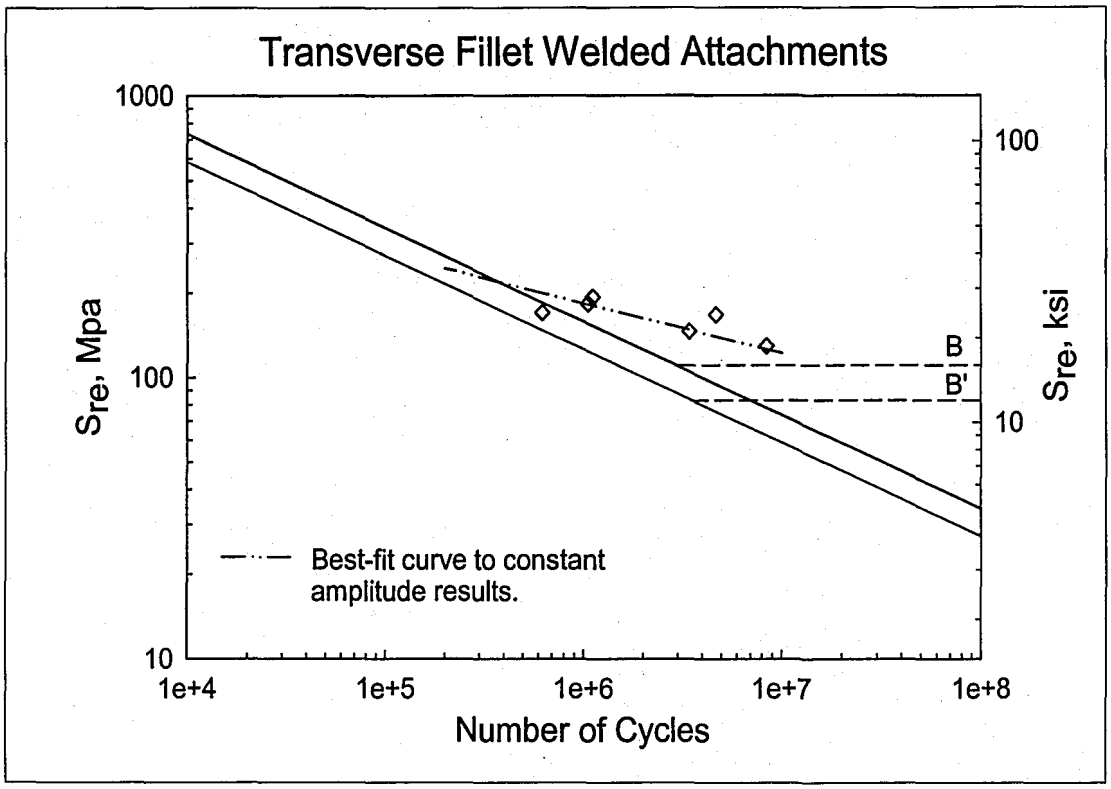

Figure 3.3.1 - Variable Amplitude Fatigue Test Data for Austenitic Stainless Steel

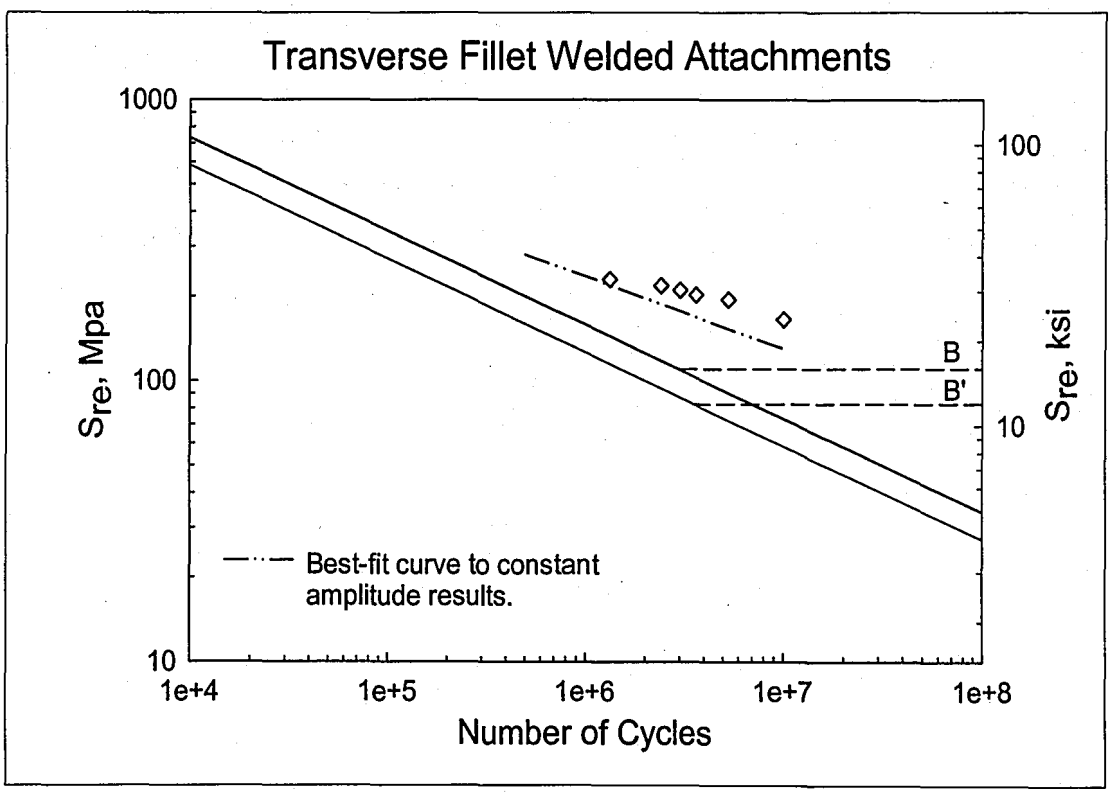

Figure 3.3.2 - Variable Amplitude Fatigue Data for Duplex Stainless Steel

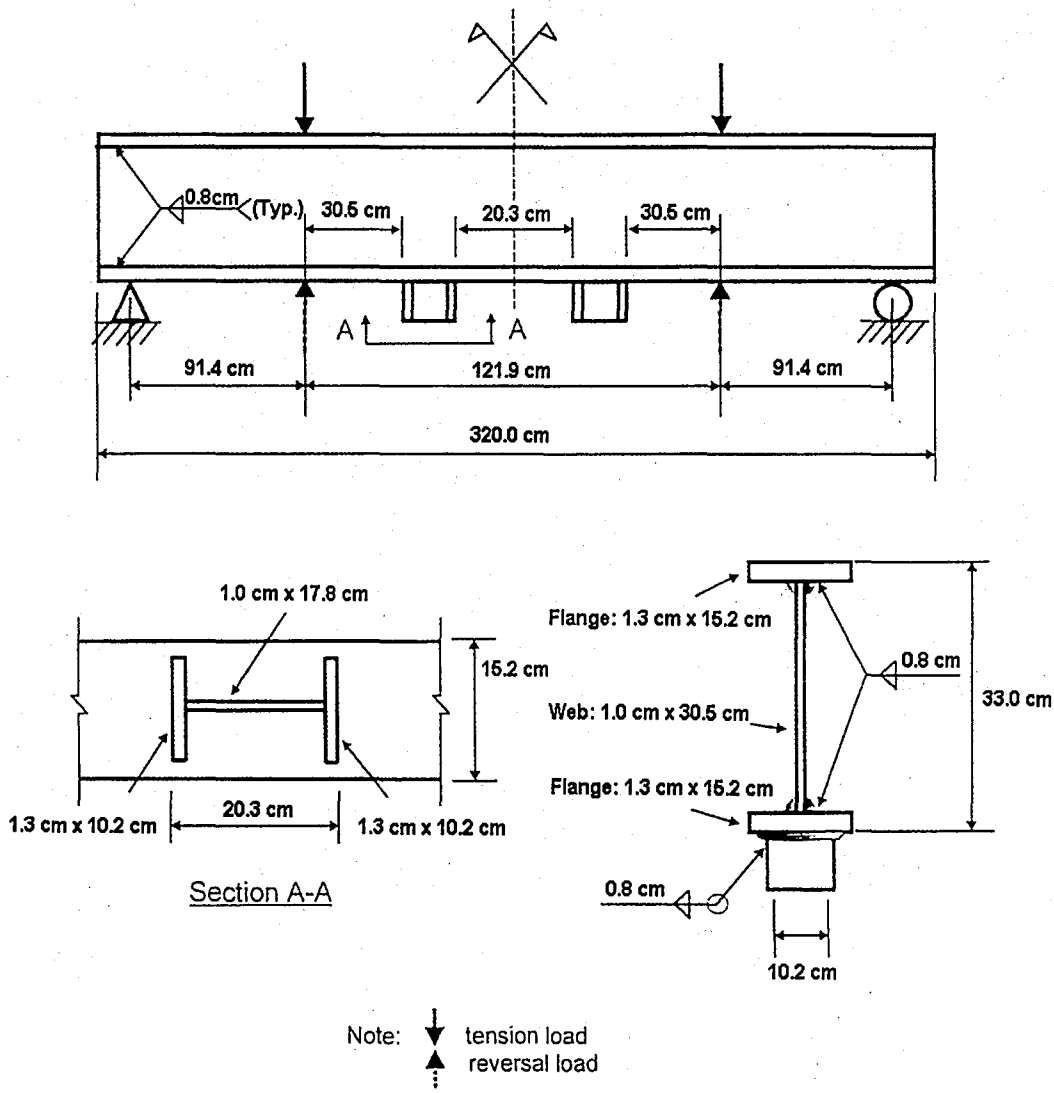

Figure 4.1.1 – Schematic of Simulated Bulkhead Attachment Specimens (6).

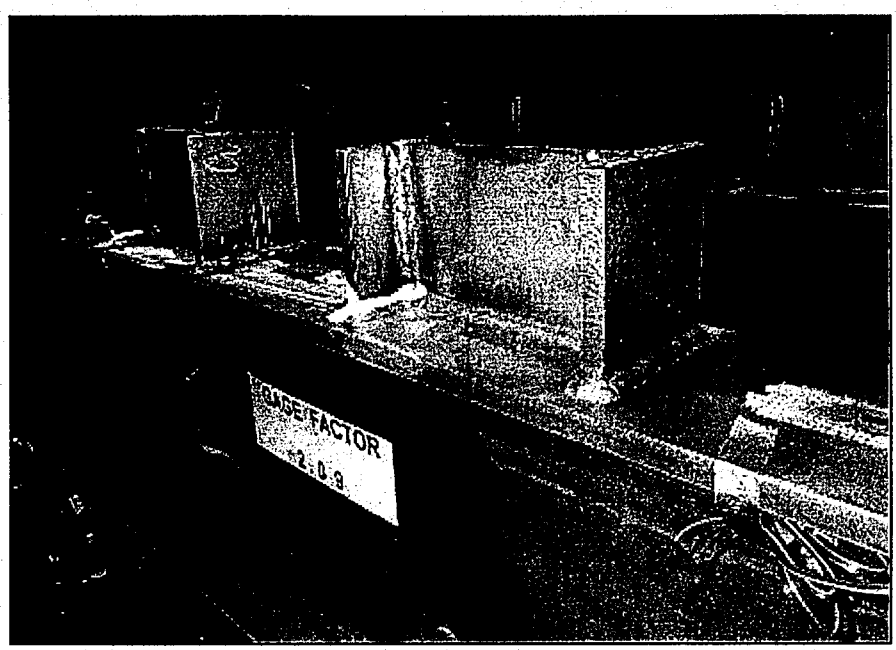

Figure 4.1.2 - AL-6XN Bulkhead Attachments Fillet Welded to the Flange of the Test Specimen

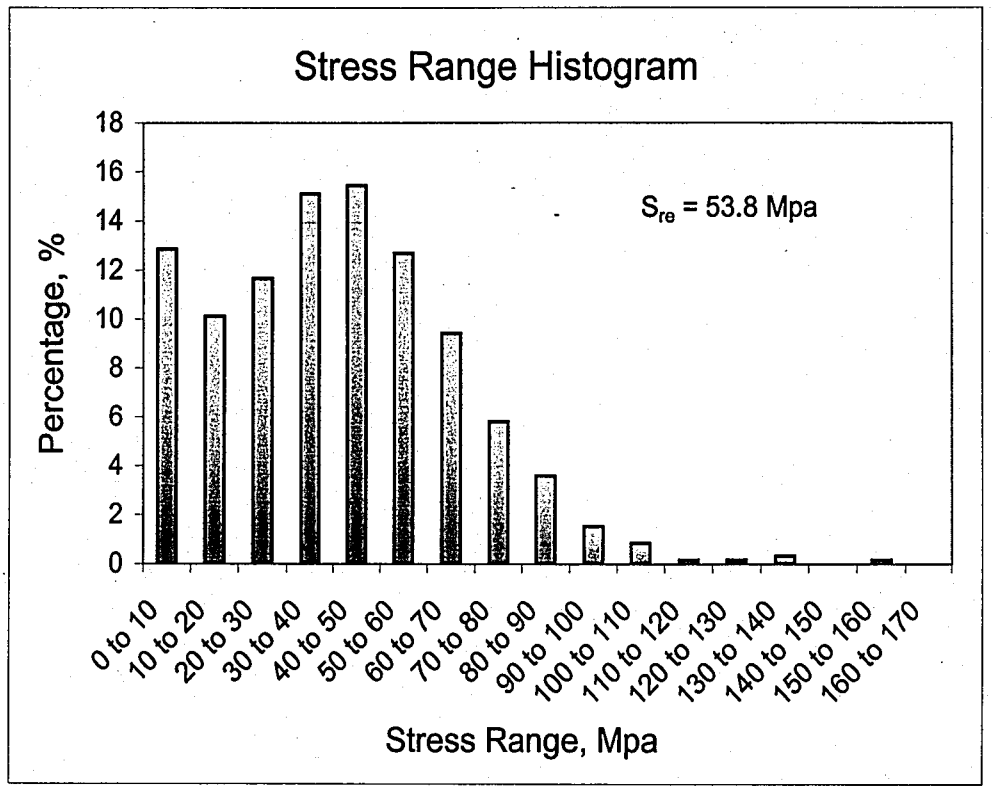

Figure 4.3.1 - Stress Range Histogram

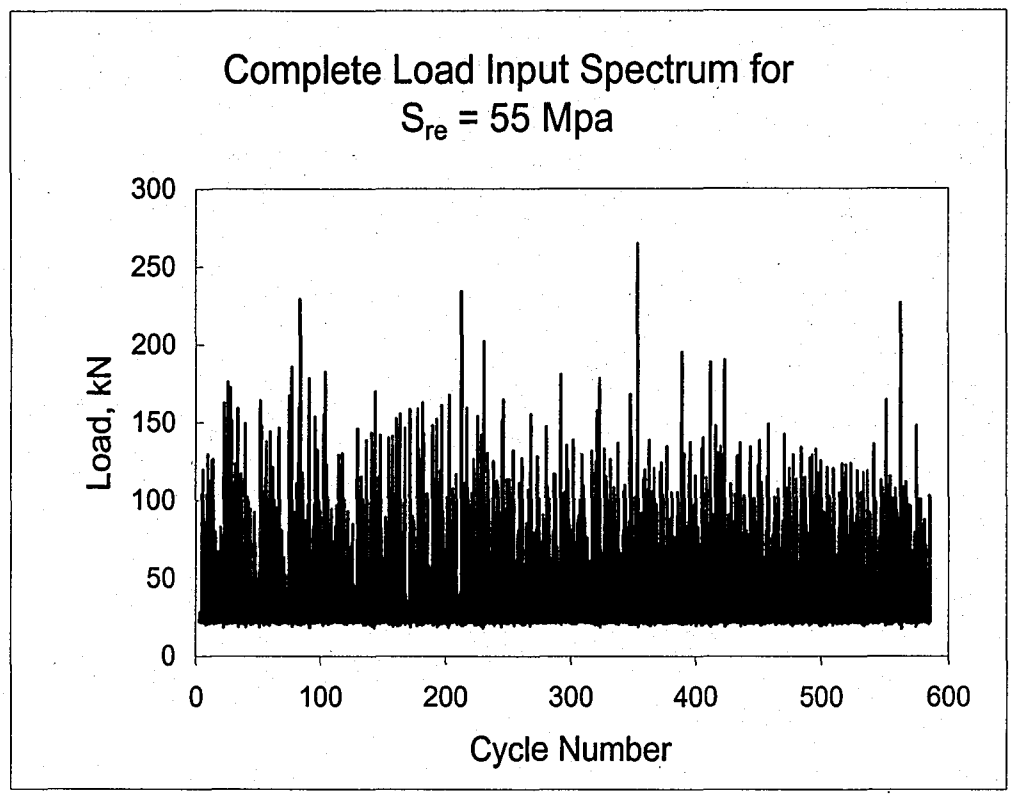

Figure 4.3.2 - Complete Random Load Input Spectrum for S_{re} = 55 Mpa

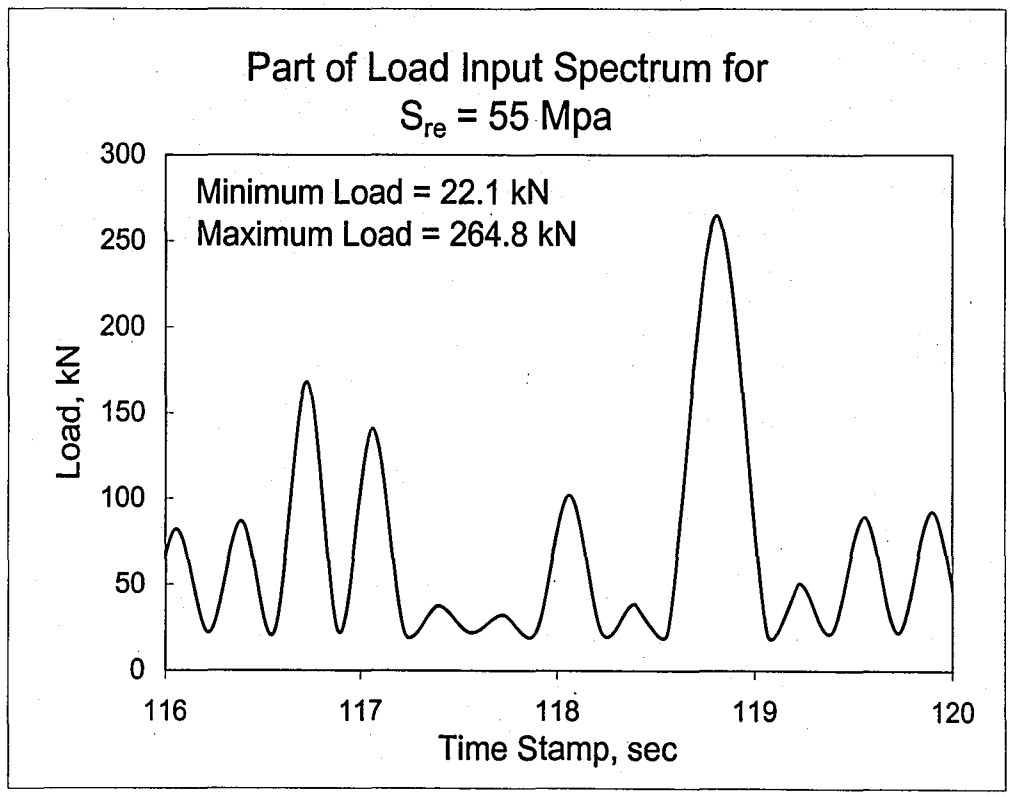

Figure 4.3.3 - Part of Load Input Spectrum for S_{re} = 55 Mpa

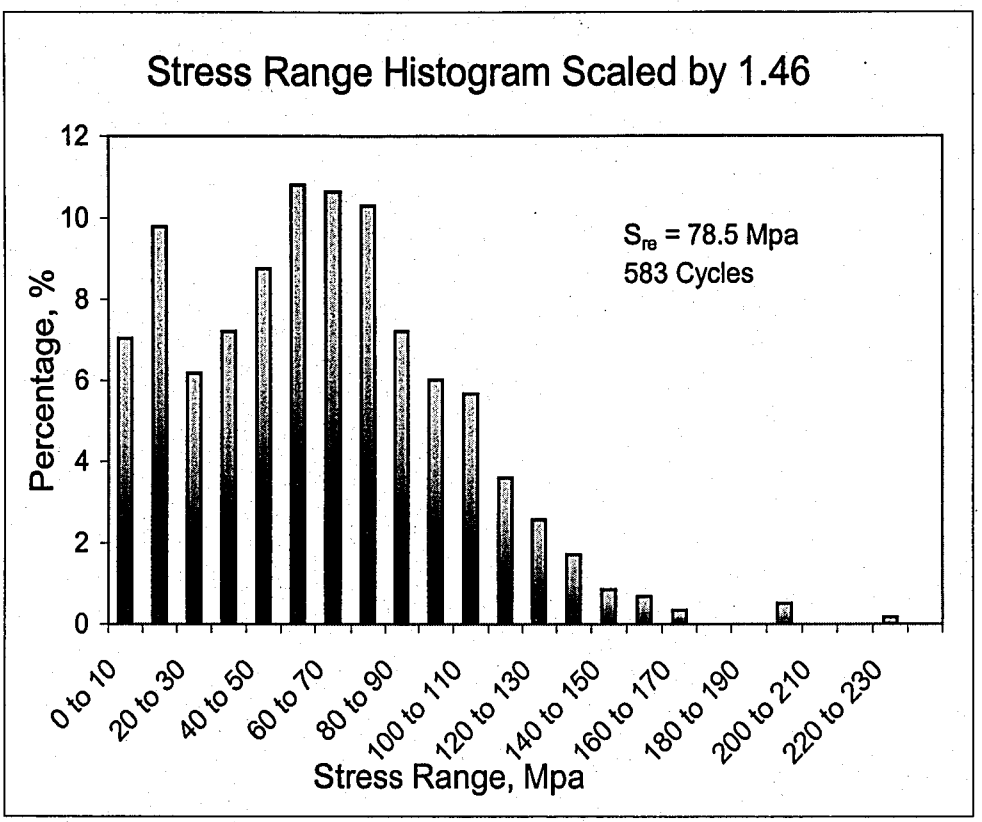

Figure 4.3.4 - Stress Range Histogram Scaled by 1.46

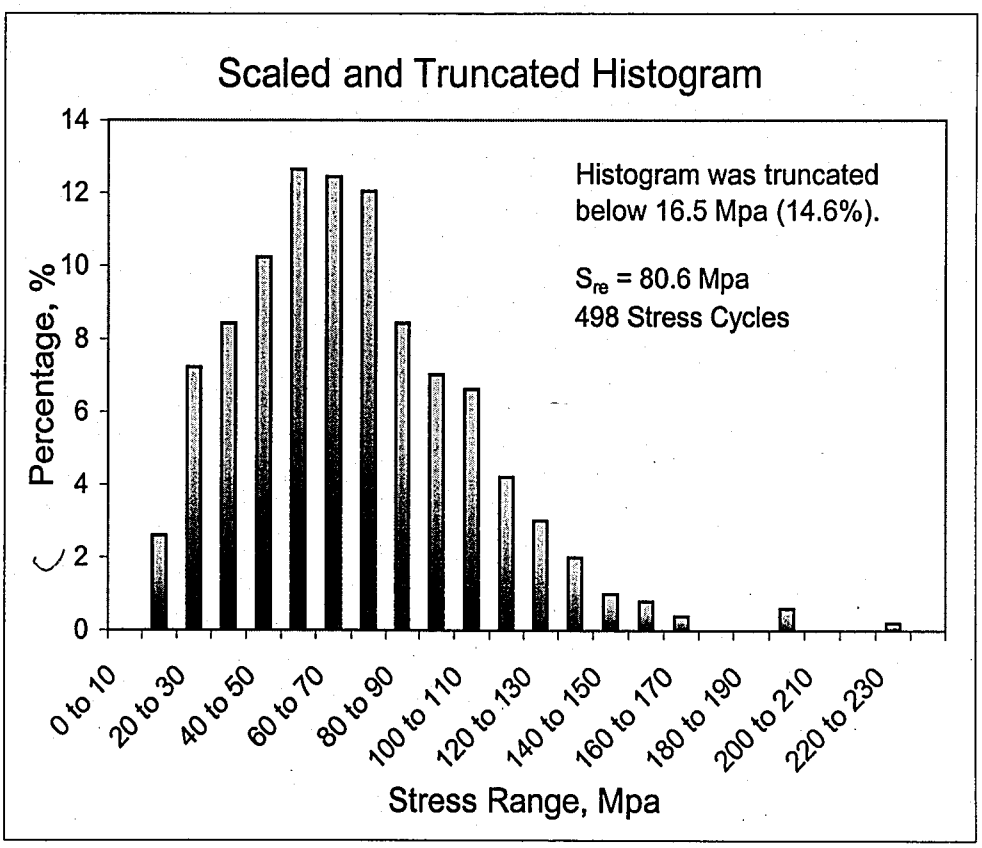

Figure 4.3.5 - Stress Range Histogram Scaled by 1.46 and Truncated

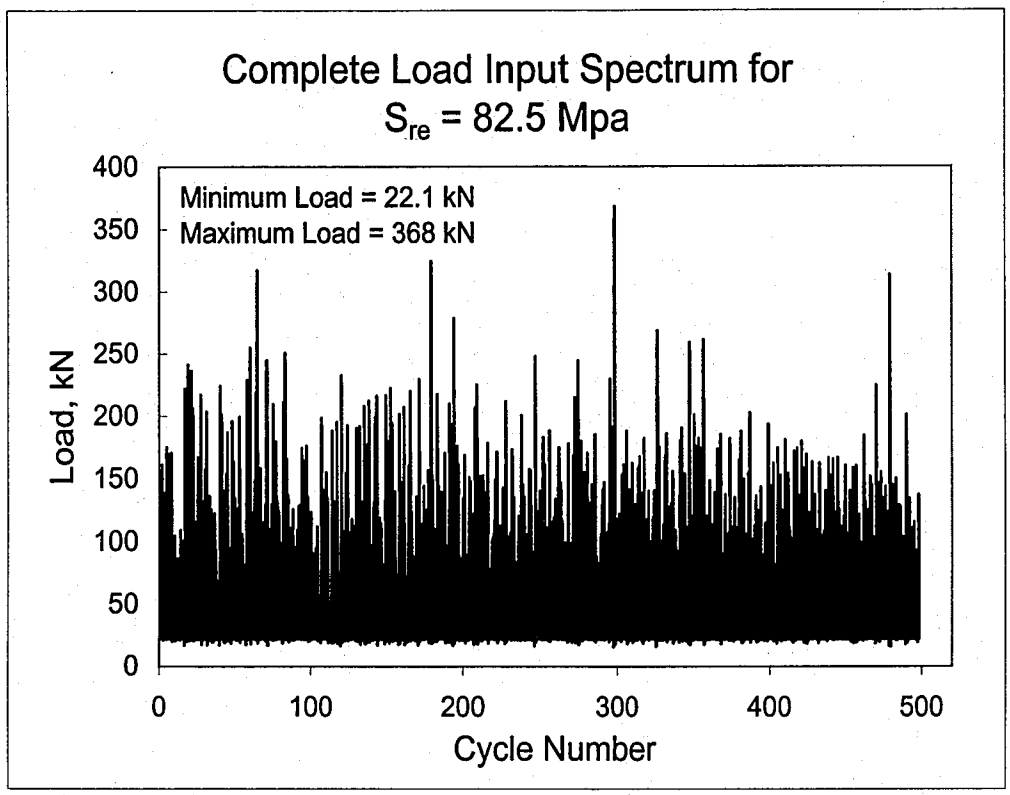

Figure 4.3.6 - Complete Random Load Input Spectrum for S_{re} = 82.5 Mpa

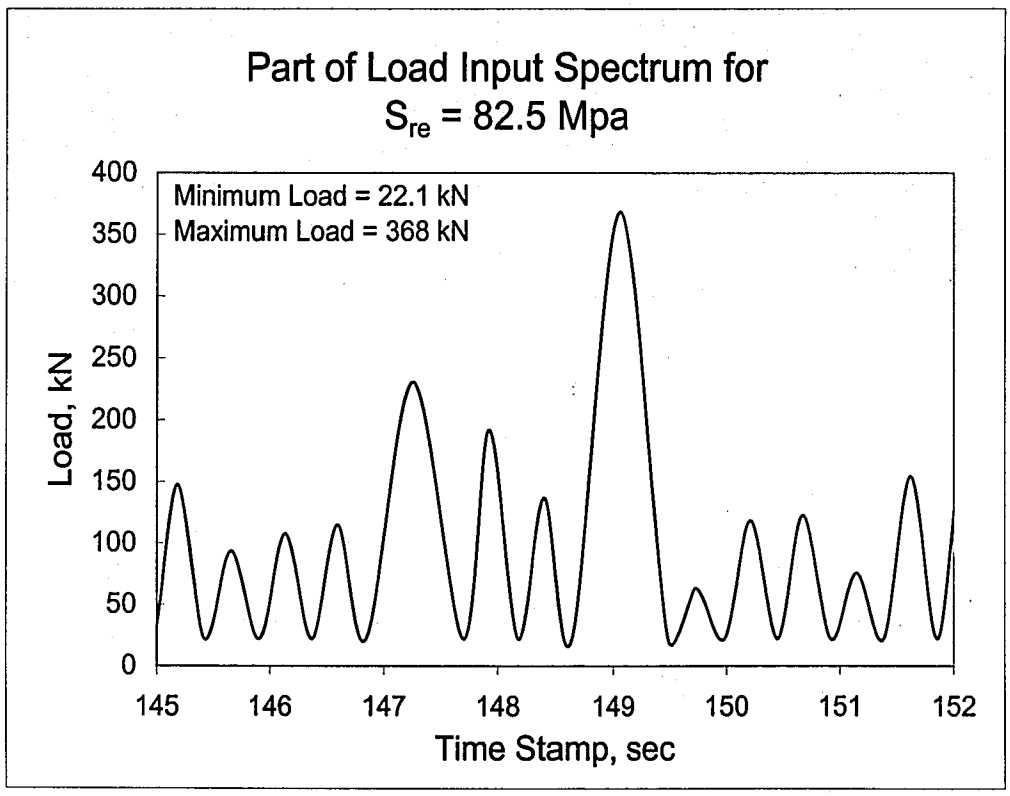

Figure 4.3.7 - Partial Load Input Spectrum for S_{re} = 82.5 Mpa

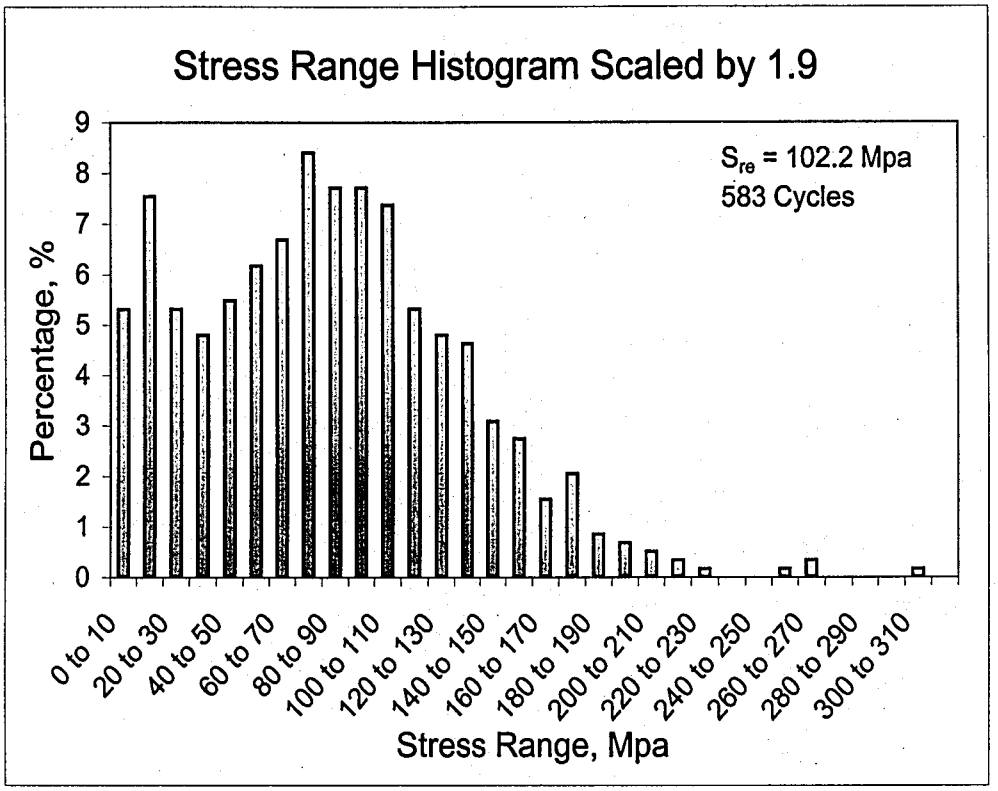

Figure 4.3.8 - Stress Range Histogram Scaled by 1.9

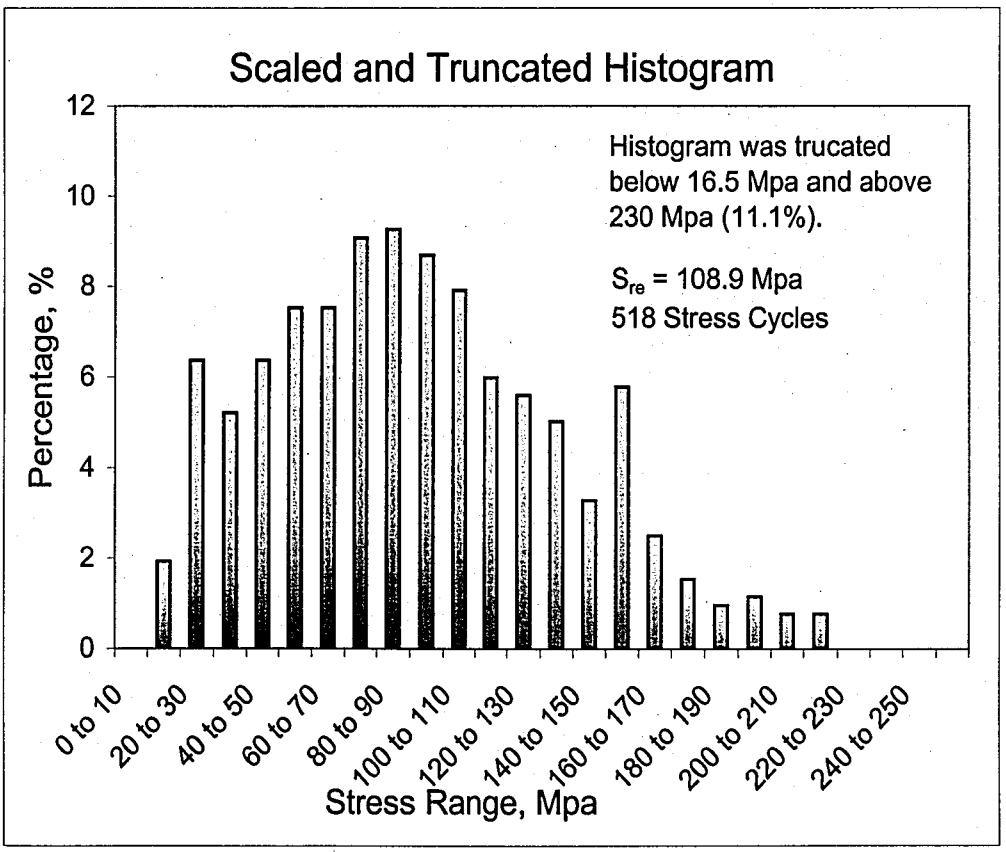

Figure 4.3.9 - Stress Range Histogram by 1.9 and Truncated

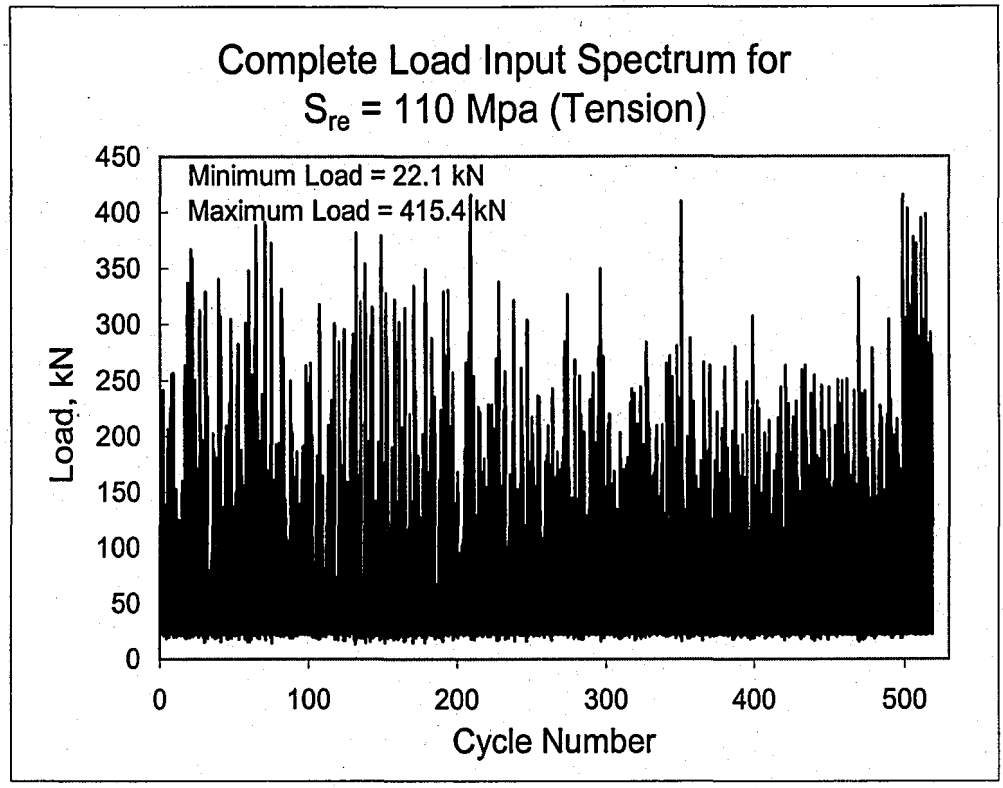

Figure 4.3.10 - Complete Random Load Input Spectrum for S_{re} = 110 Mpa, Tension

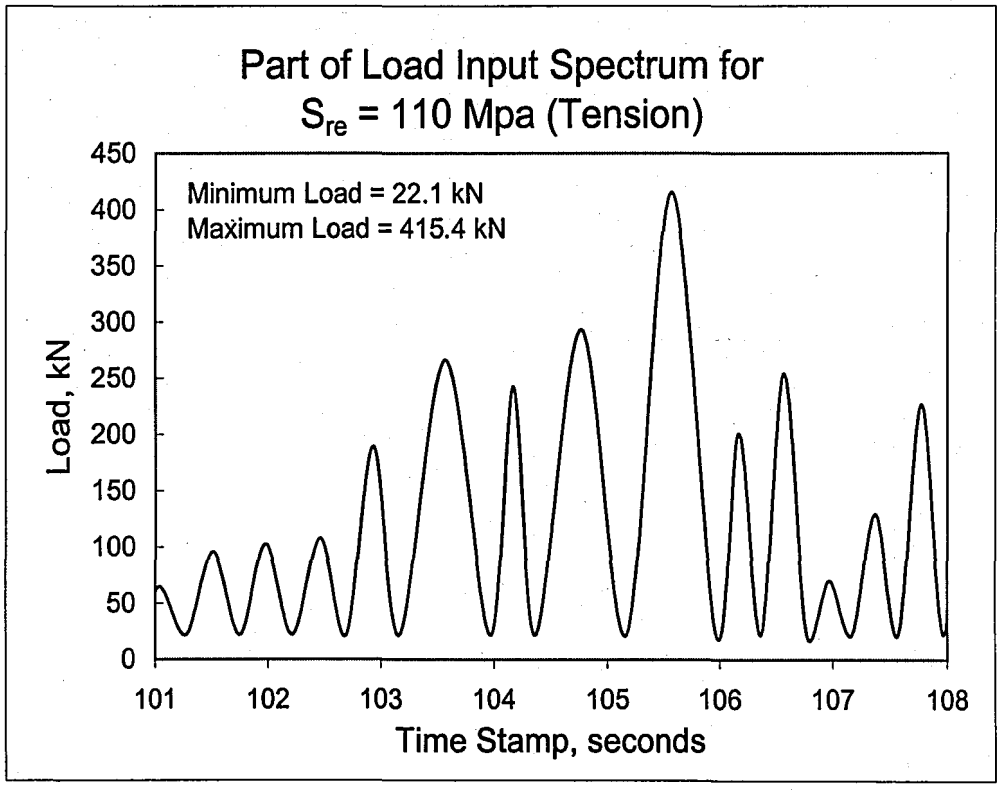

Figure 4.3.11 - Part of Load Input Spectrum for S_{re} = 110 Mpa, Tension

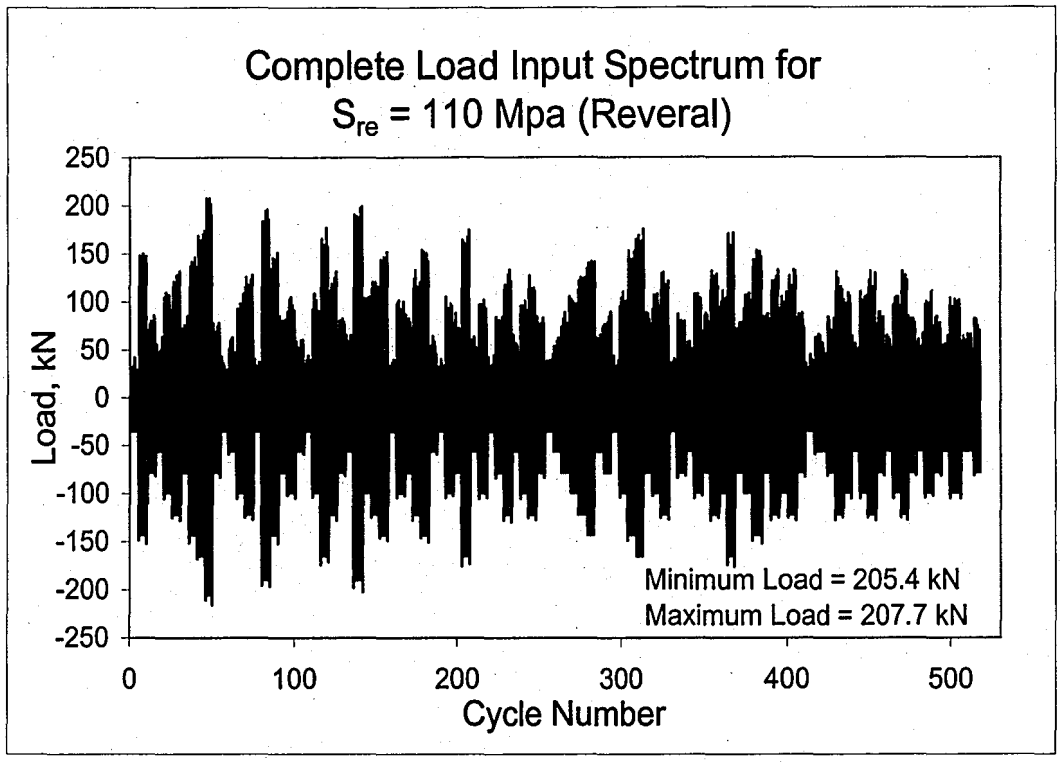

Figure 4.3.12 - Complete Load Input Spectrum for S_{re} = 110 Mpa, Reversal

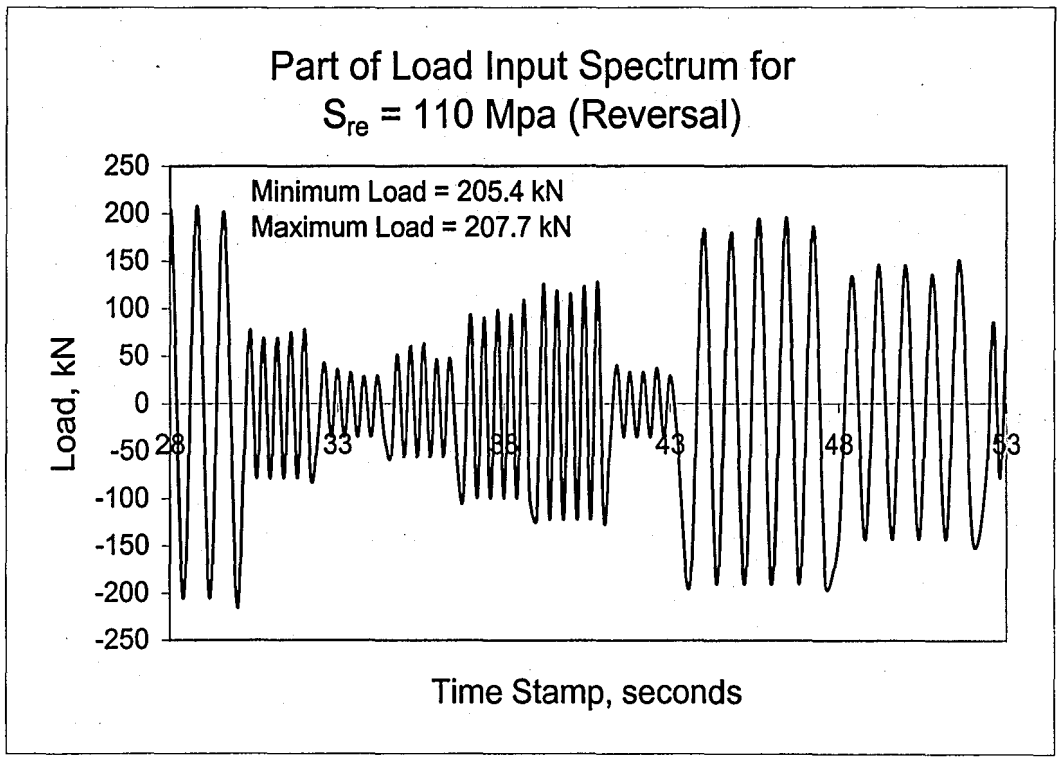

Figure 4.3.13 - Part of Load Input Spectrum for S_{re} = 110 Mpa, Reversal

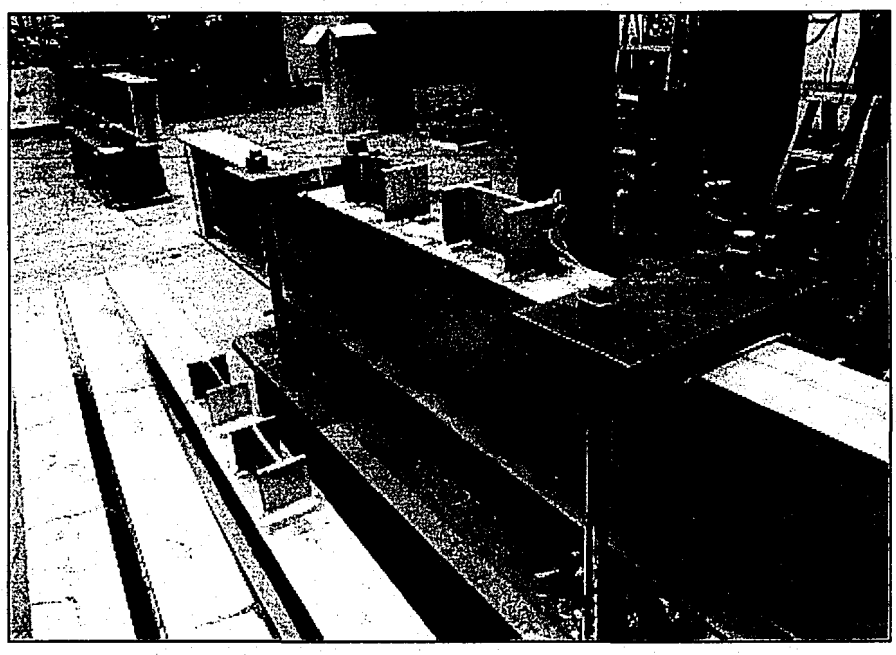

Figure 4.4.1 - Location of Bulkhead Attachments in Constant Moment Region

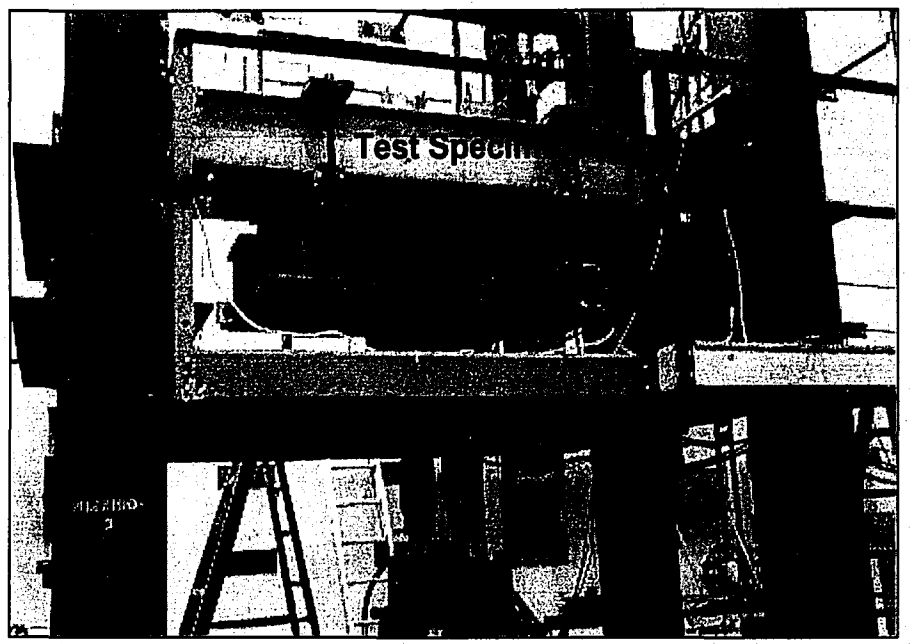

Figure 4.4.2 - Test Frame Located in ATLSS Laboratory

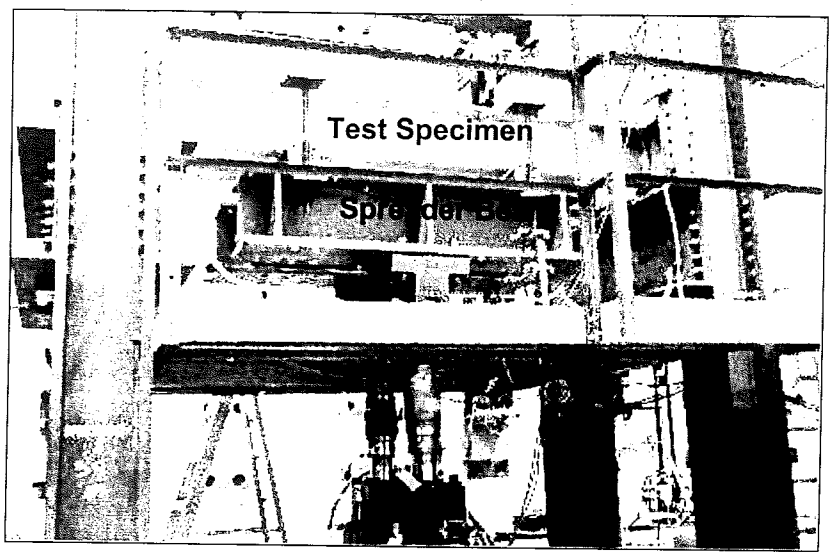

Figure 4.4.2 - Test Frame Located in ATLSS Laboratory

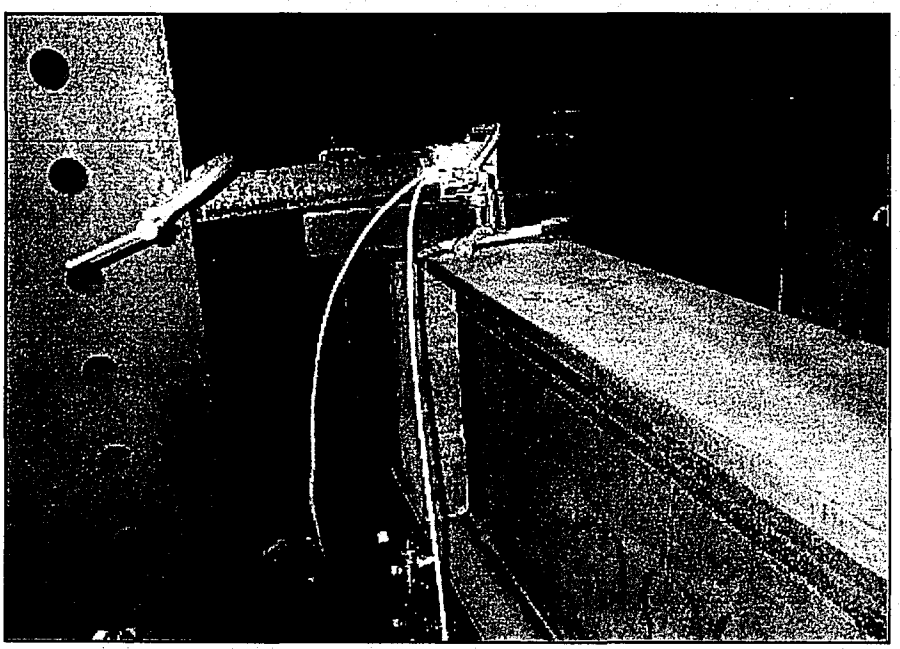

Figure 4.4.3 - Mechanical Limit Switch Located at the End of the Test Specimen

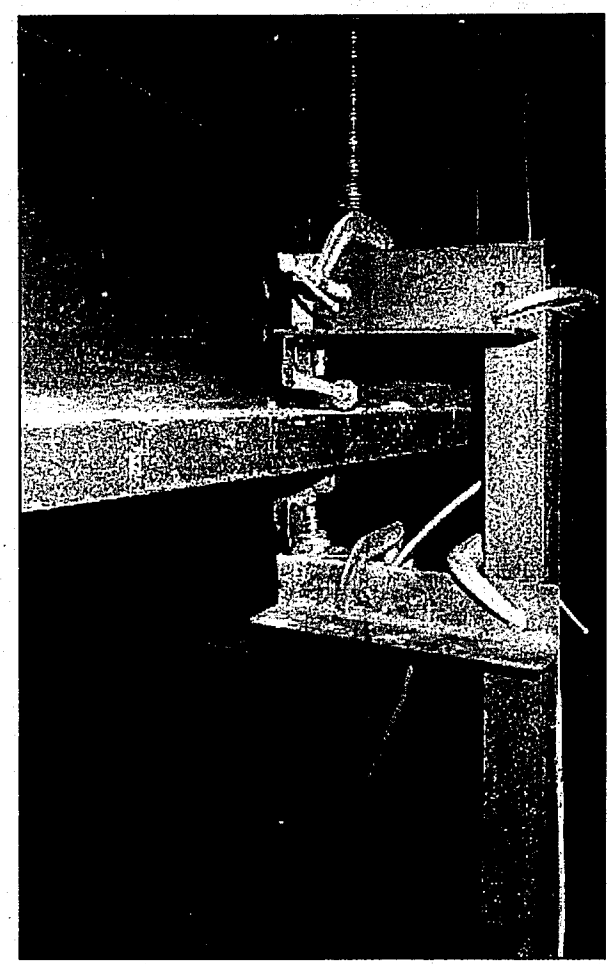

Figure 4.4.4 - Mechanical Limit Switch Located Around the Spreader Beam

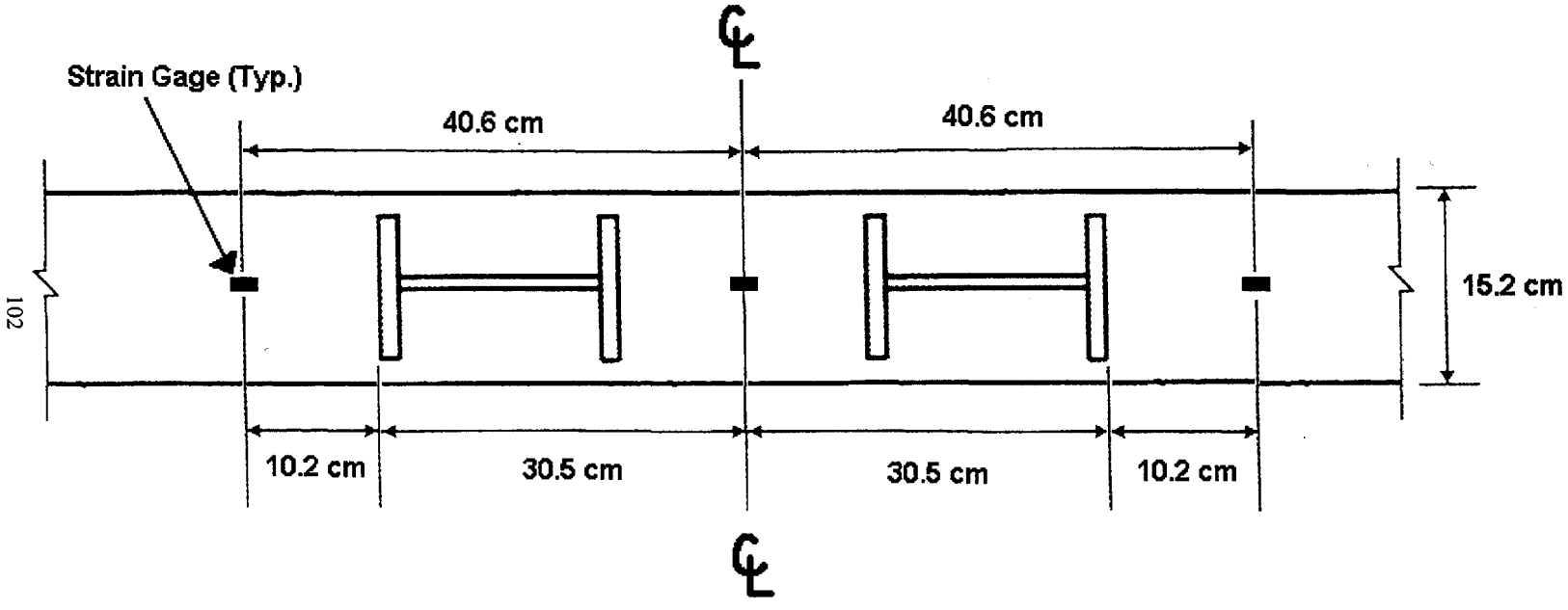

Figure 4.4.5 – Strain Gage Location

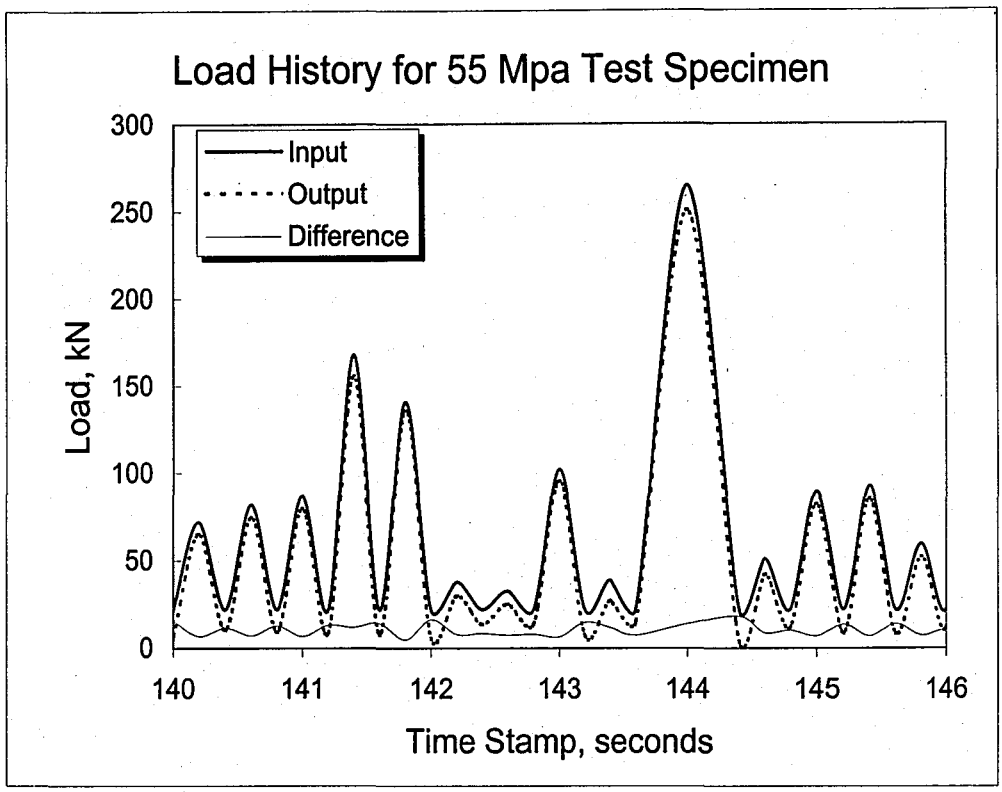

Figure 5.1.1 - Partial Loading History for 55 Mpa Test Specimen

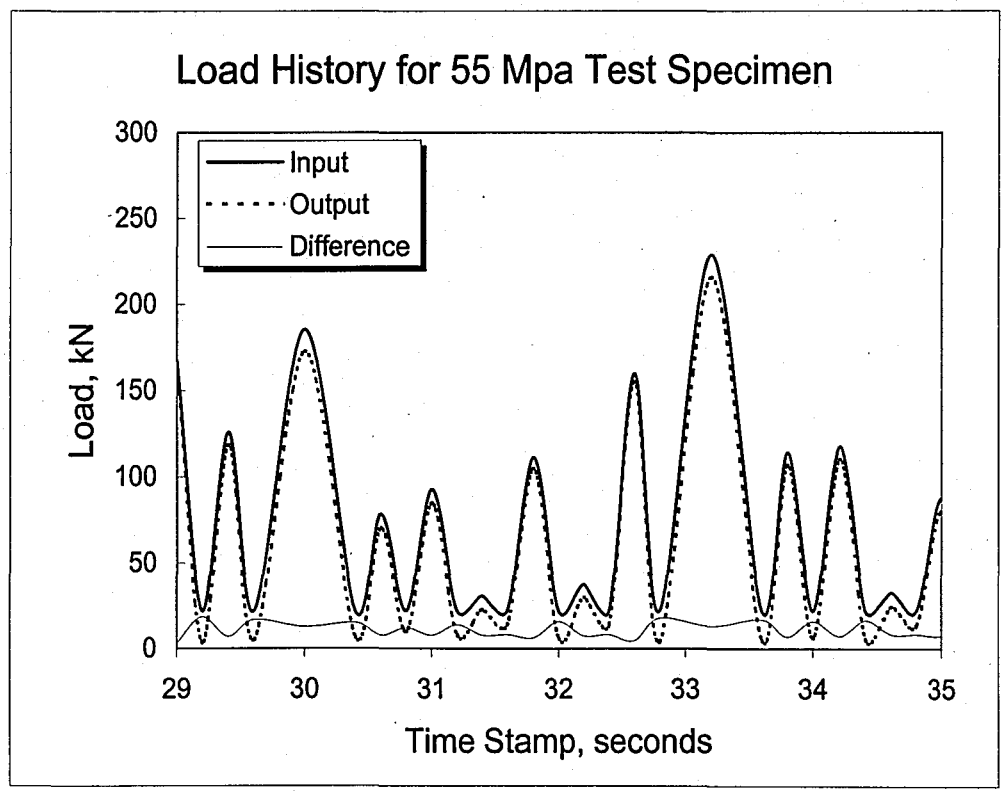

Figure 5.1.2 - Partial Loading History for 55 Mpa Test Specimen

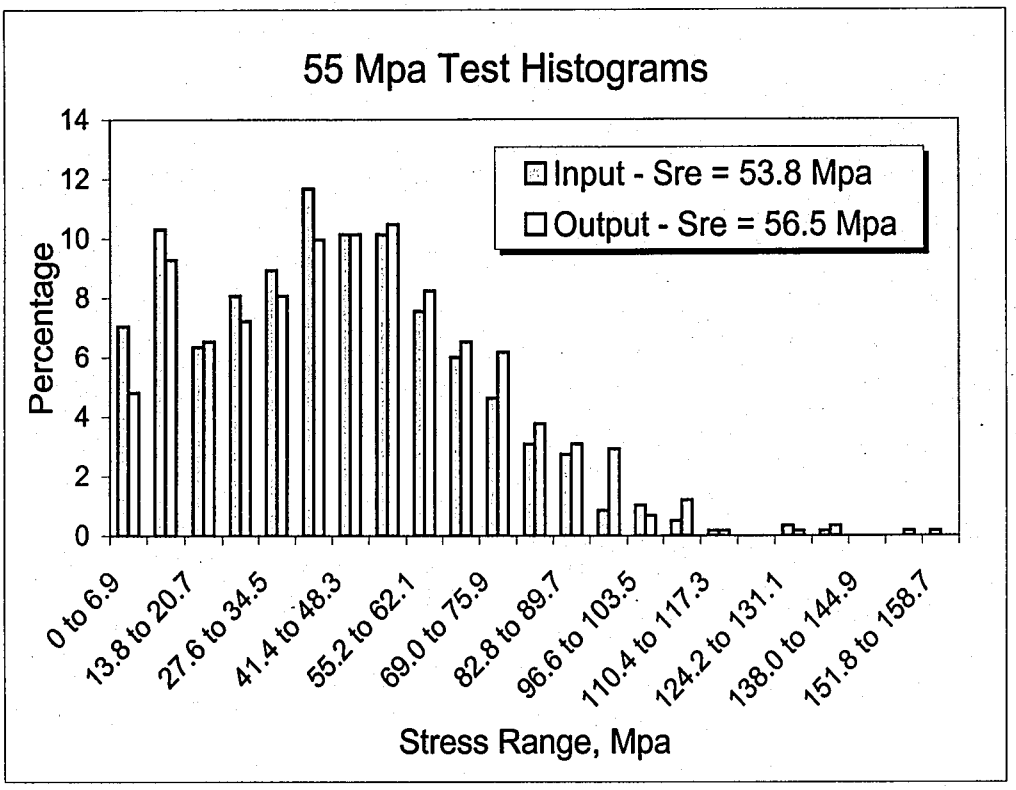

Figure 5.1.3 - Comparison of Control Input and Feedback Output Stress Range Histograms

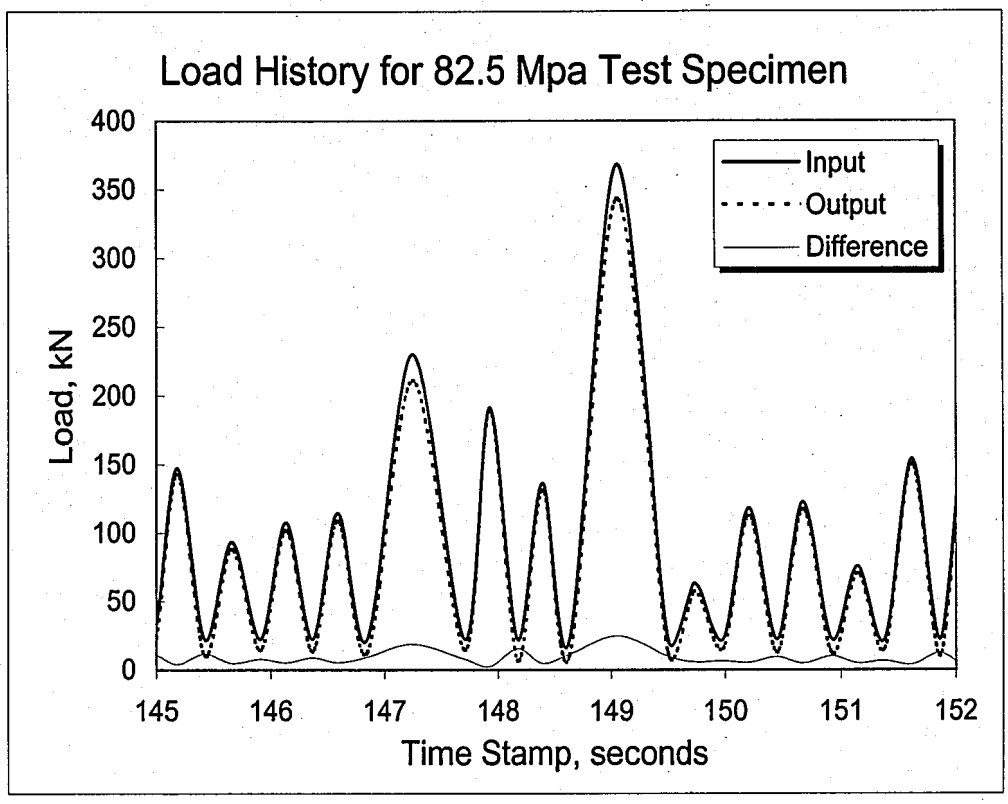

Figure 5.1.4 - Partial Loading History for 82.5 Mpa Test Specimen

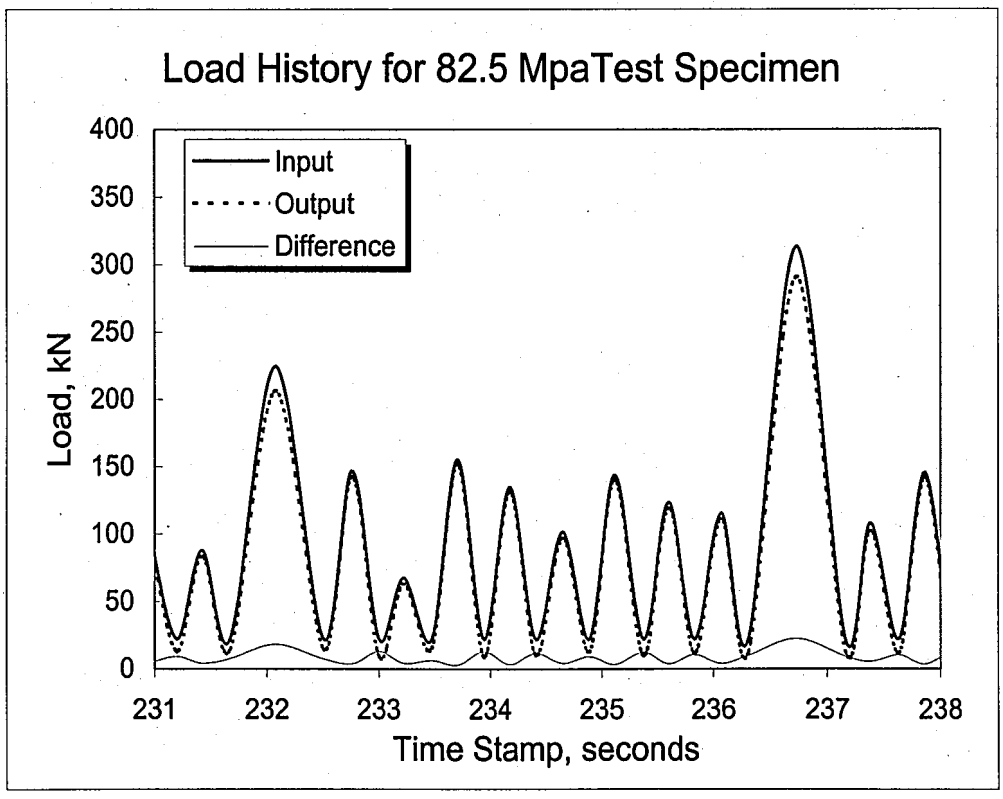

Figure 5.1.5 - Partial Loading History for 82.5 Mpa Test Specimen

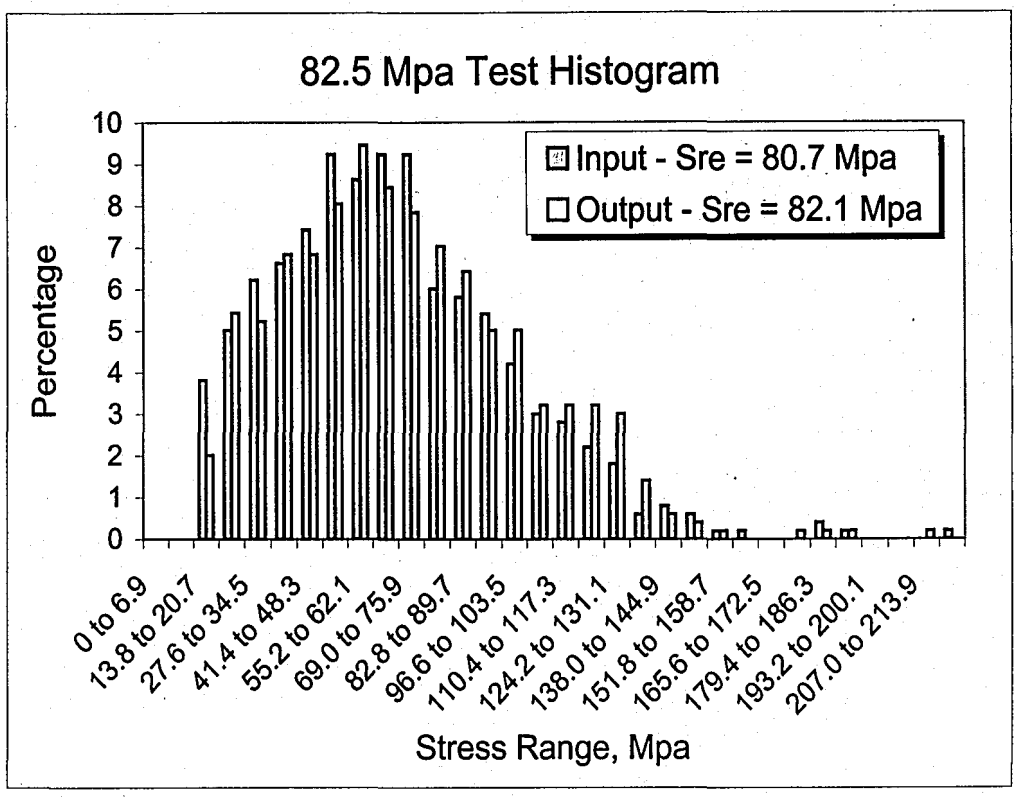

Figure 5.1.6 - Comparison of Control Input and Feedback Output Stress Range Histograms

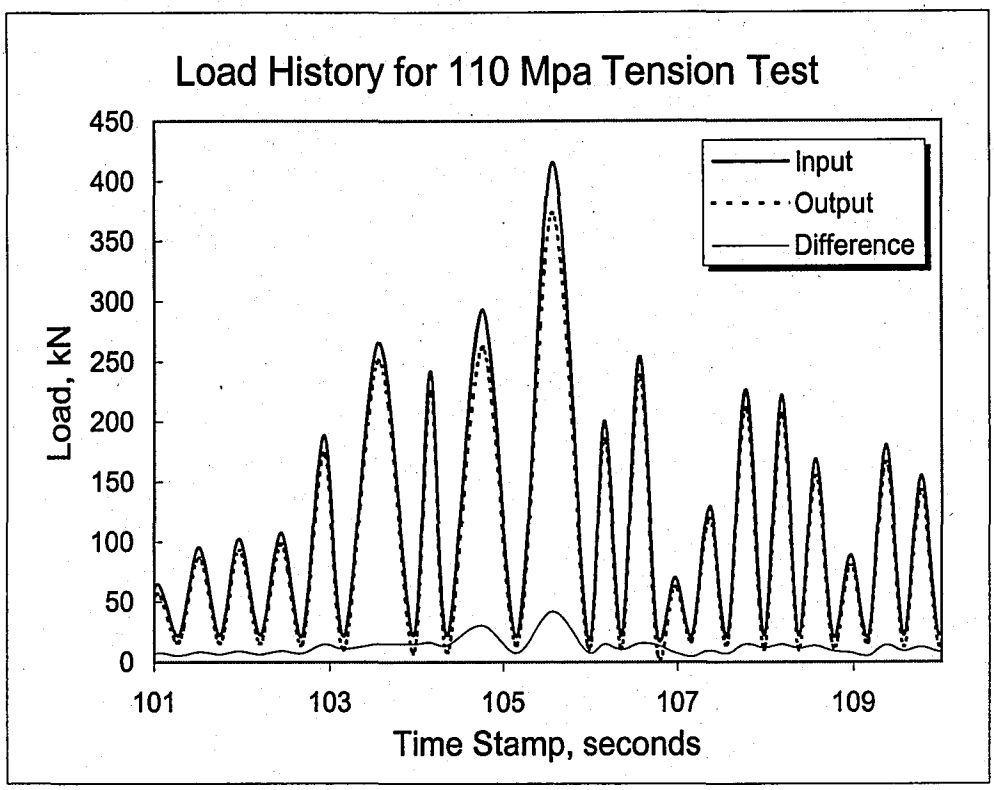

Figure 5.1.7 - Partial Loading History for 110 Mpa Tension Specimen

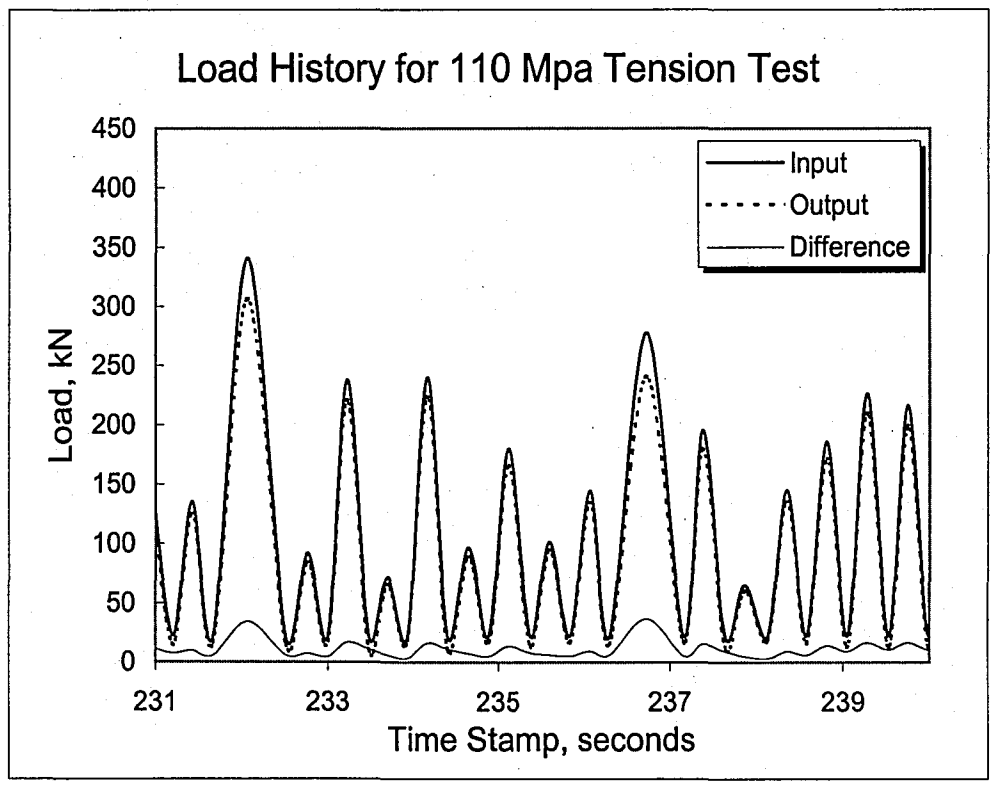

Figure 5.1.8 - Partial Loading History for 110 Mpa Tension Specimen

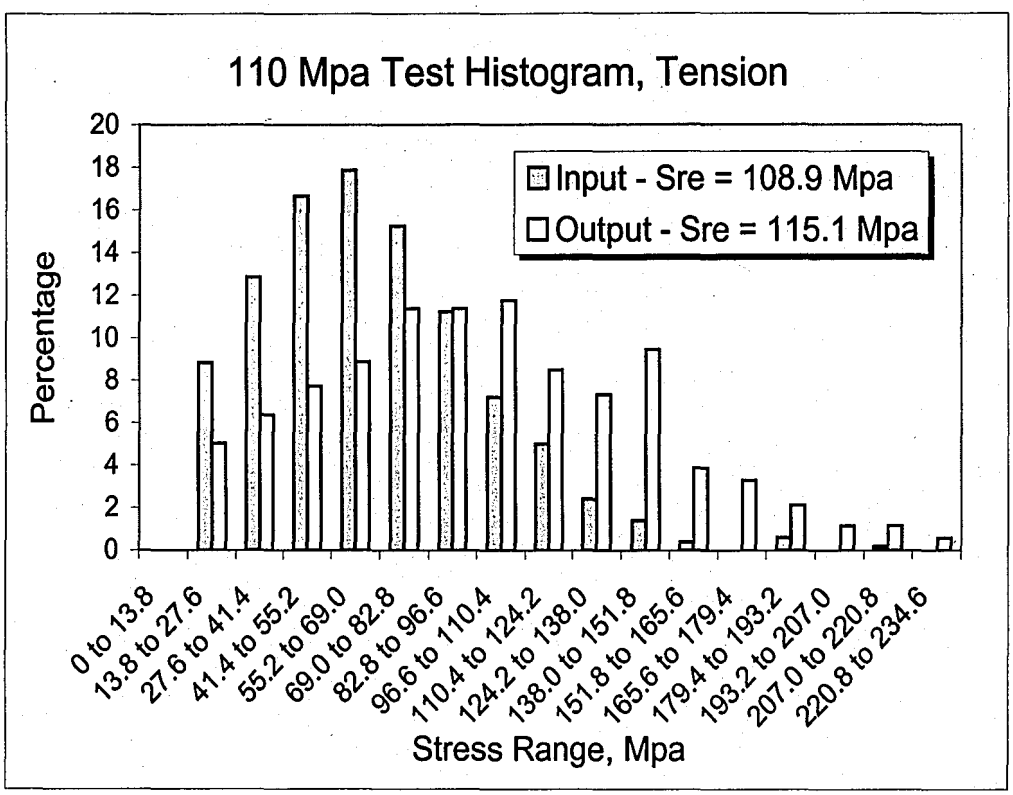

Figure 5.1.9 - Comparison of Control Input and Feedback Output Stress Range Histograms

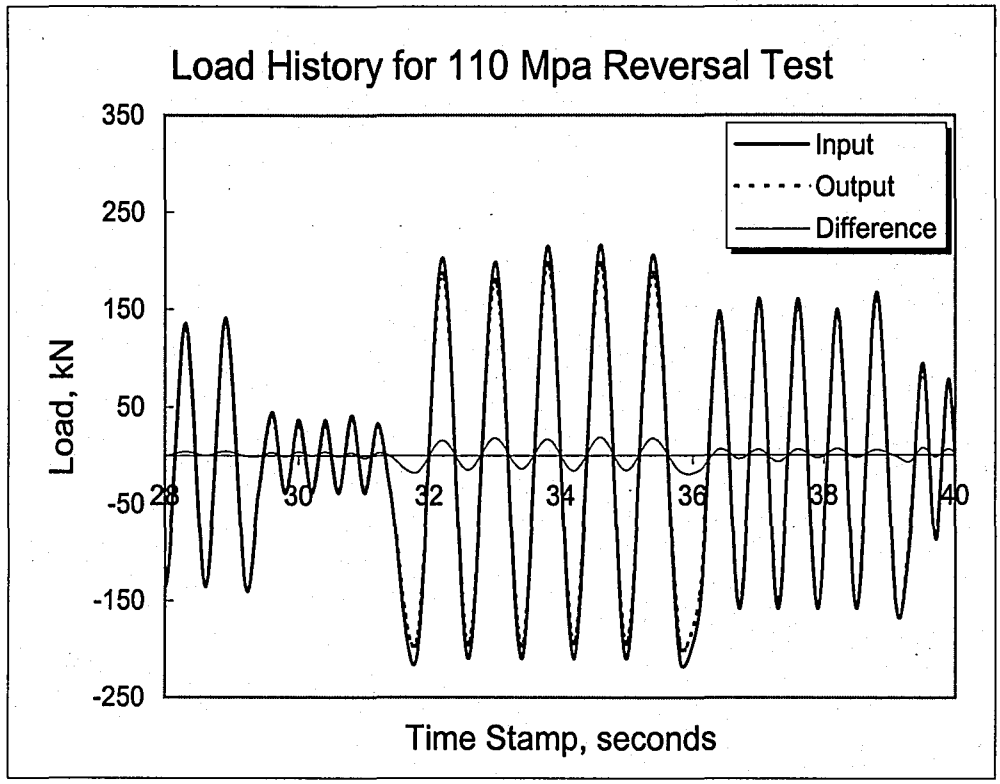

Figure 5.1.10 - Partial Loading History for 110 Mpa Reversal Specimen

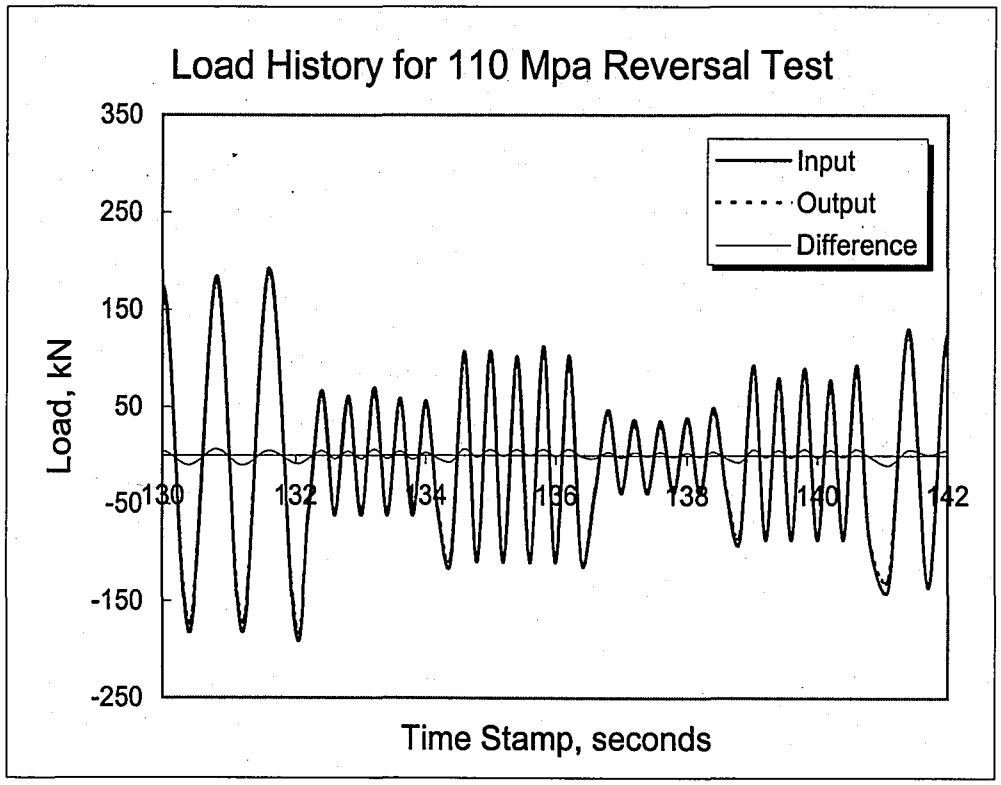

Figure 5.1.11 - Partial Loading History for 110 Mpa Reversal Specimen

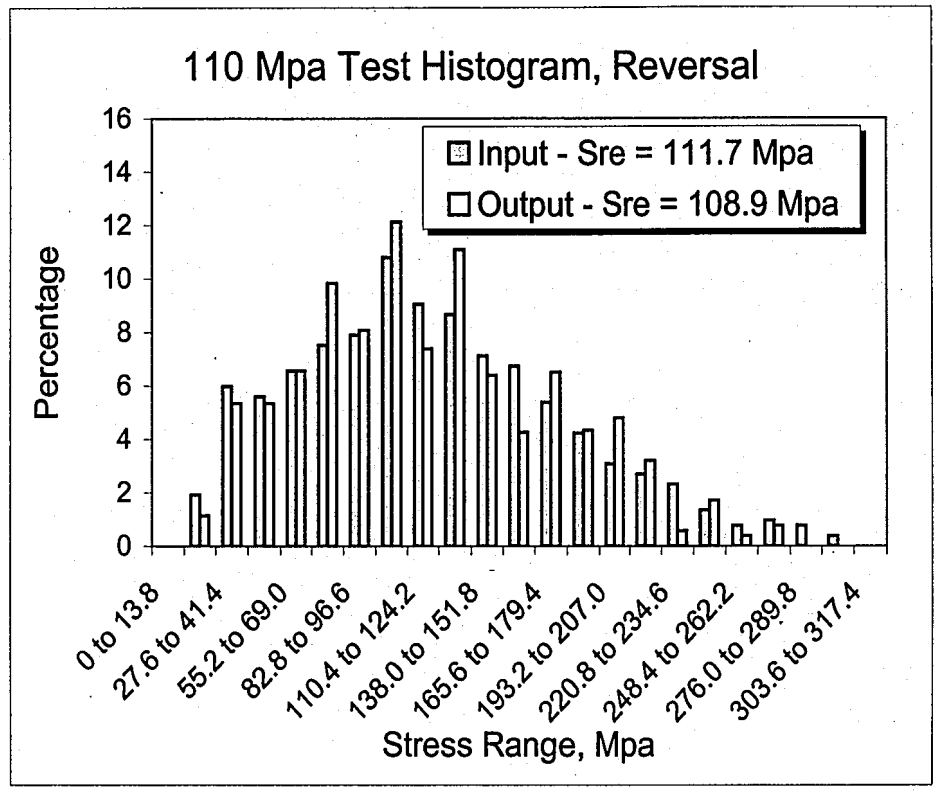

Figure 5.1.12 - Comparison of Control Input and Feedback Output Stress Range Histograms

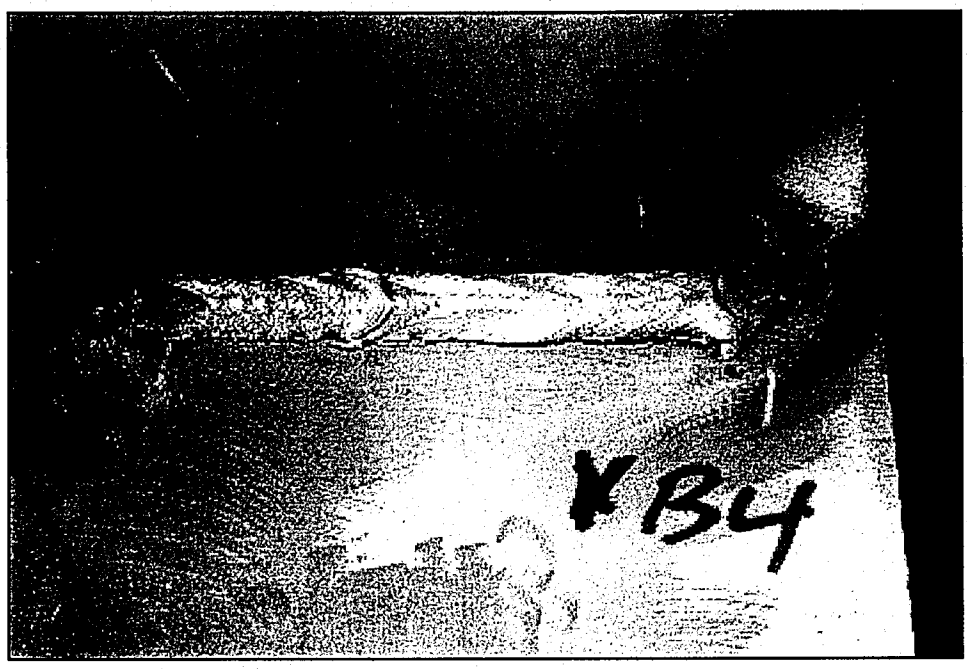

Figure 5.2.1 - Typical Fatigue Crack Formed
at Transverse Fillet Weld Toe

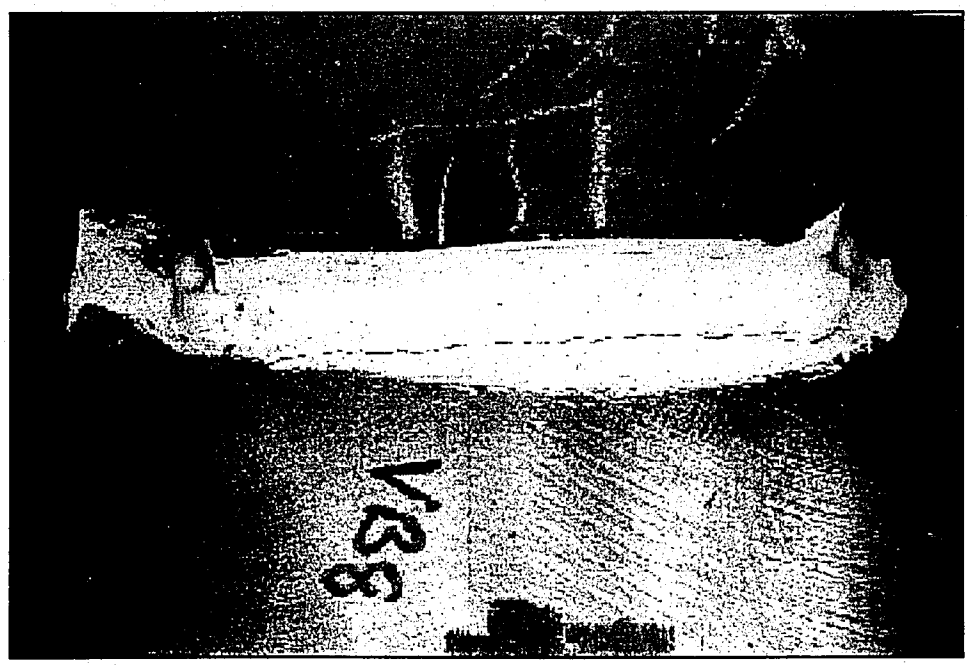

Figure 5.2.2 - Typical Fatigue Crack Formed in Smart Paint
at Transverse Fillet Weld Toe

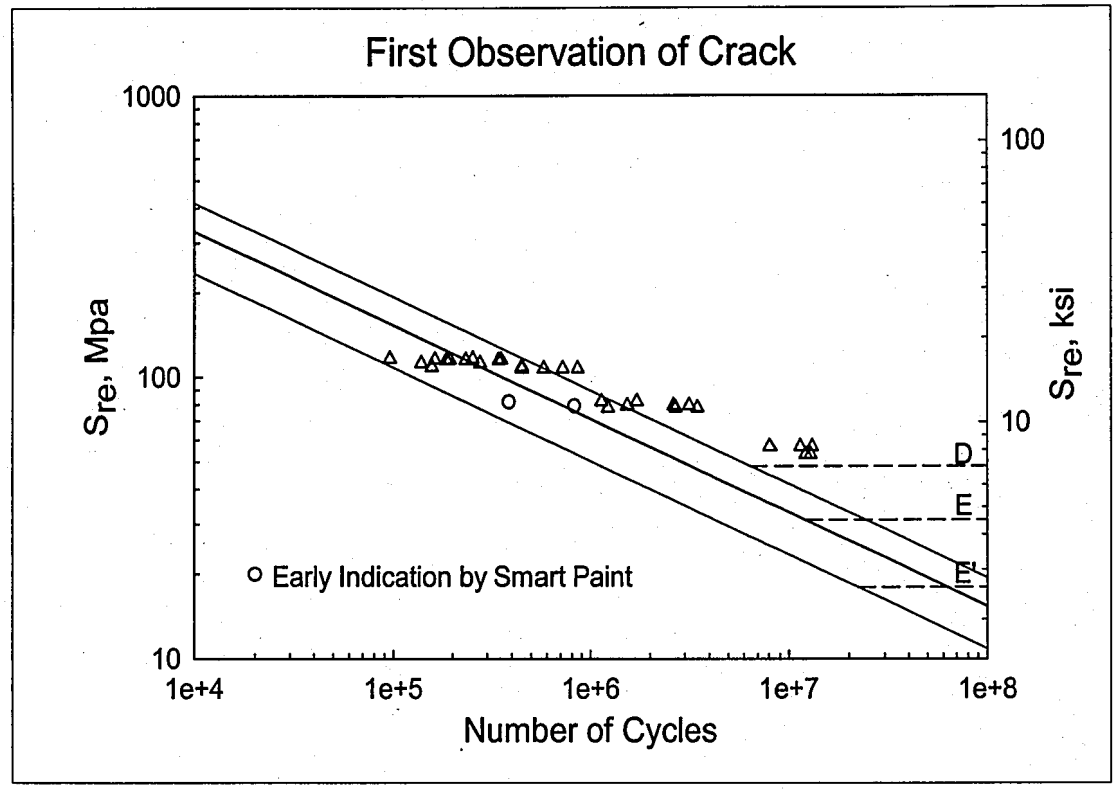

Figure 5.2.3 - S-N Data for First Observation of Cracking

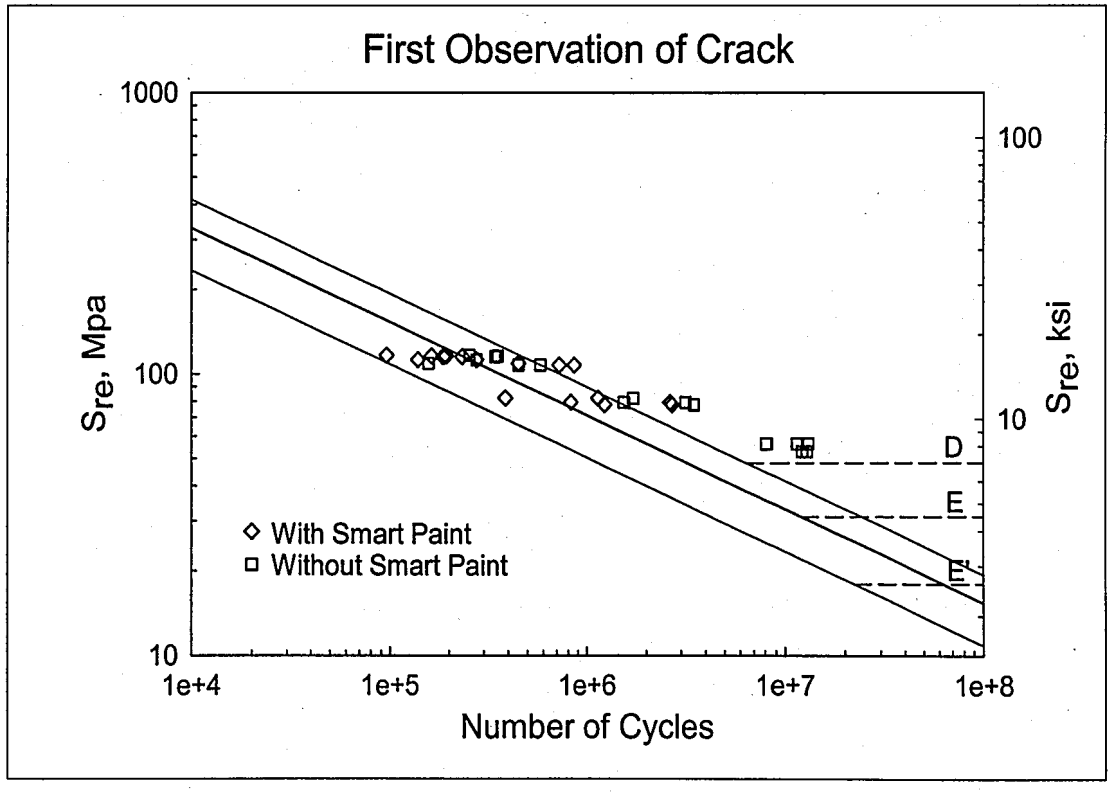

Figure 5.2.4 - S-N Data for First Observation of Cracking,
Welds with and without Smartpaint

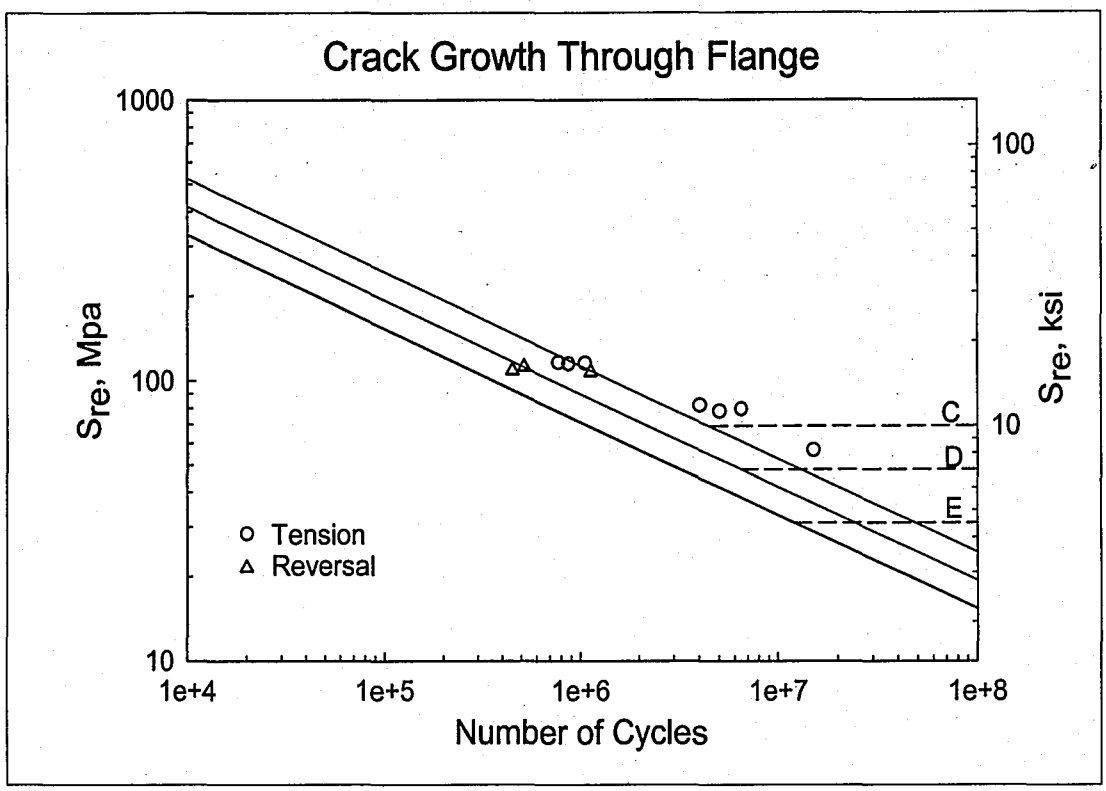

Figure 5.2.5 - Variable Amplitude Fatigue Results

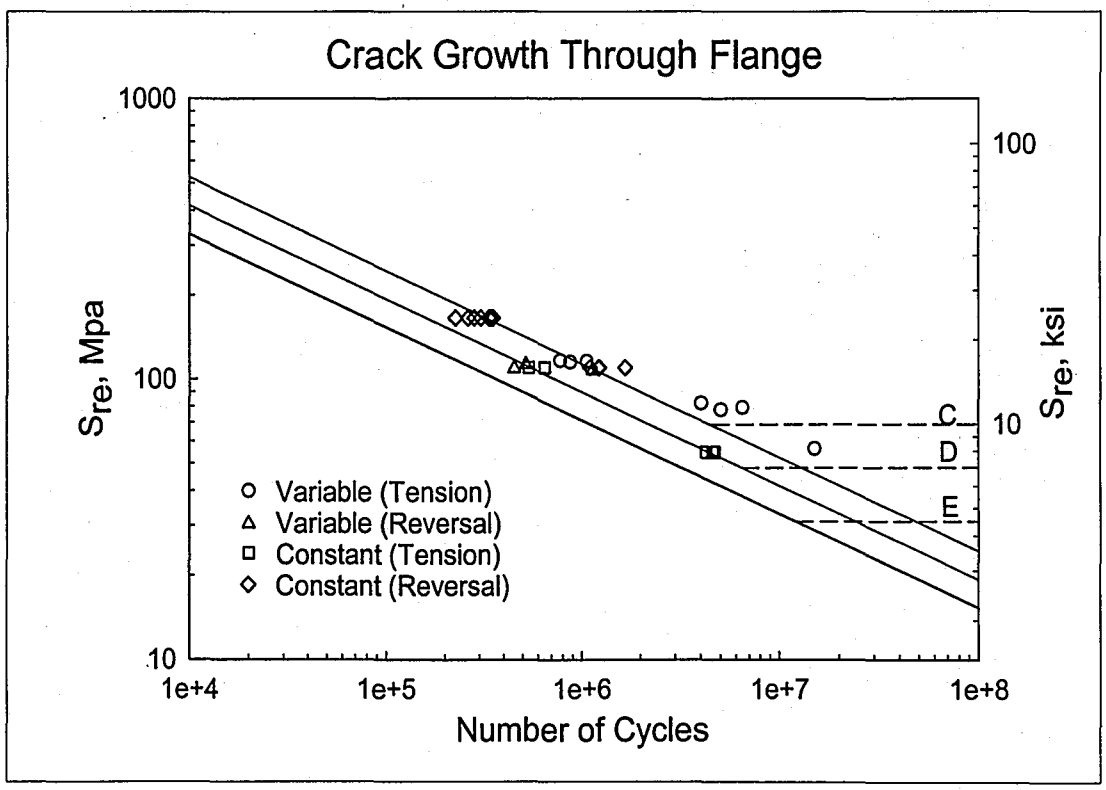

Figure 5.2.6 - Variable Amplitude Fatigue Results Plotted with Constant Amplitude Fatigue Results

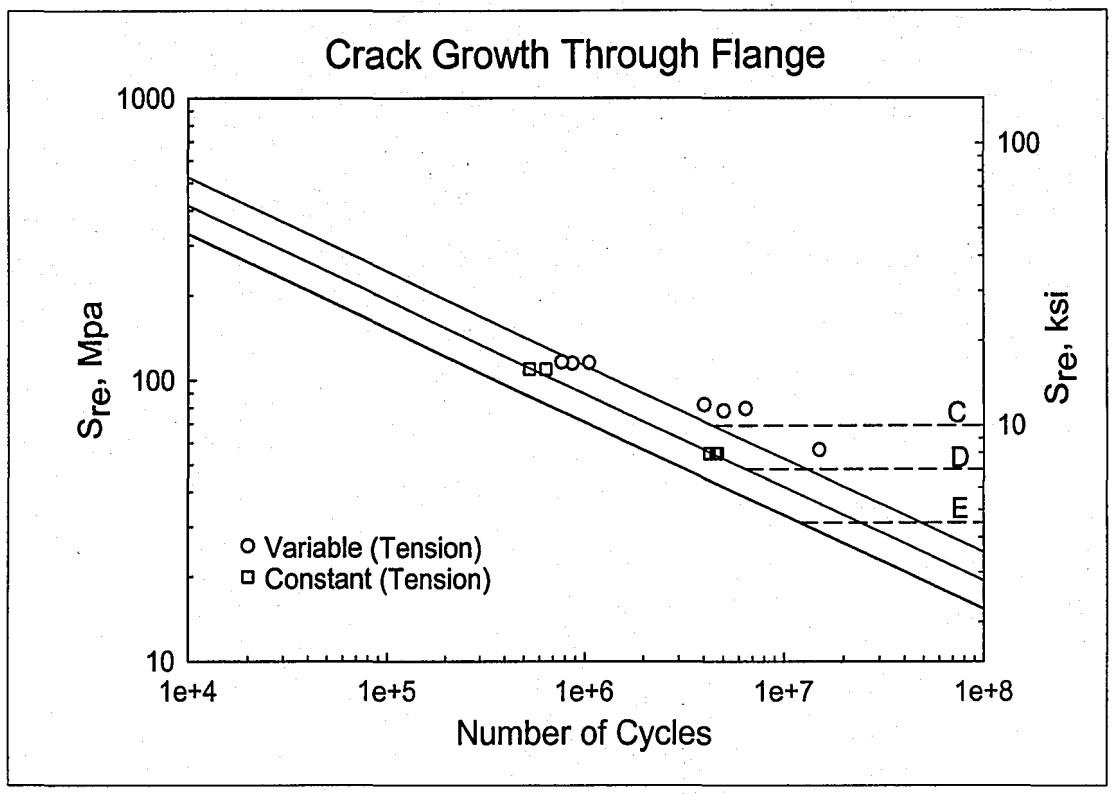

Figure 5.2.7 - Comparison of Variable Amplitude and Constant Amplitude Fatigue Results - Tension Only

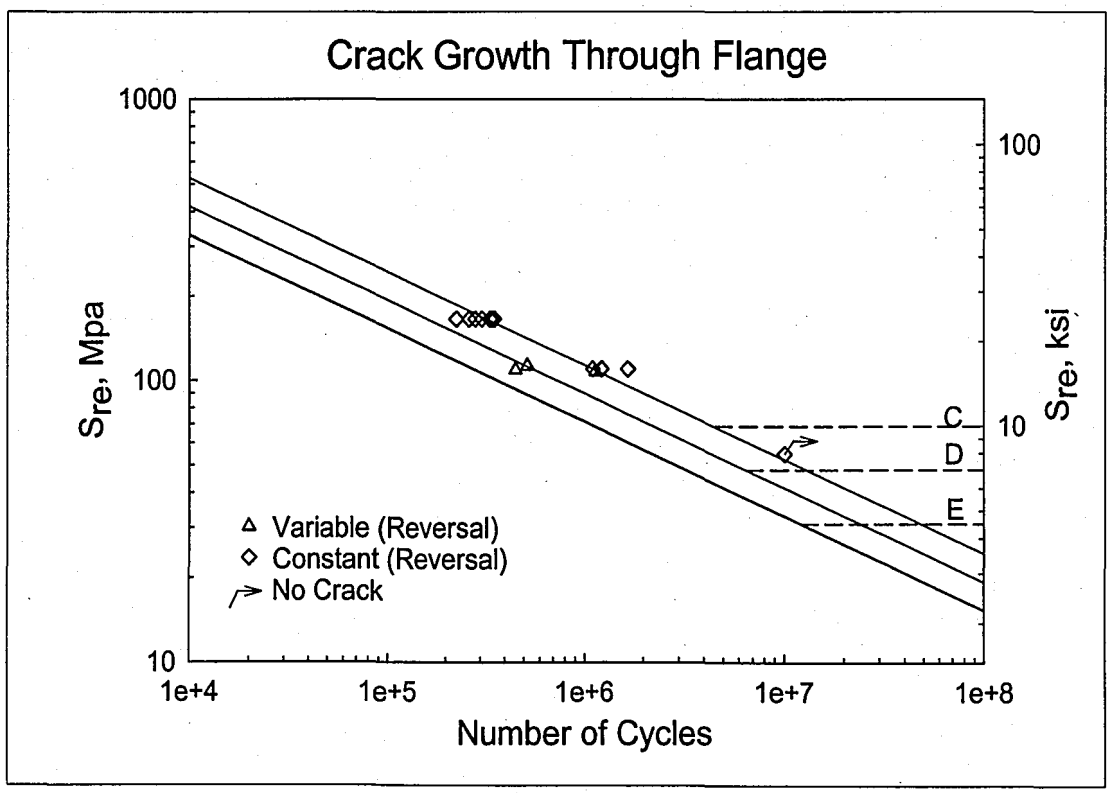

Figure 5.2.8 - Comparison of Variable Amplitude and Constant Amplitude Fatigue Results - Reversal Only

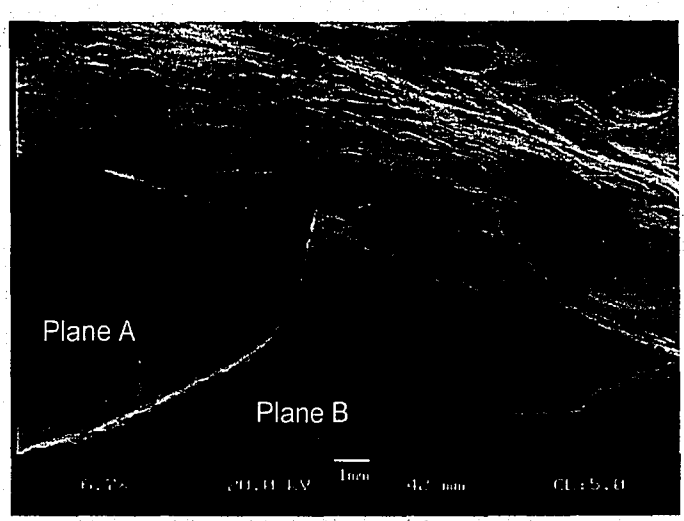

(a) View of Two Separate Cracks Joining

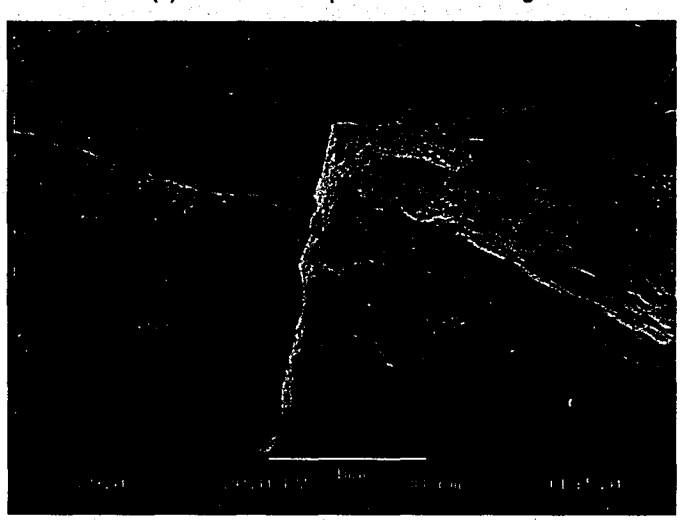

(b) View of Slag Inclusion

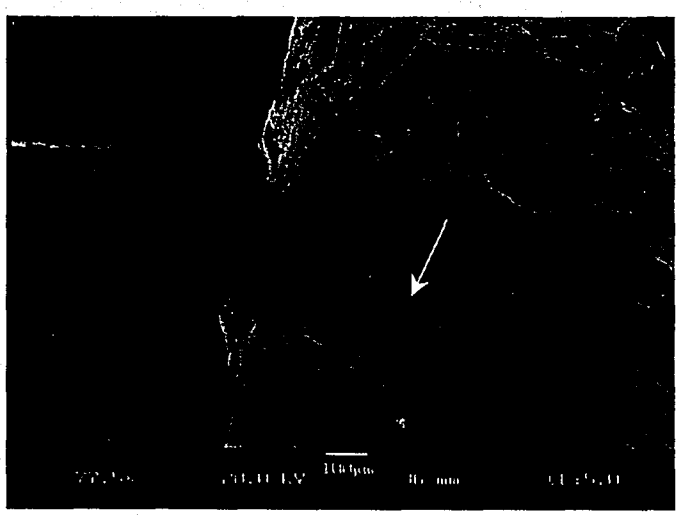

(c) View of Hole due to Slag Inclusion

Figure 5.2.9 - SEM Micrograph of Slag Inclusion and the Joining of Two Cracks Along Separate Planes in Beam VB10

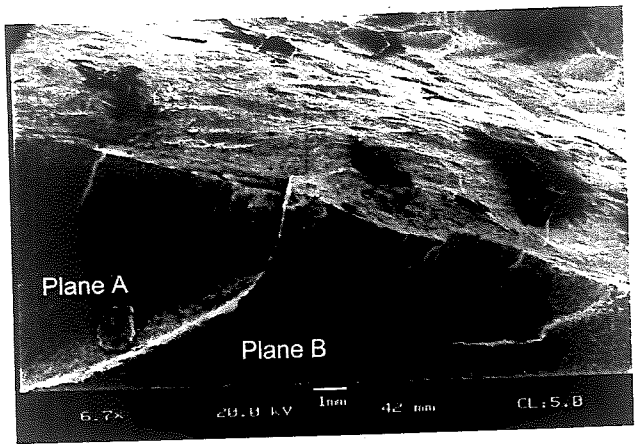

(a) View of Two Separate Cracks Joining

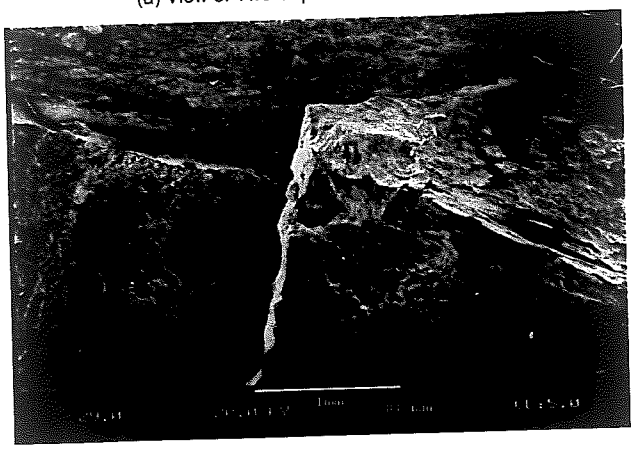

(b) View of Slag Inclusion

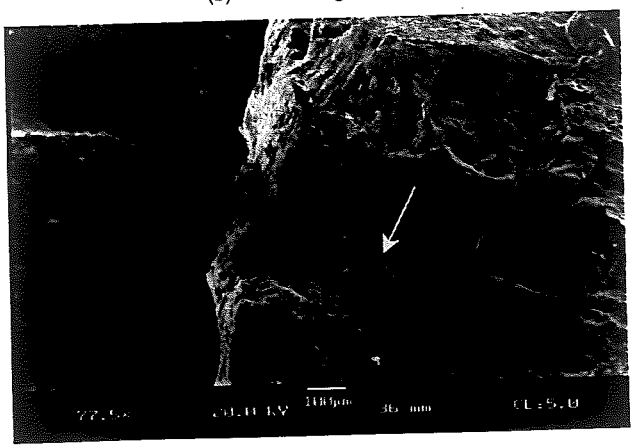

(c) View of Hole due to Slag Inclusion

Figure 5.2.9 - SEM Micrograph of Slag Inclusion and the Joining of Two Cracks Along Separate Planes in Beam VB10

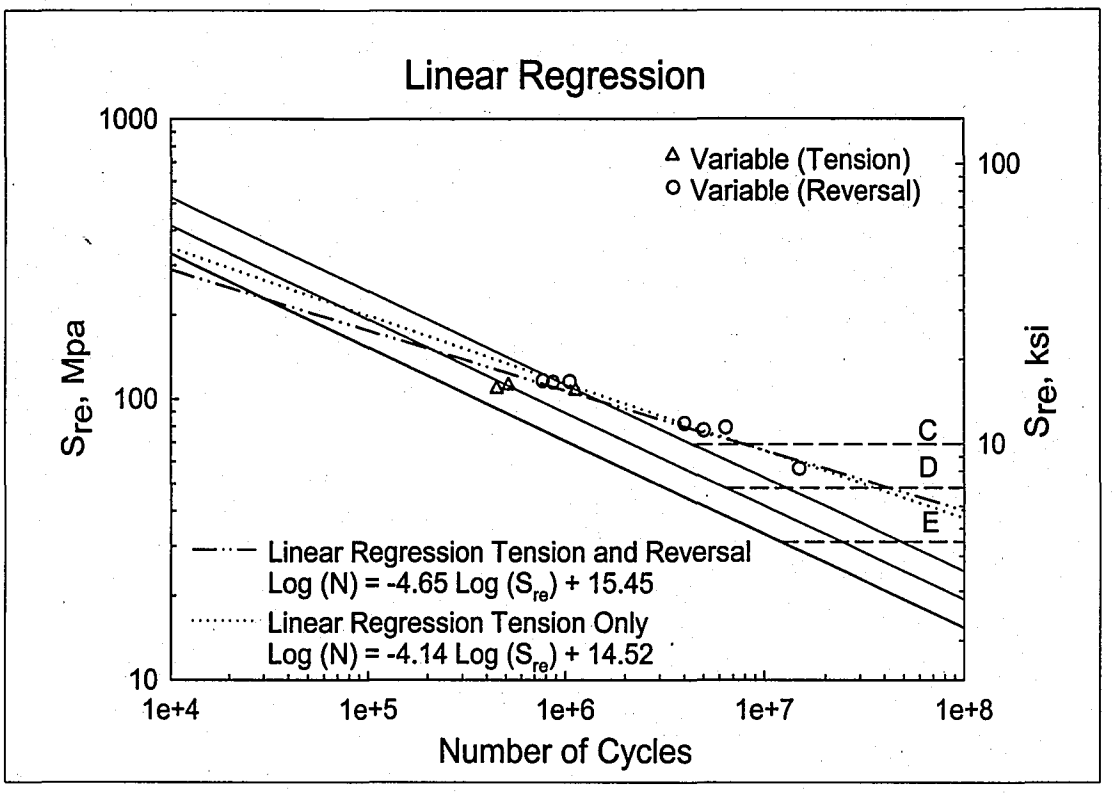

Figure 5.2.10 - Linear Regression Results for Tension Alone Data and Tension with Reversal Data

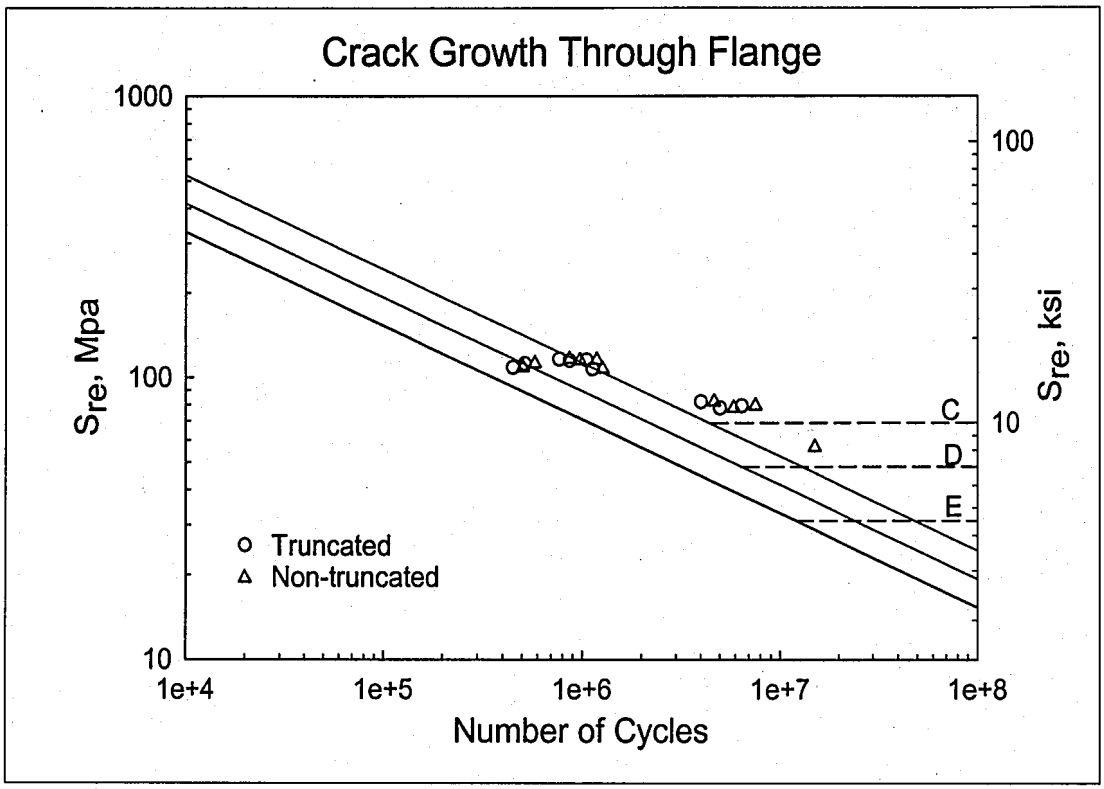

Figure 5.3.1 - Comparing Variable Amplitude Fatigue Results with Truncated and Non-truncated Spectrums

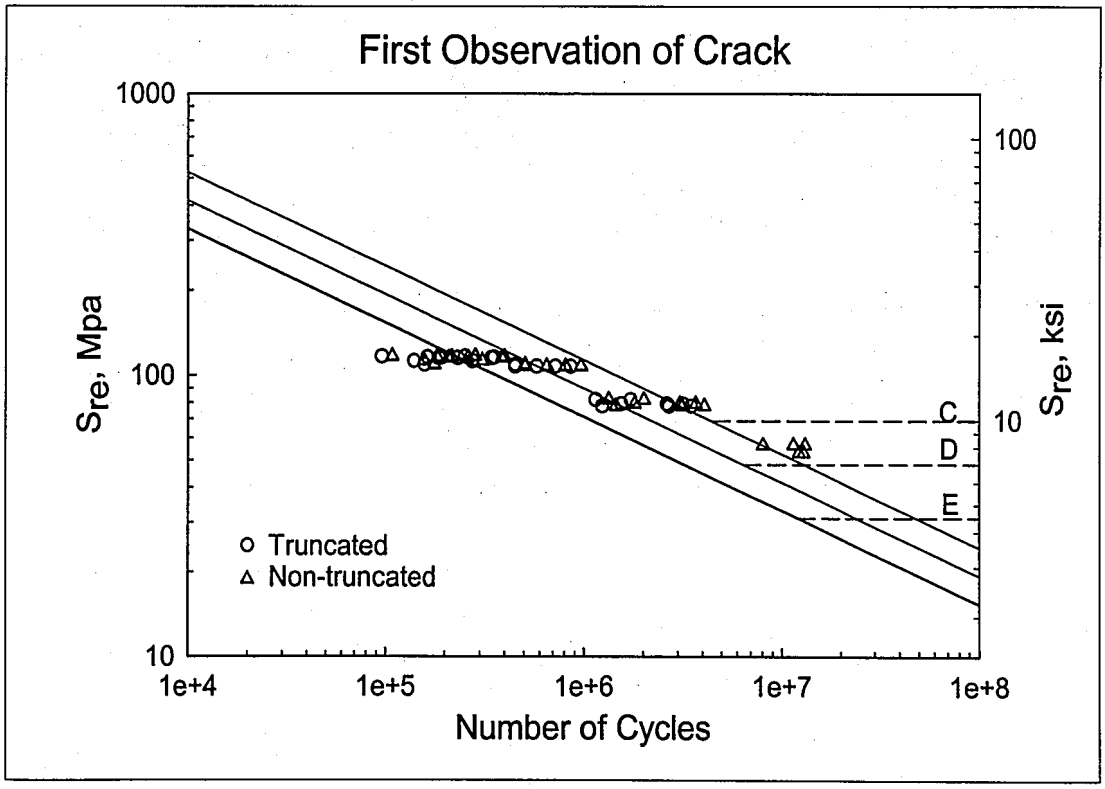

Figure 5.3.2 - Comparing Variable Amplitude Fatigue Results with Truncated and Non-truncated Spectrums

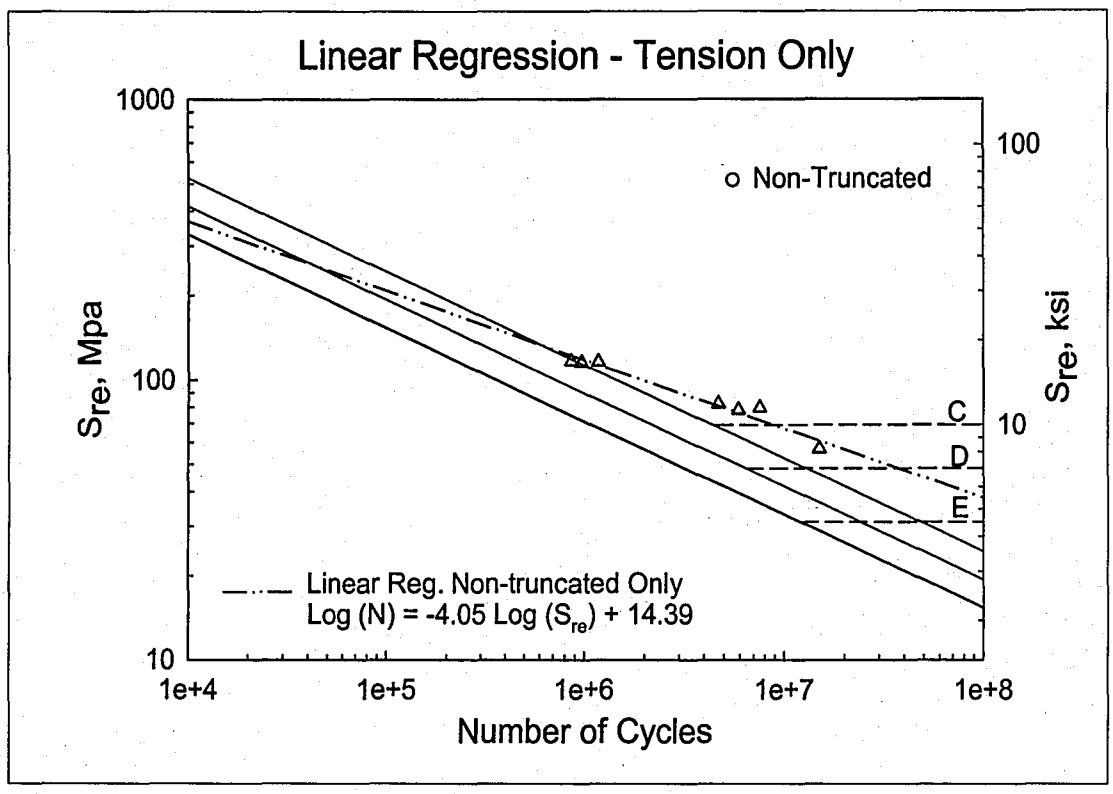

Figure 5.3.3 - Linear Regression Results for Non-truncated Tension Tests

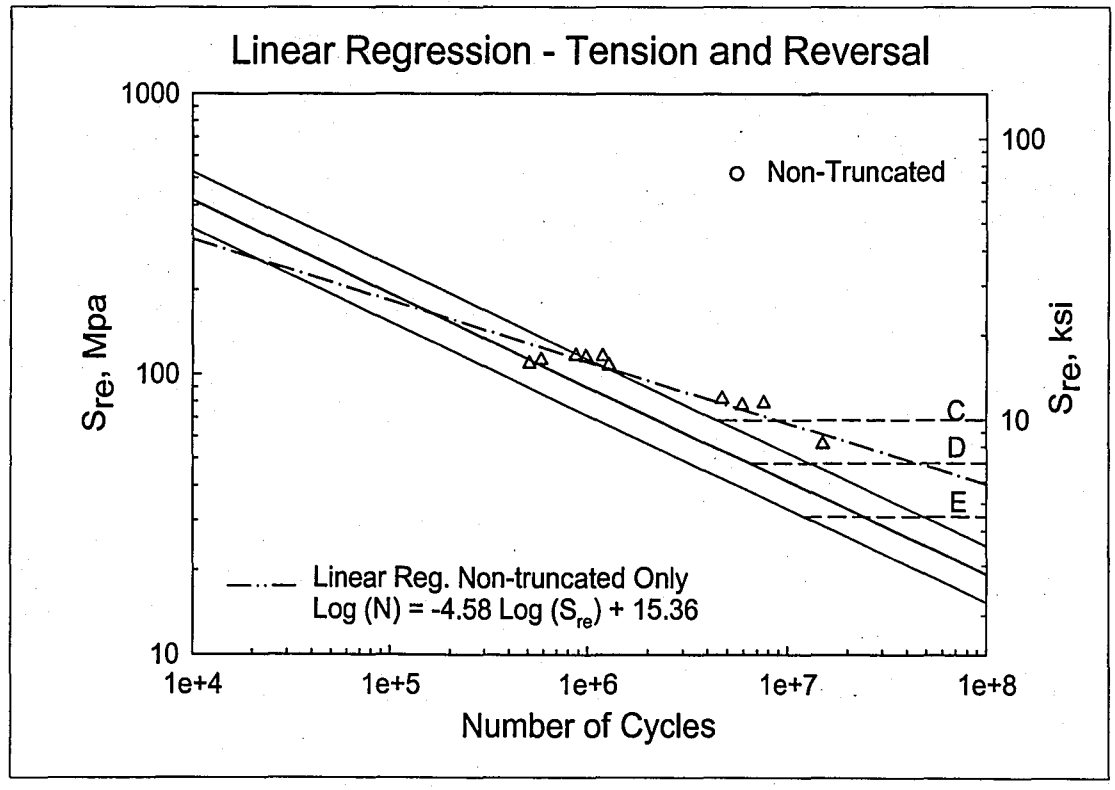

Figure 5.3.4 - Linear Regression Results for Non-truncated Tension and Reversal Tests

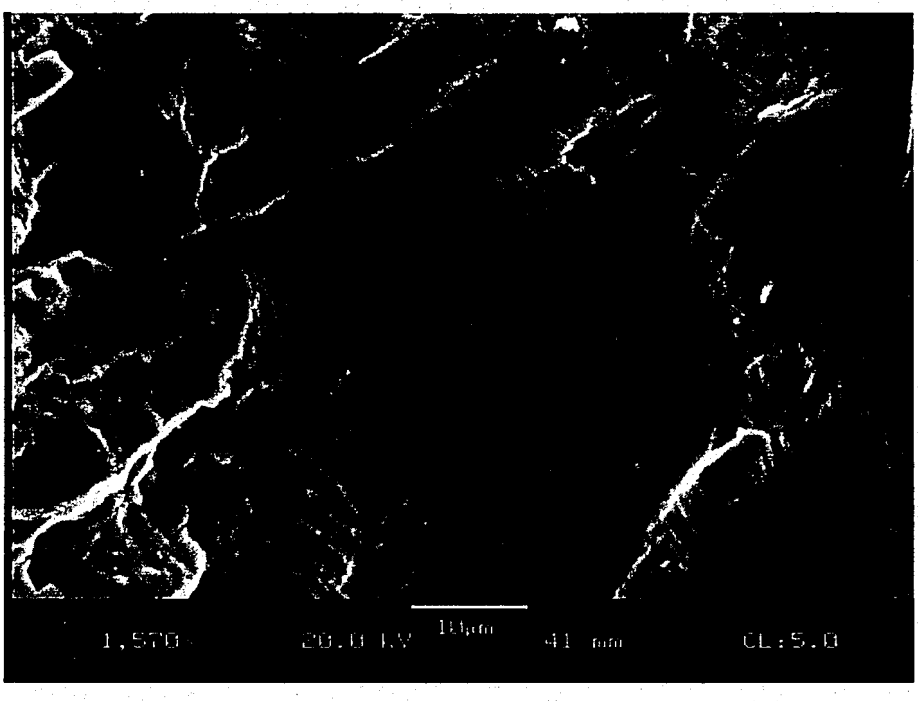

Figure 5.4.1 - Variable Amplitude Fatigue Striations from VB12

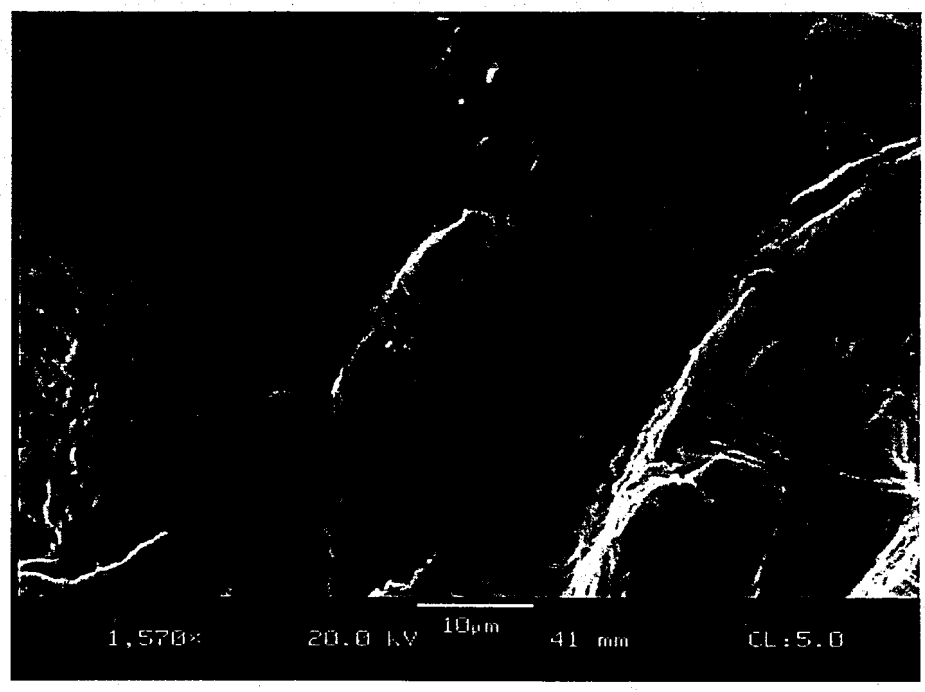

Figure 5.4.2 - Variable Amplitude Fatigue Striations from VB12

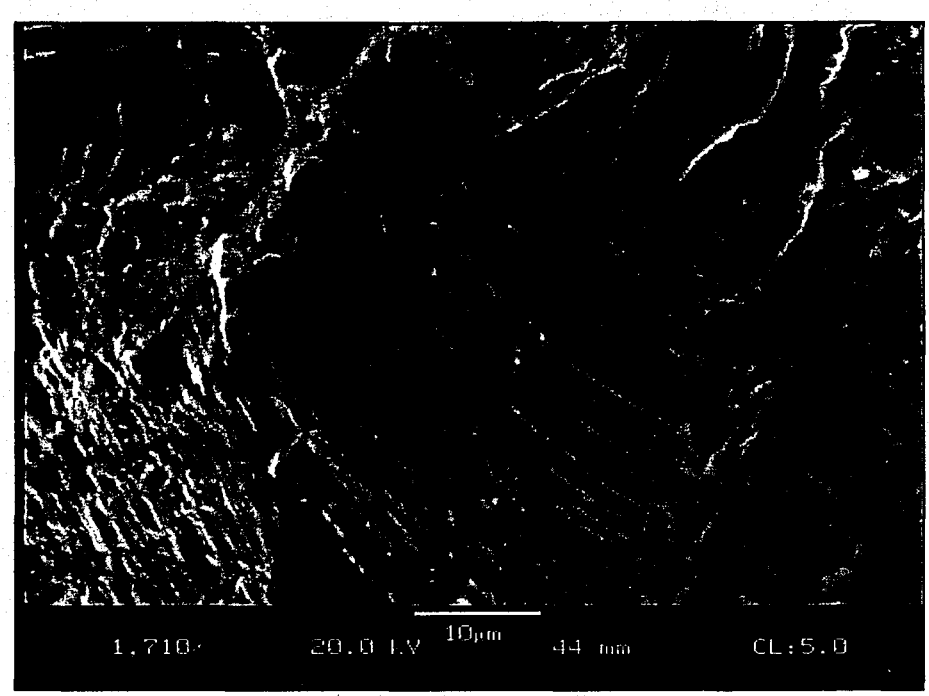

Figure 5.4.3 - Variable Amplitude Fatigue Striations from VB7

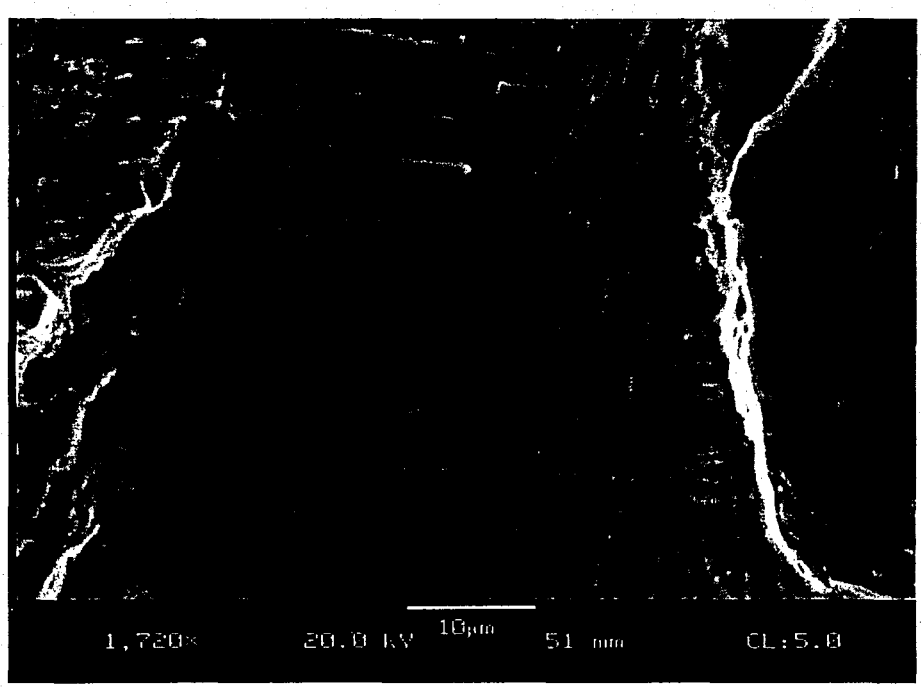

Figure 5.4.4 - Variable Amplitude Fatigue Striations from VB5

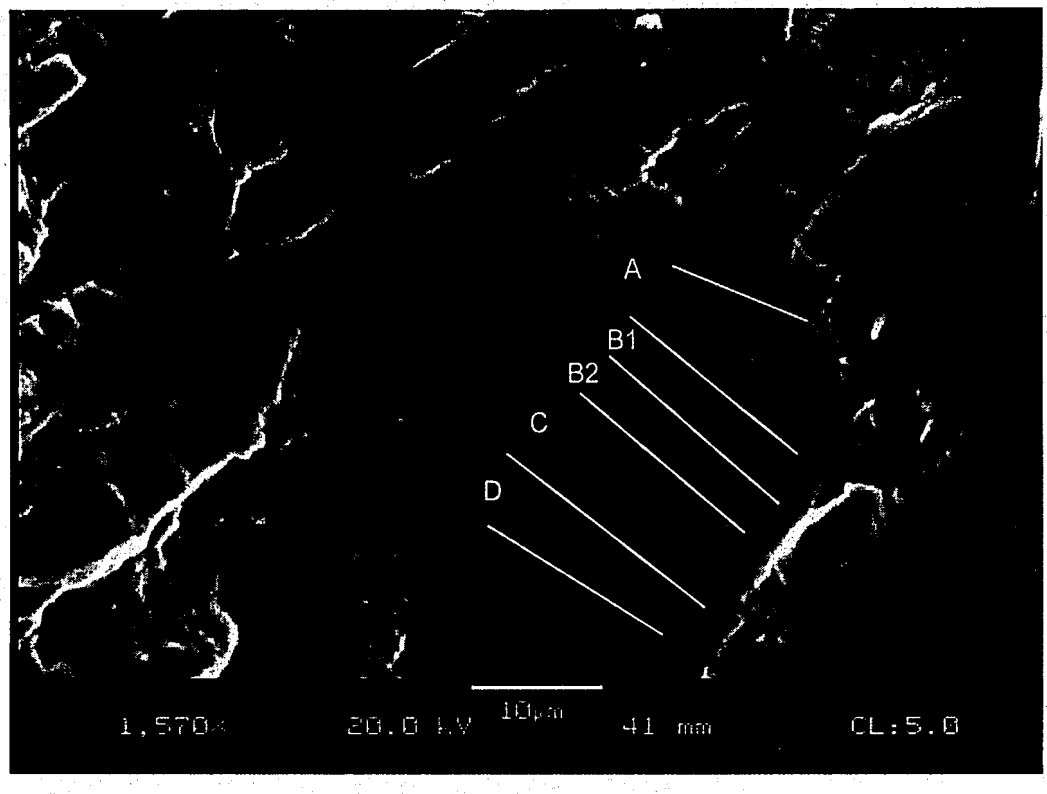

Figure 5.4.5 - Variable Amplitude Fatigue Striations - VB12

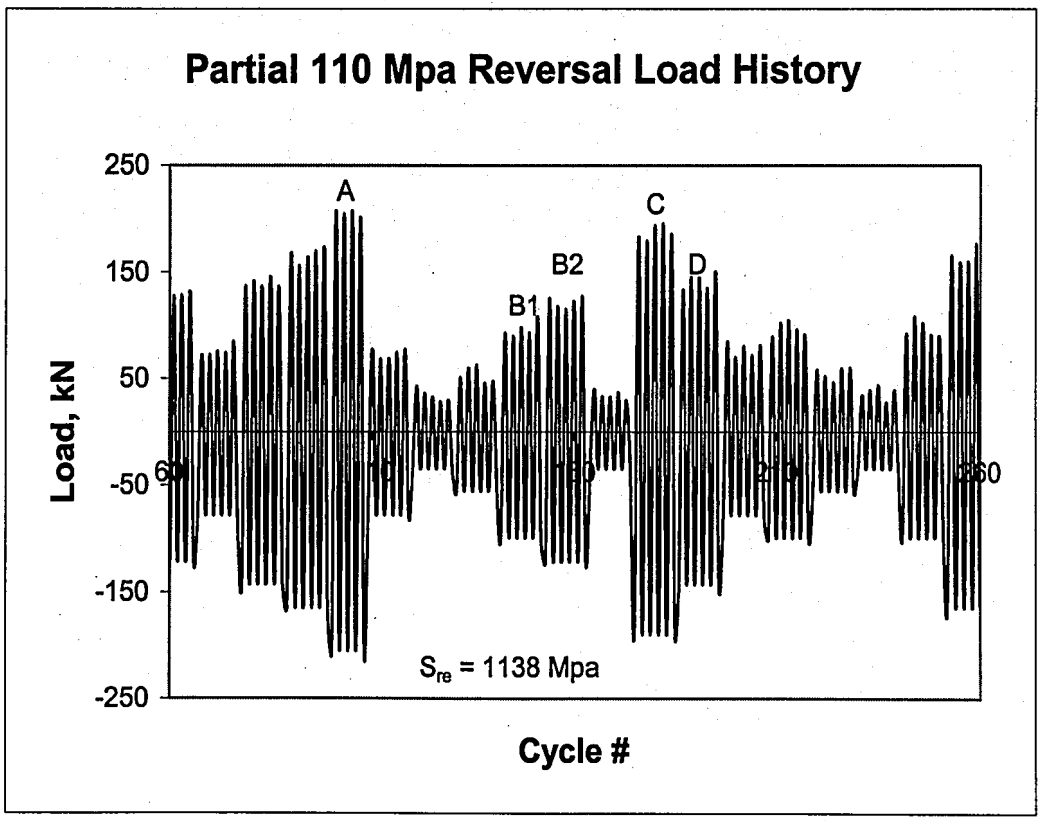

Figure 5.4.6 - Load History Causing Fatigue Striations in Figure 5.4.5

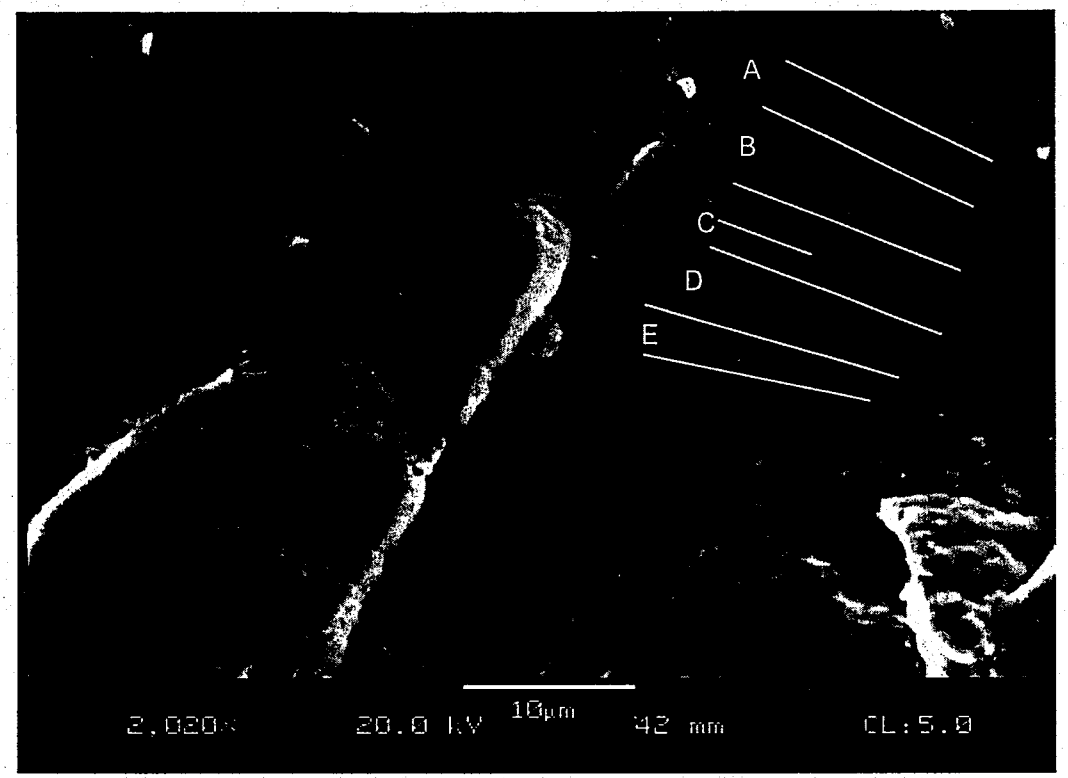

Figure 5.4.7 - Variable Amplitude Fatigue Striations - VB12

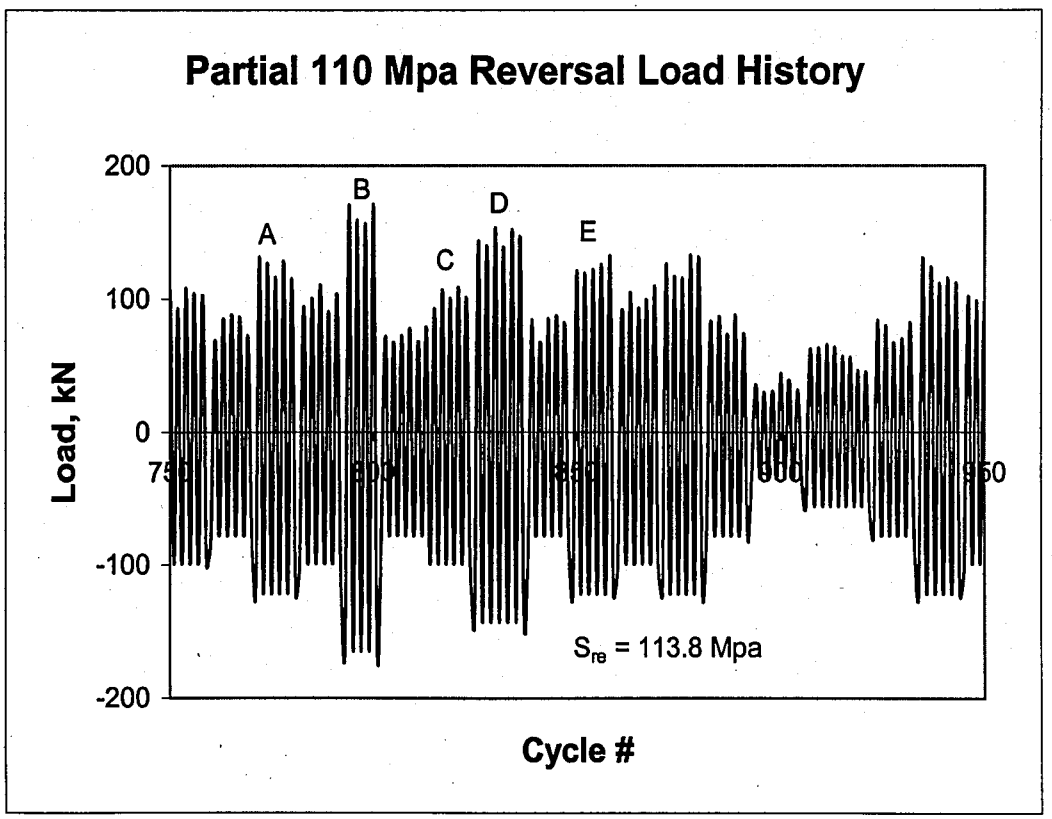

Figure 5.4.8 - Load History Causing Fatigue Striations in Figure 5.4.7

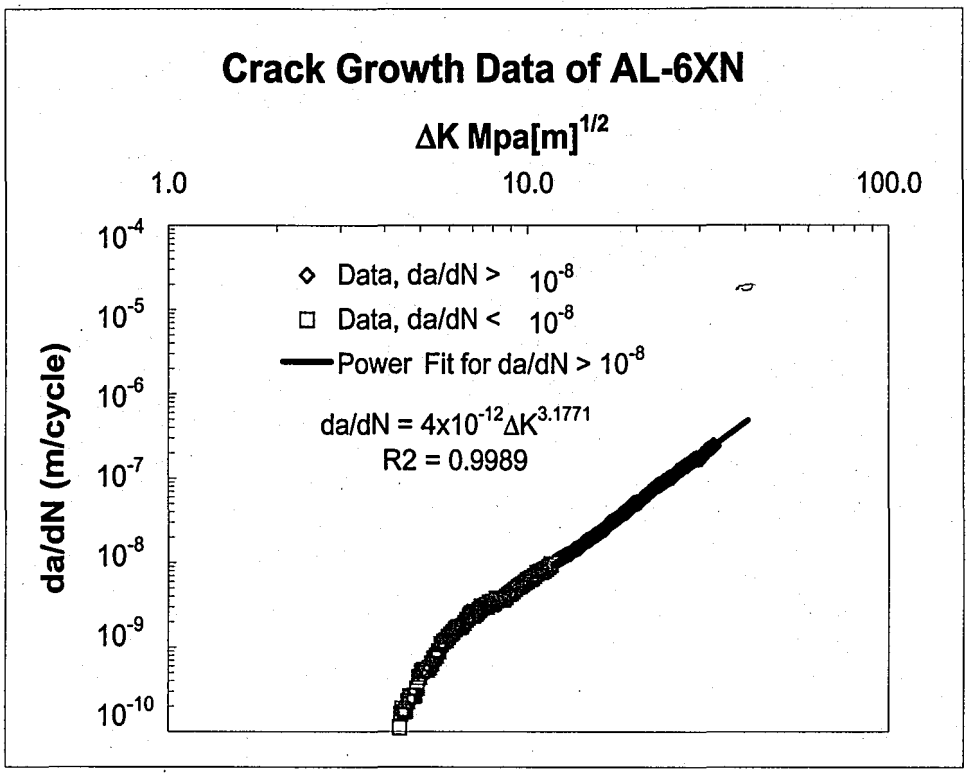

Figure 5.4.9 - Summary of Crack Growth Data of AL-6XN Austenitic Stainless Steel

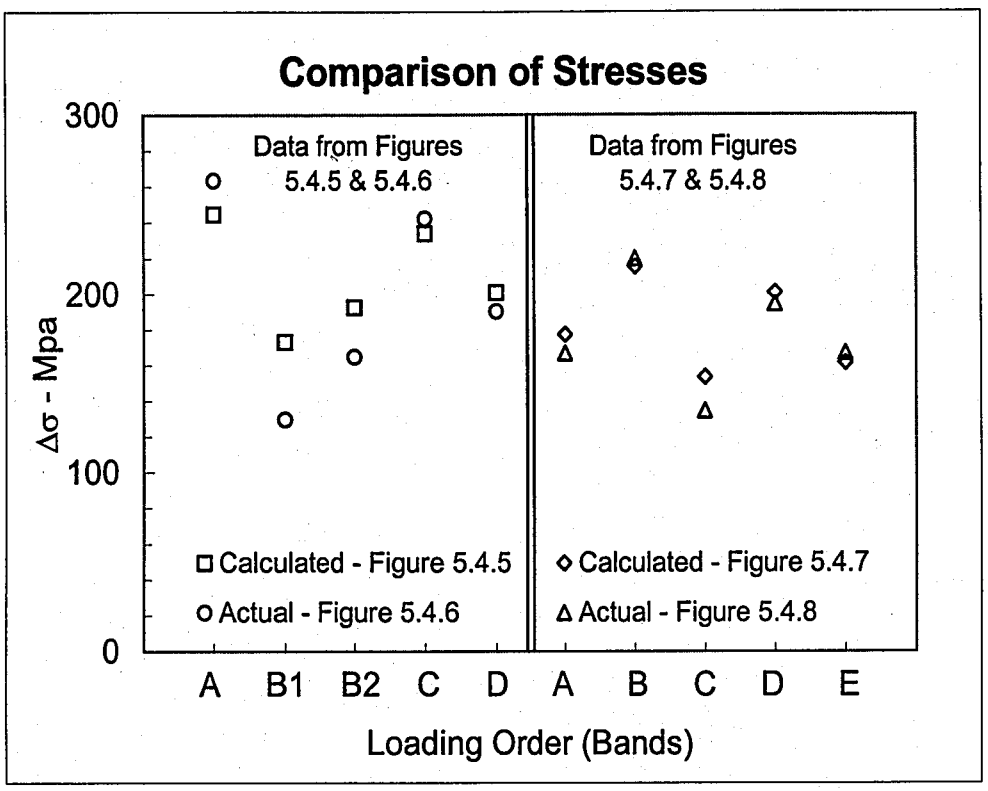

Figure 5.4.10 - Comparison of Actual and Calculated Stress Ranges, by Loading Order

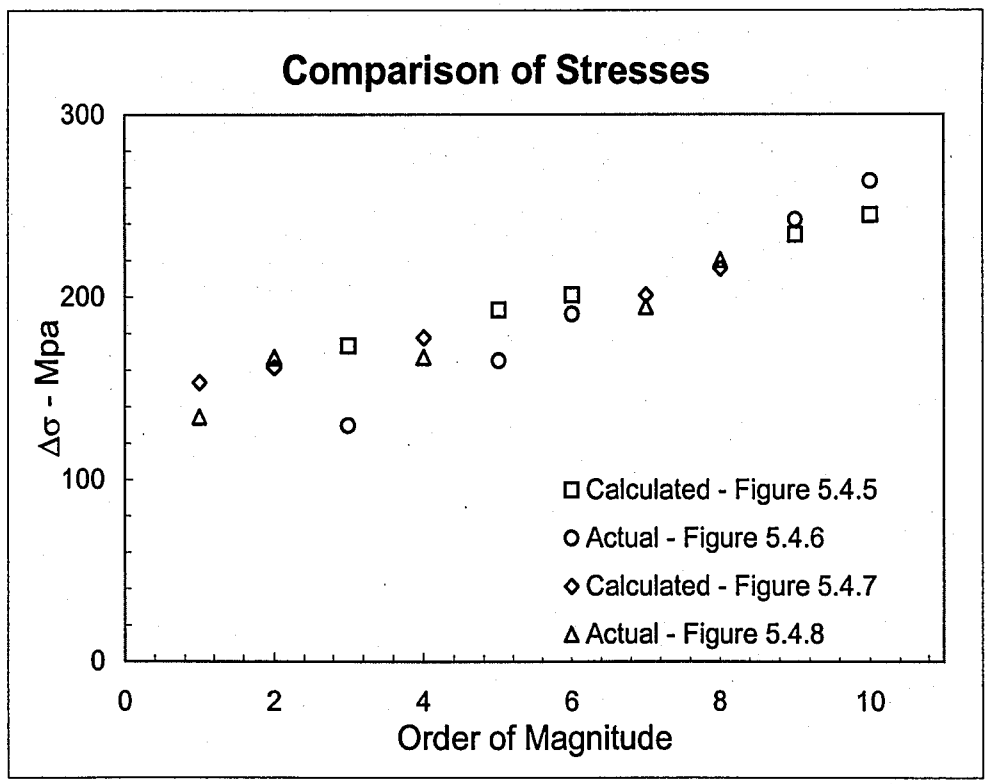

Figure 5.4.11 - Comparison of Actual and Calculated Stress Ranges, in Order of Magnitude

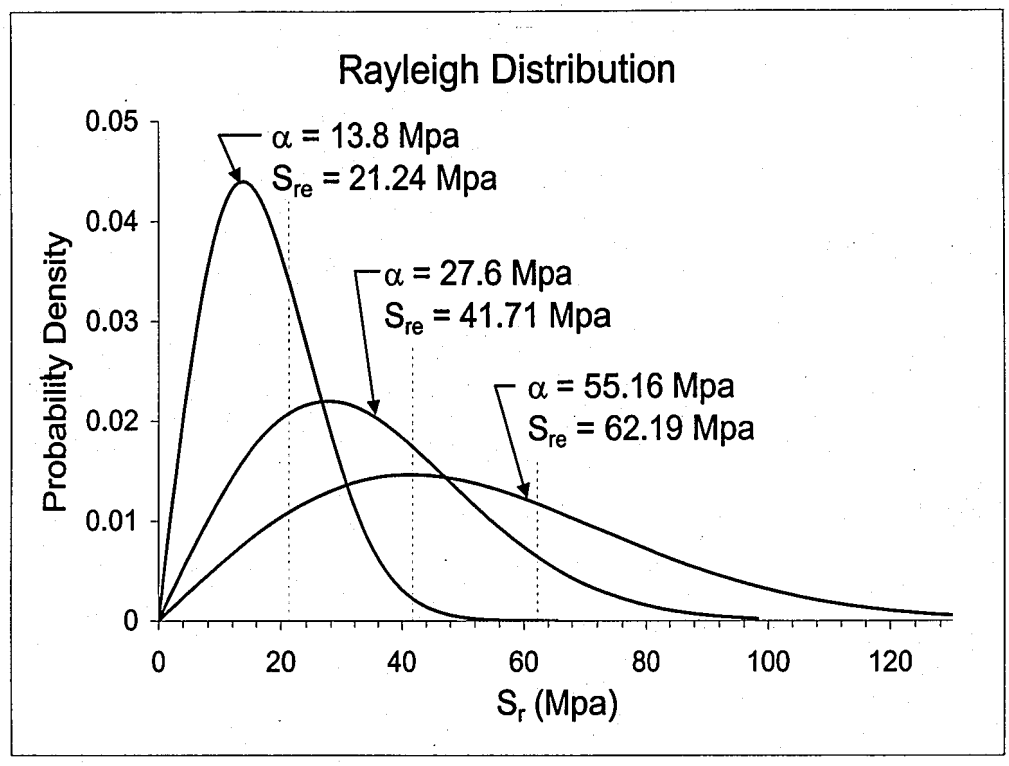

Figure 6.3.1 - Typical Rayleigh Distributions

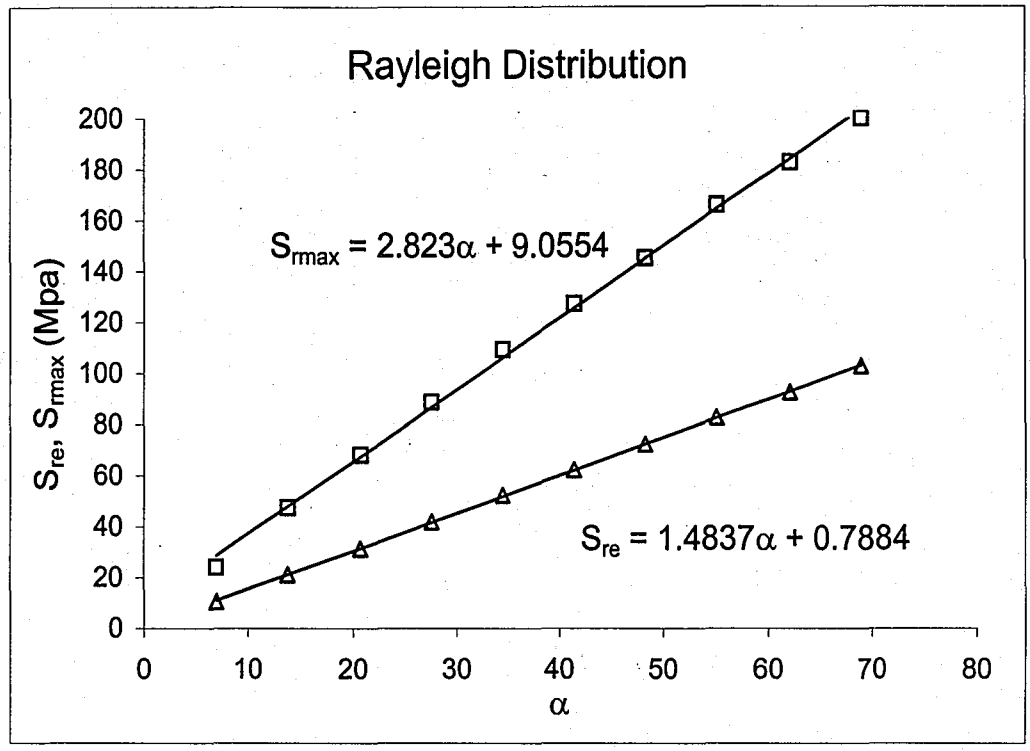

Figure 6.3.2 - S_{re} and S_{rmax} for Several Rayleigh Distributions

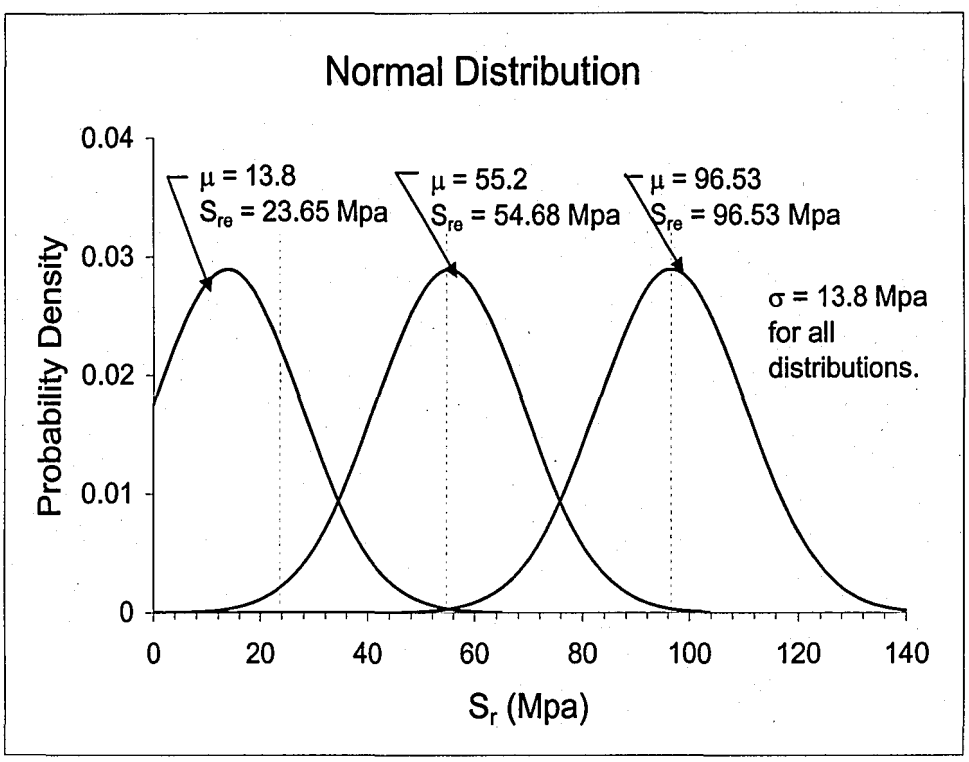

Figure 6.3.3 - Typical Normal Distributions

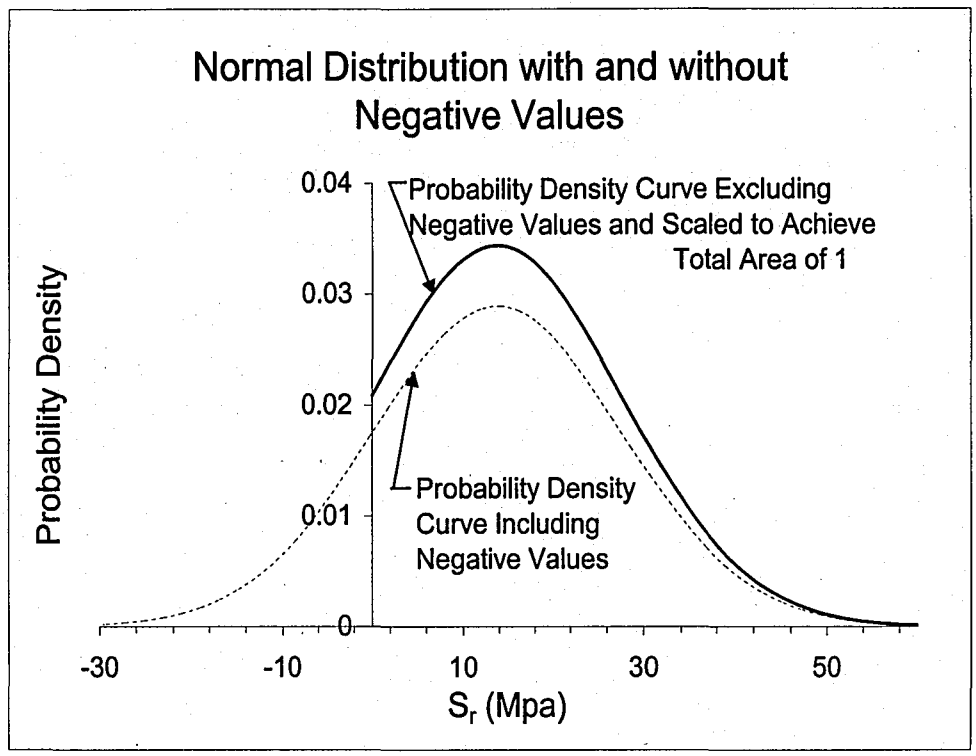

Figure 6.3.4 - Normal Distribution with and without Negative Values

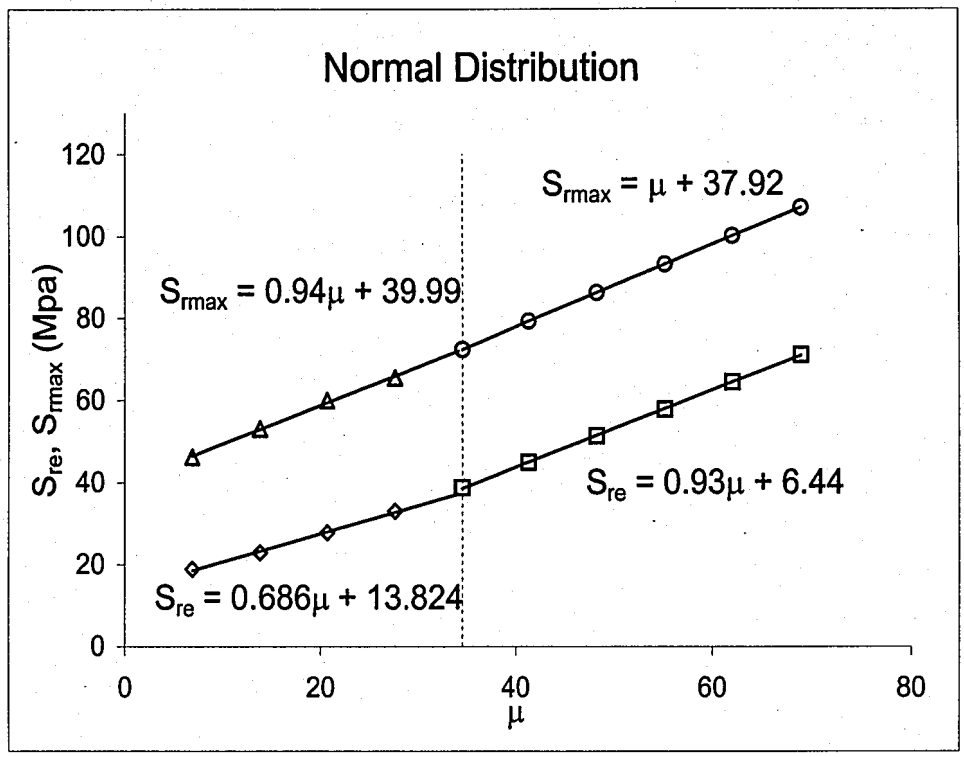

Figure 6.3.5 - S_{re} and S_{rmax} Data for Several Normal Distributions

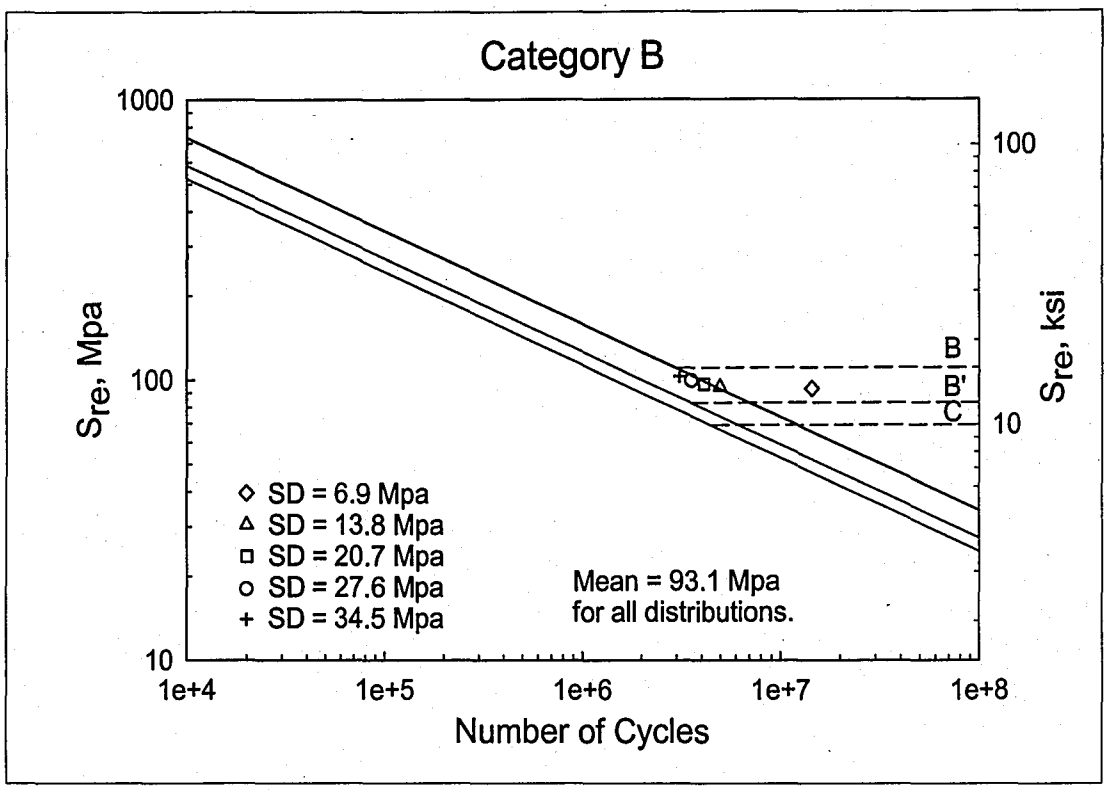

Figure 6.3.6 - Normal Distribution with Constant Mean Values and Varying Standard Deviations (SD)

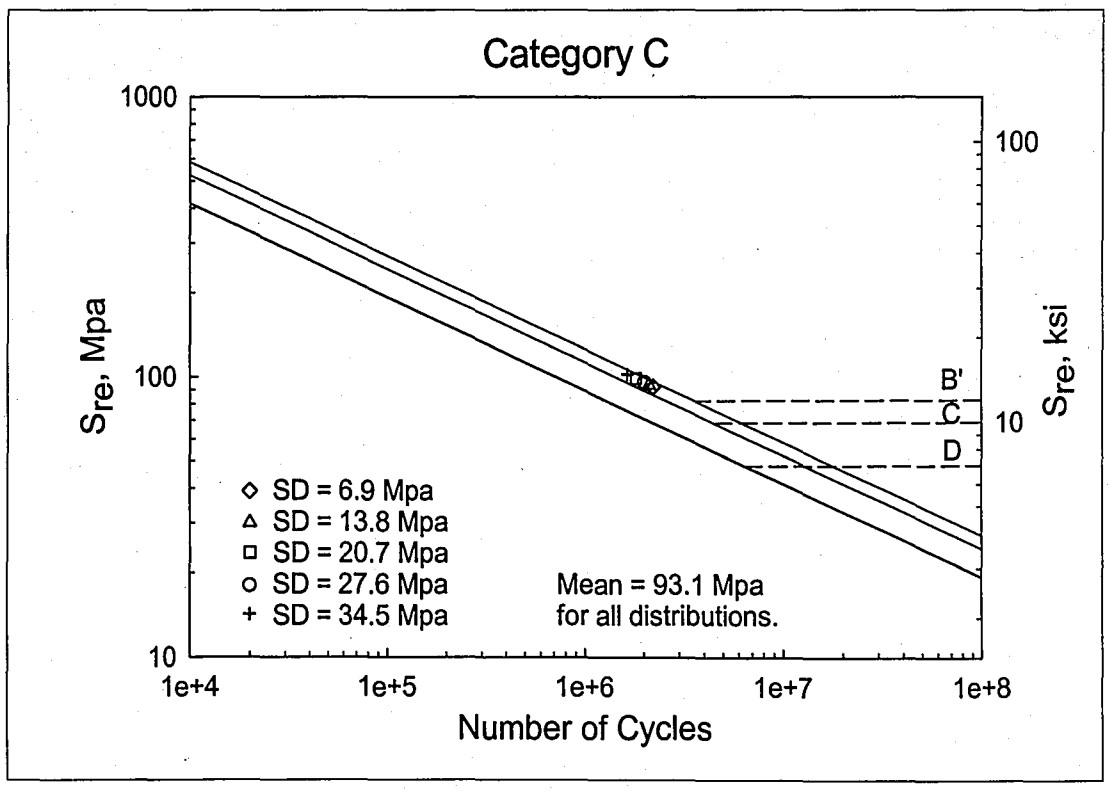

Figure 6.3.7 - Normal Distribution with Constant Mean Values and Varying Standard Deviations (SD)

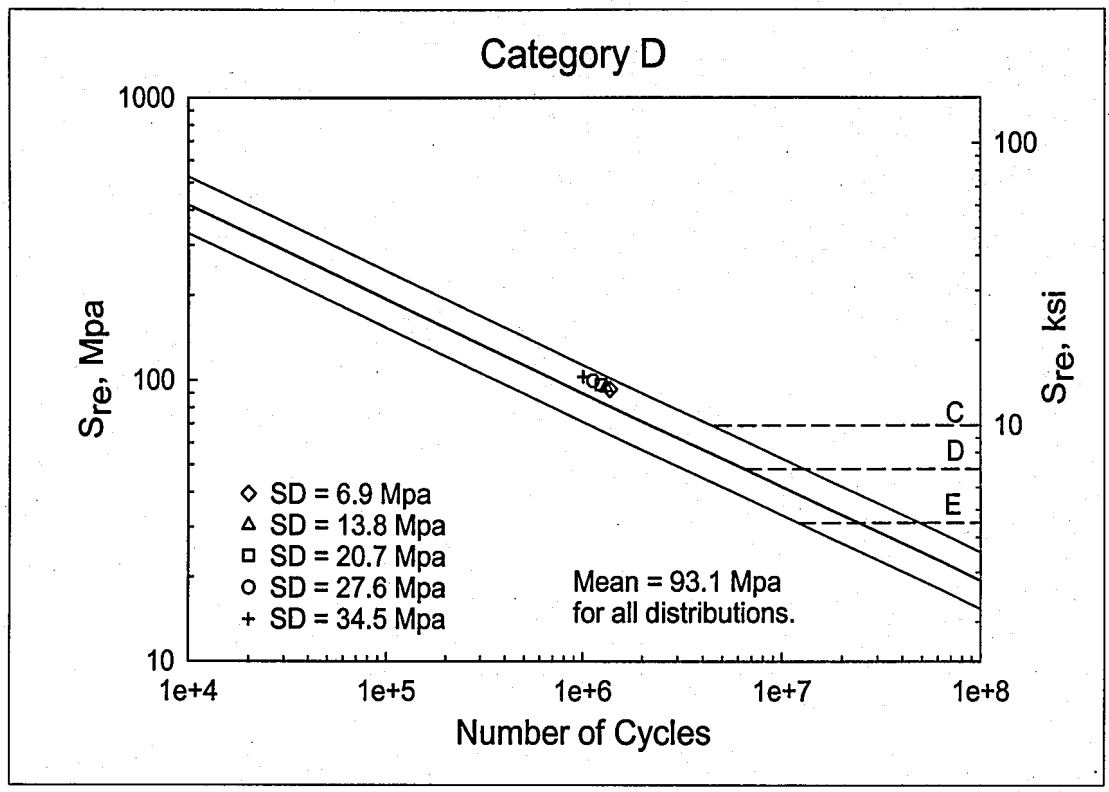

Figure 6.3.8 - Normal Distribution with Constant Mean Values and Varying Standard Deviations (SD)

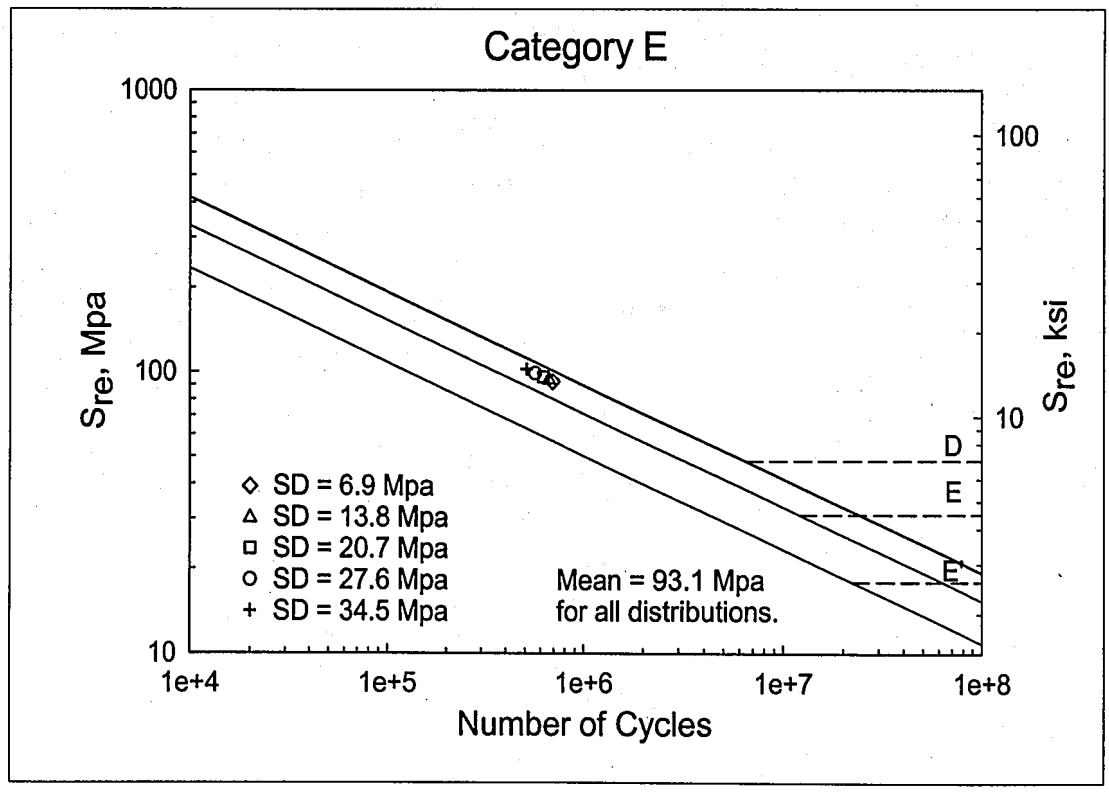

Figure 6.3.9 - Normal Distribution with Constant Mean Values and Varying Standard Deviations (SD)

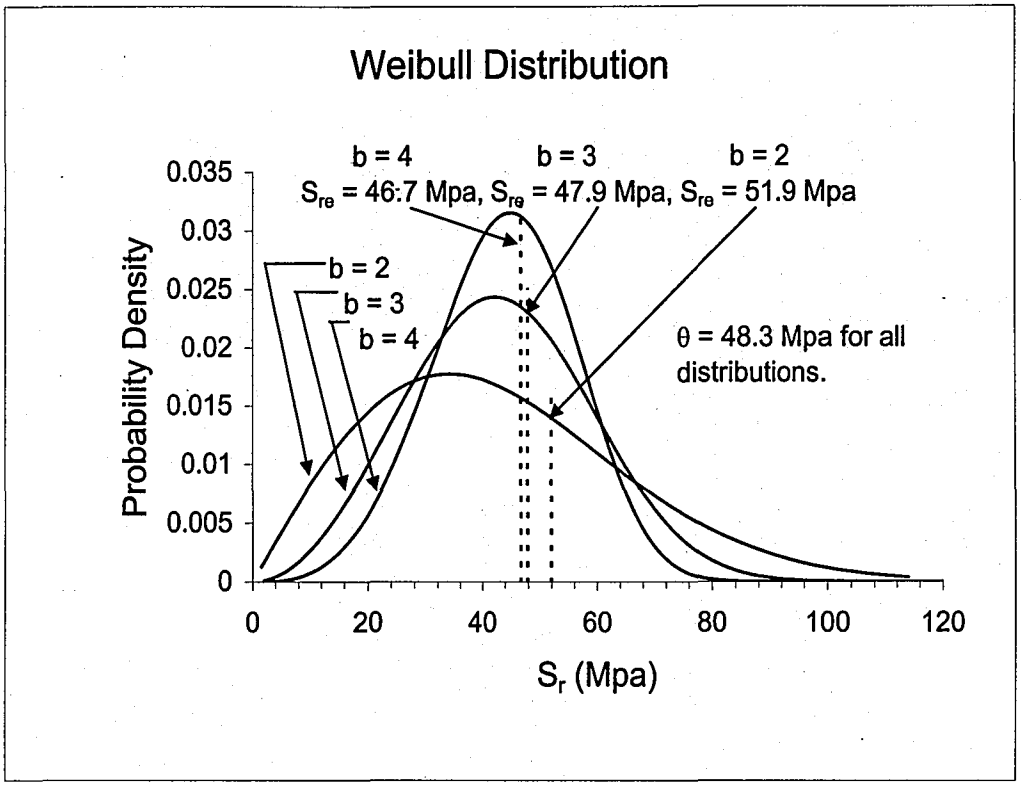

Figure 6.3.10 - Varying the Shape Parameter While Holding the Scale Parameter Constant

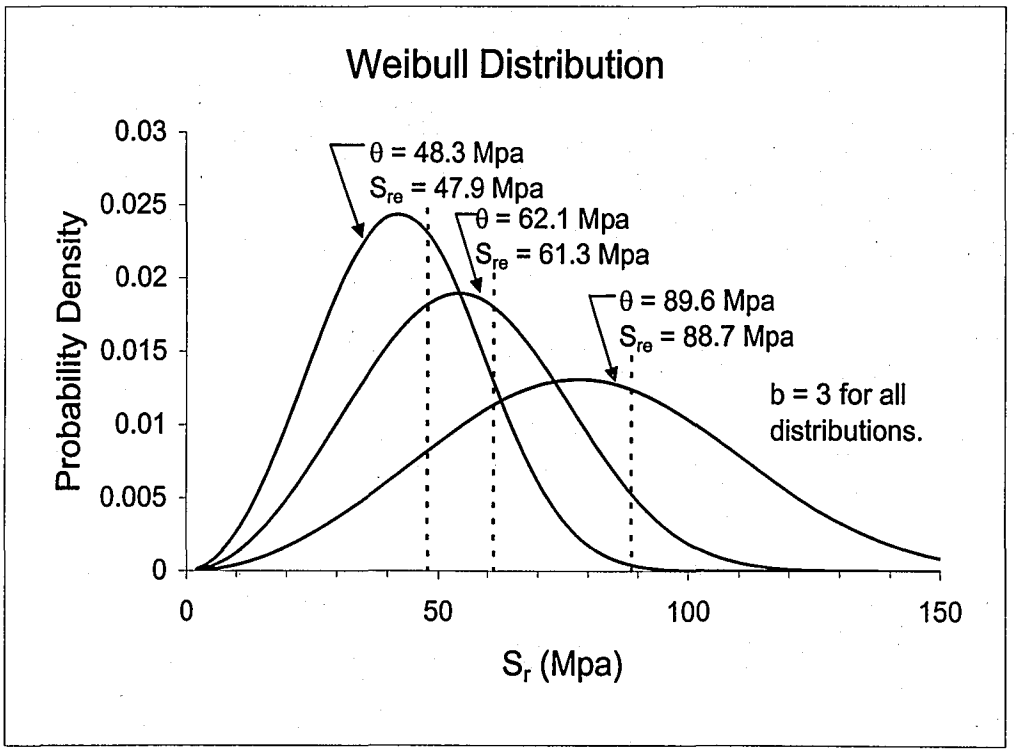

Figure 6.3.11 - Varying the Scale Parameter While Holding the Shape Parameter Constant

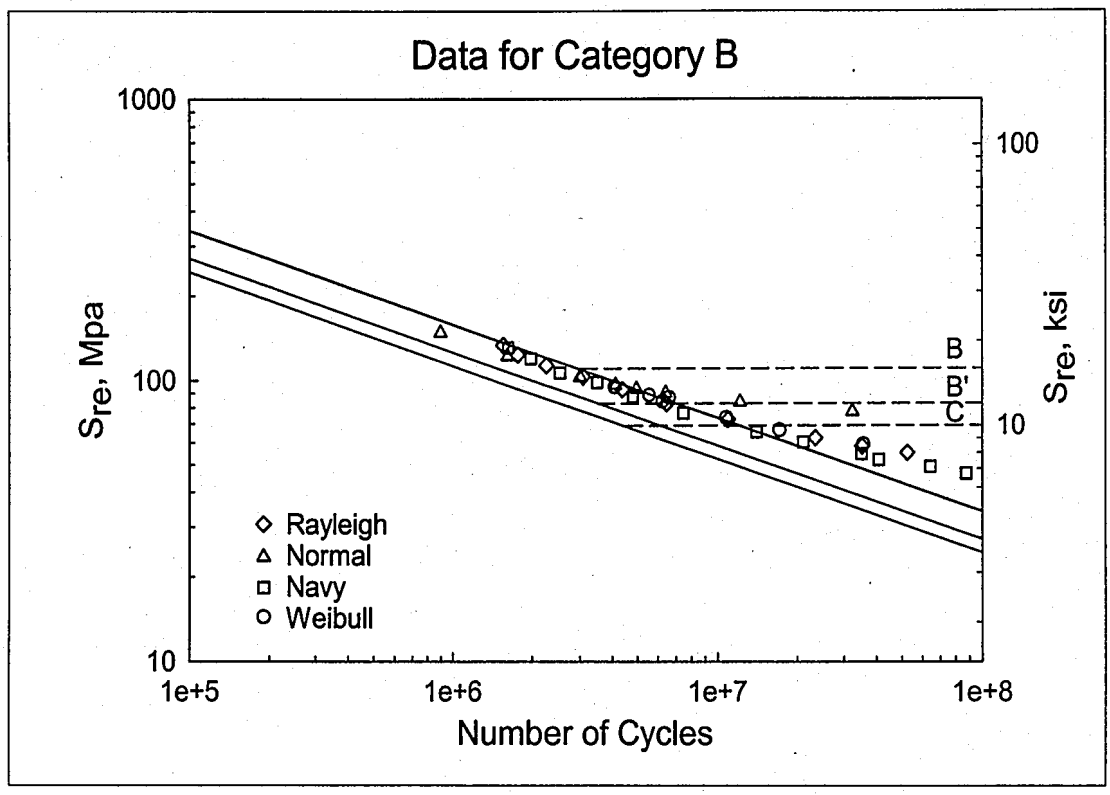

Figure 6.5.1 - S-N Data for Analytical Results Plotted with AASHTO Fatigue Curves

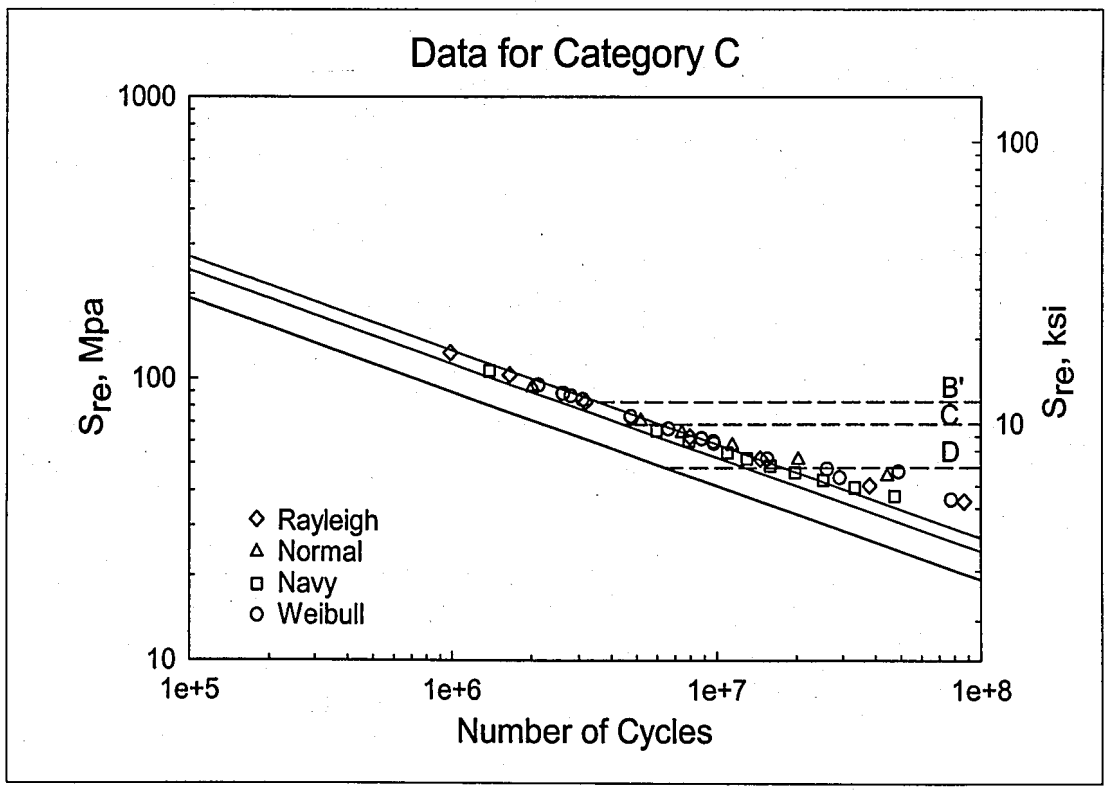

Figure 6.5.2 - S-N Data for Analytical Results Plotted with AASHTO Fatiuge Curves

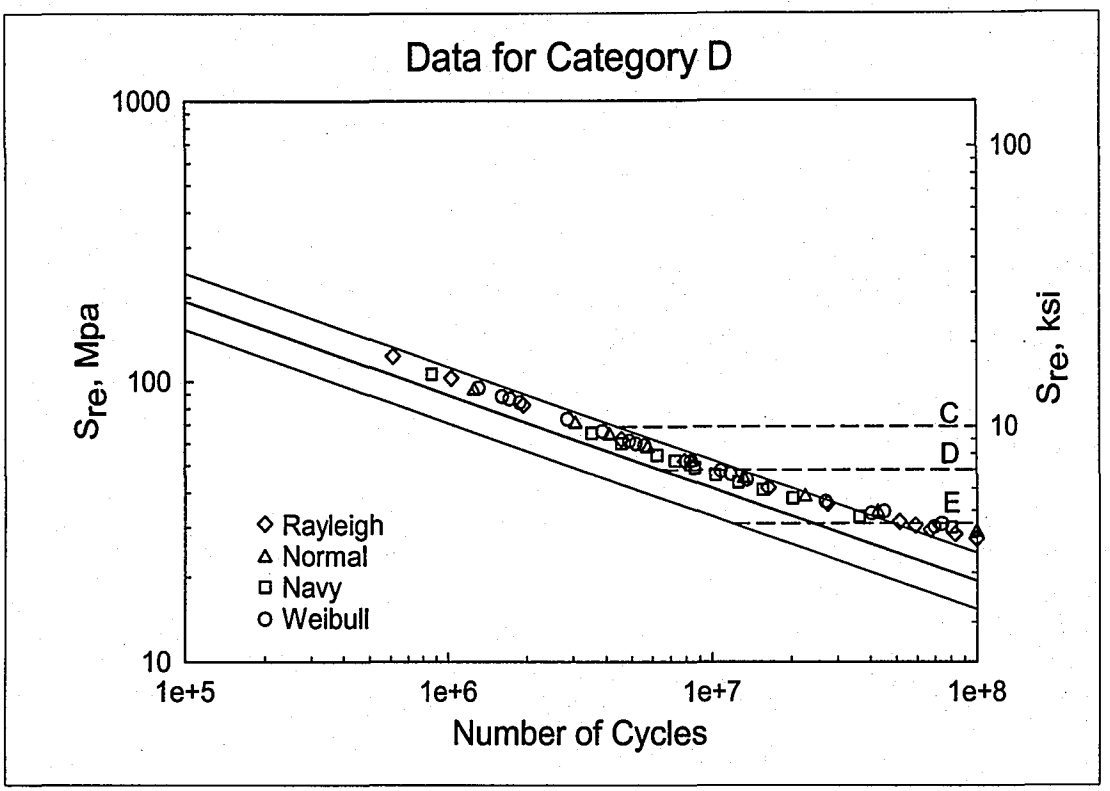

Figure 6.5.3 - S-N Data for Analytical Results Plotted with AASHTO Fatigue Curves

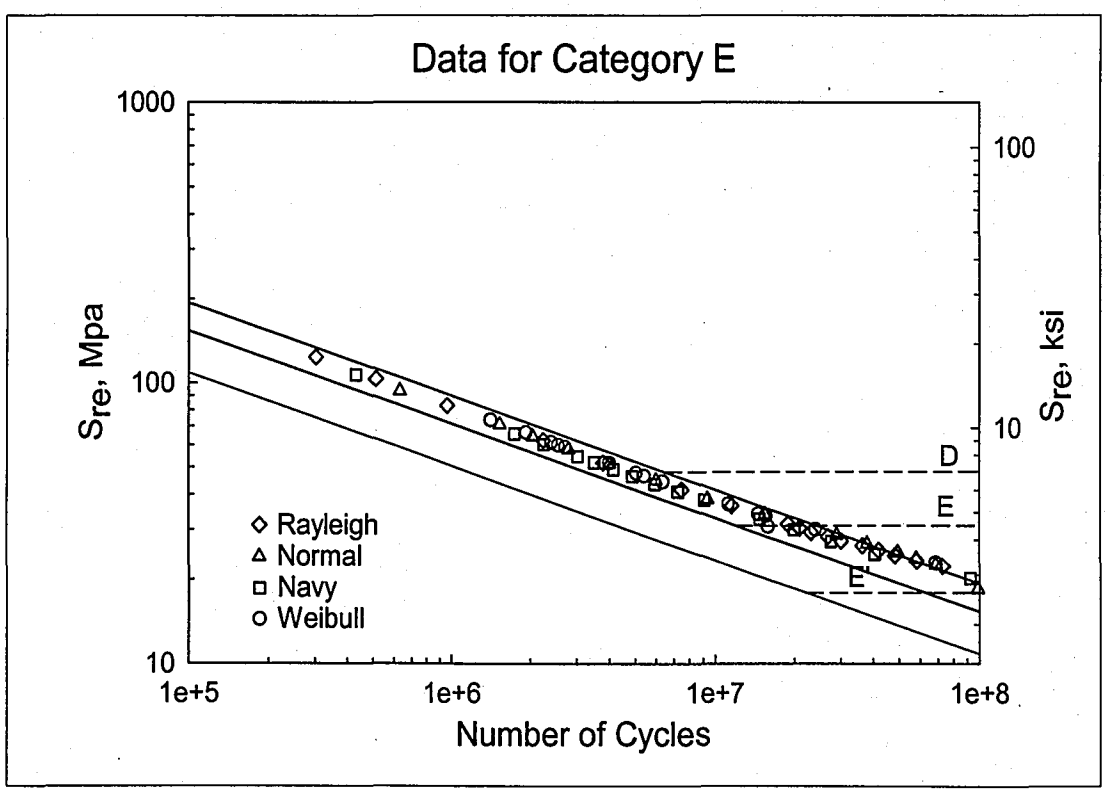

Figure 6.5.4 - S-N Data for Analytical Results Plotted with AASHTO Fatiuge Curves

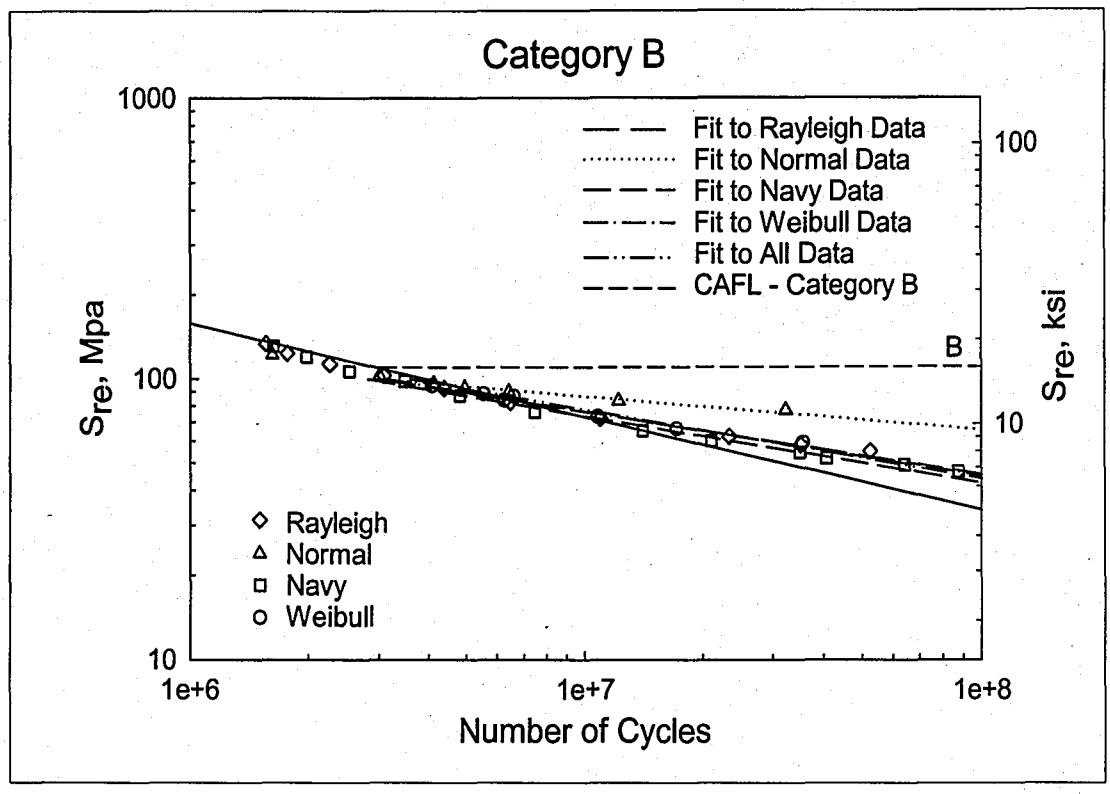

Figure 6.5.5 - Comparison of Linear Regression Below CAFL, Category B

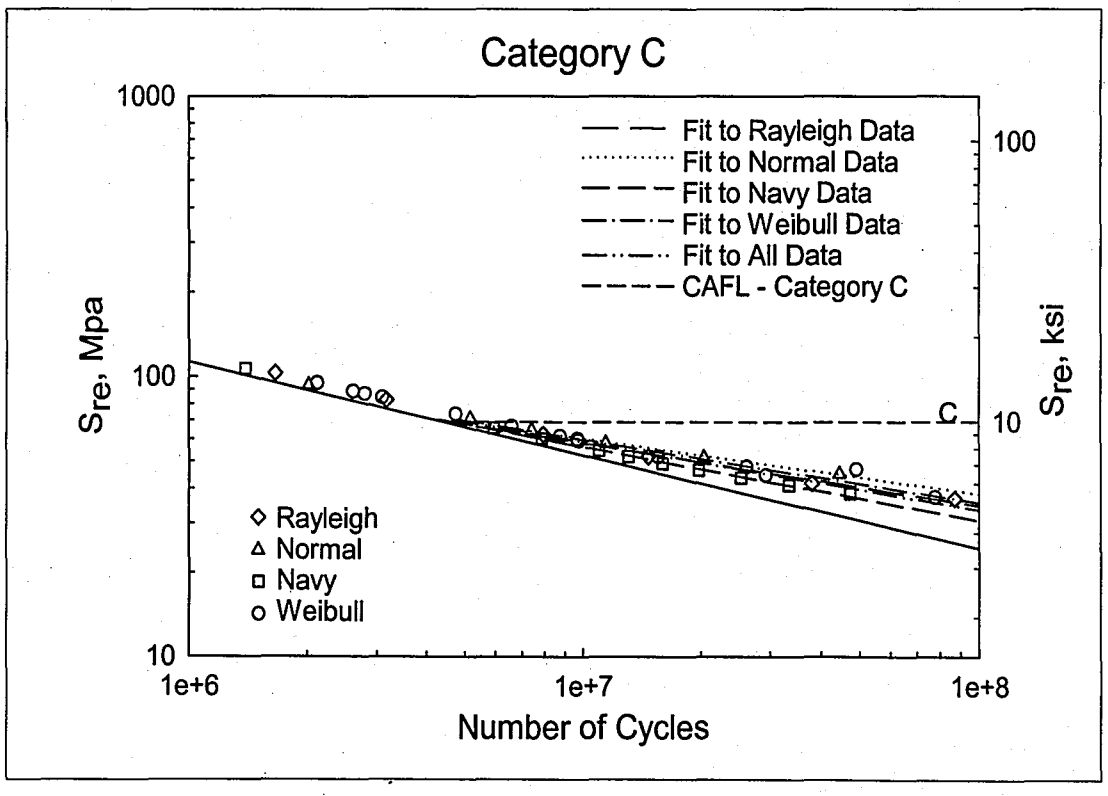

Figure 6.5.6 - Comparison of Linear Regression Below CAFL, Category C

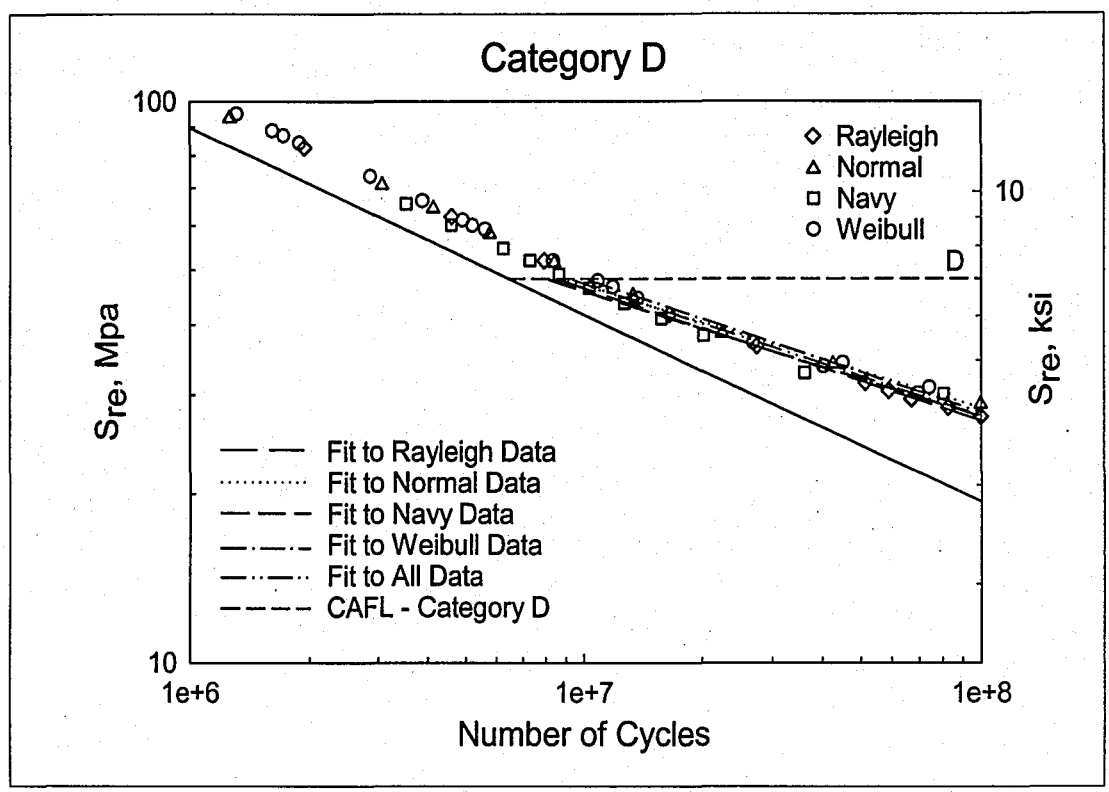

Figure 6.5.7 - Comparison of Linear Regression Below CAFL, Category D

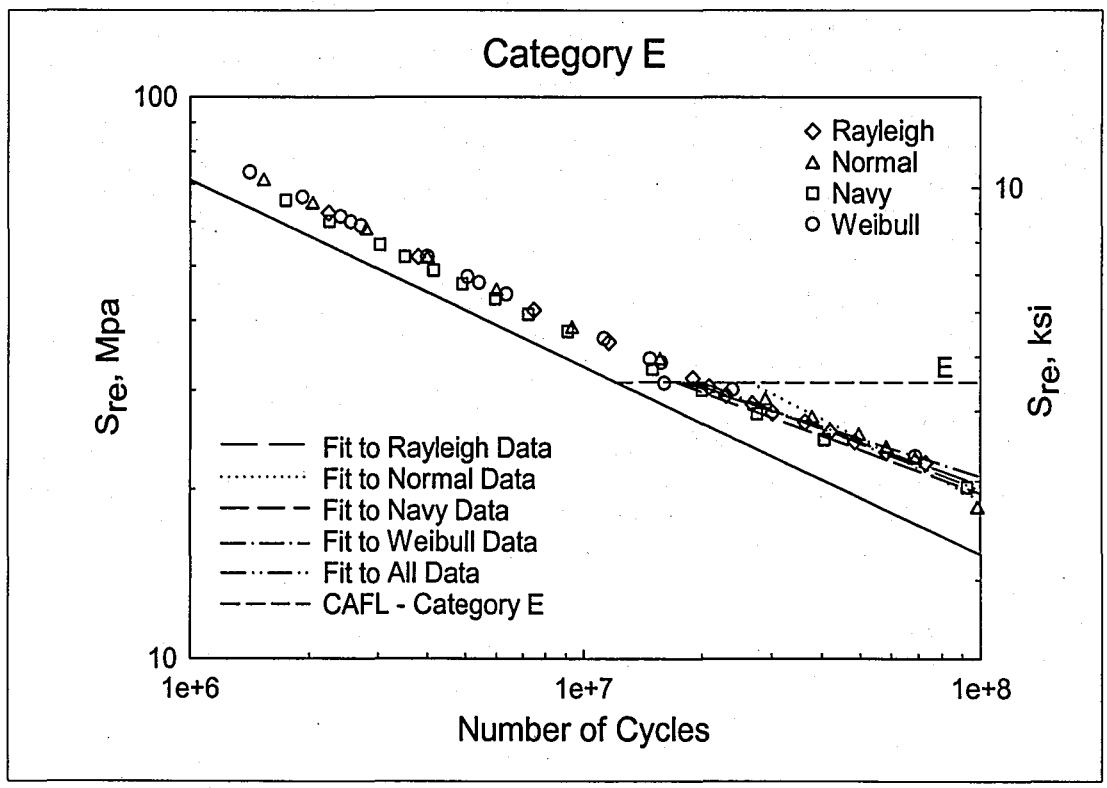

Figure 6.5.8 - Comparison of Linear Regression Below CAFL, Category E

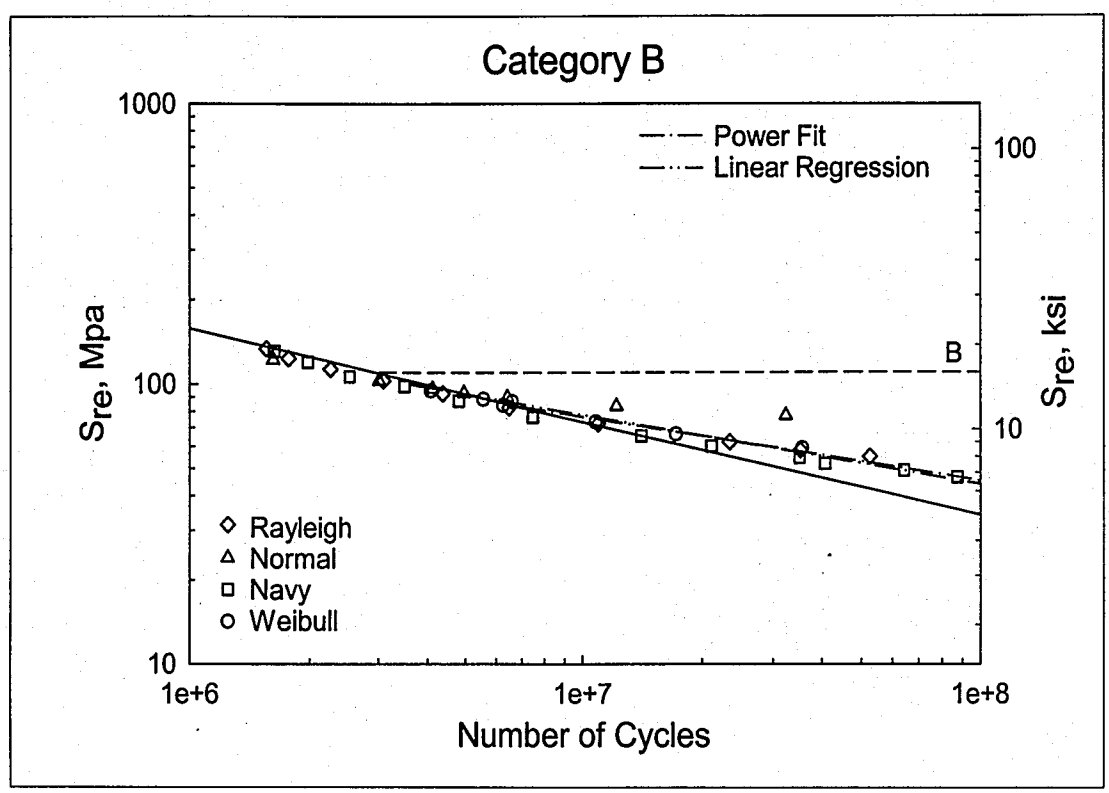

Figure 6.5.9 - Comparison of Linear Regression and Power Fit

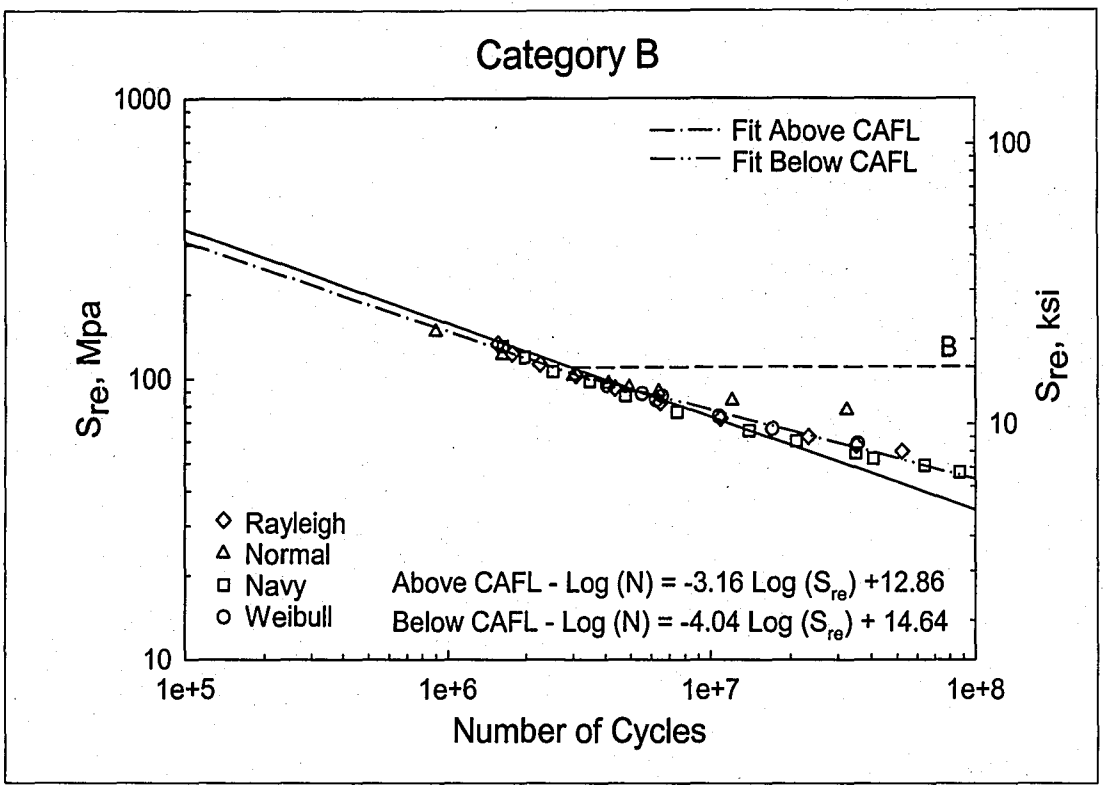

Figure 6.5.10 - Analytical Data Plotted with AASHTO Category B Curve and Linear Regression Results

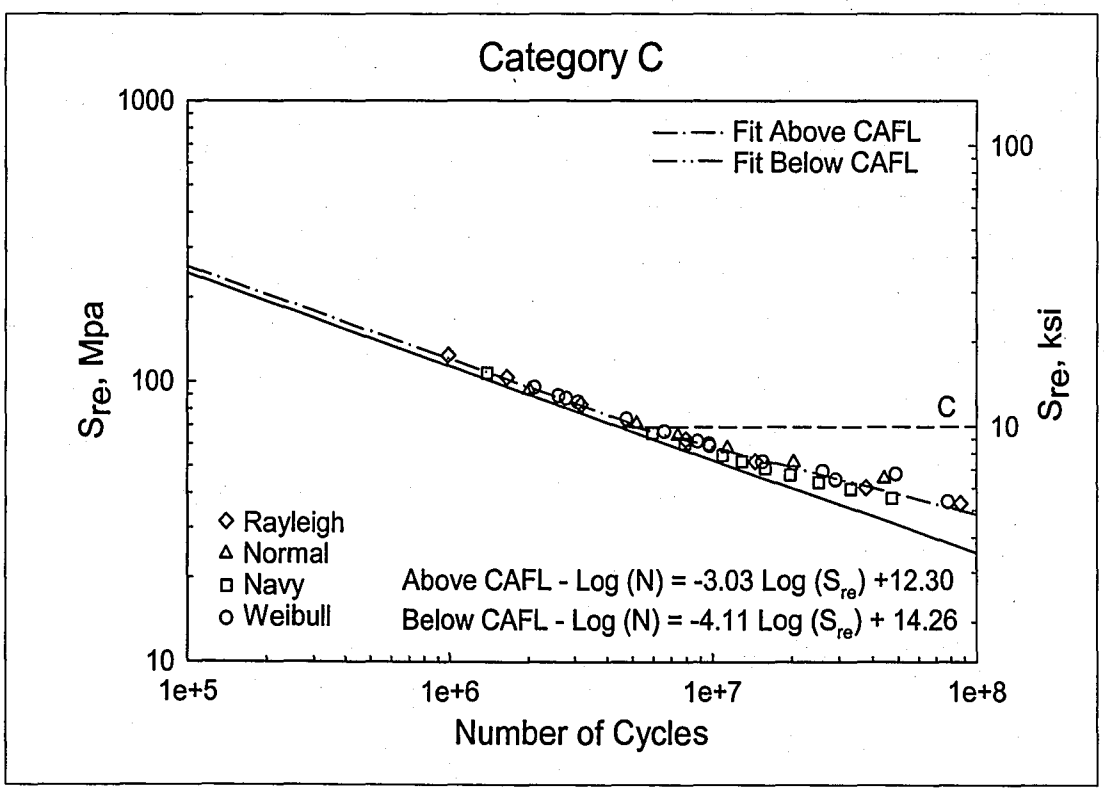

Figure 6.5.11 - Analytical Data Plotted with AASHTO Category C Fatigue Curve and Linear Regression Results

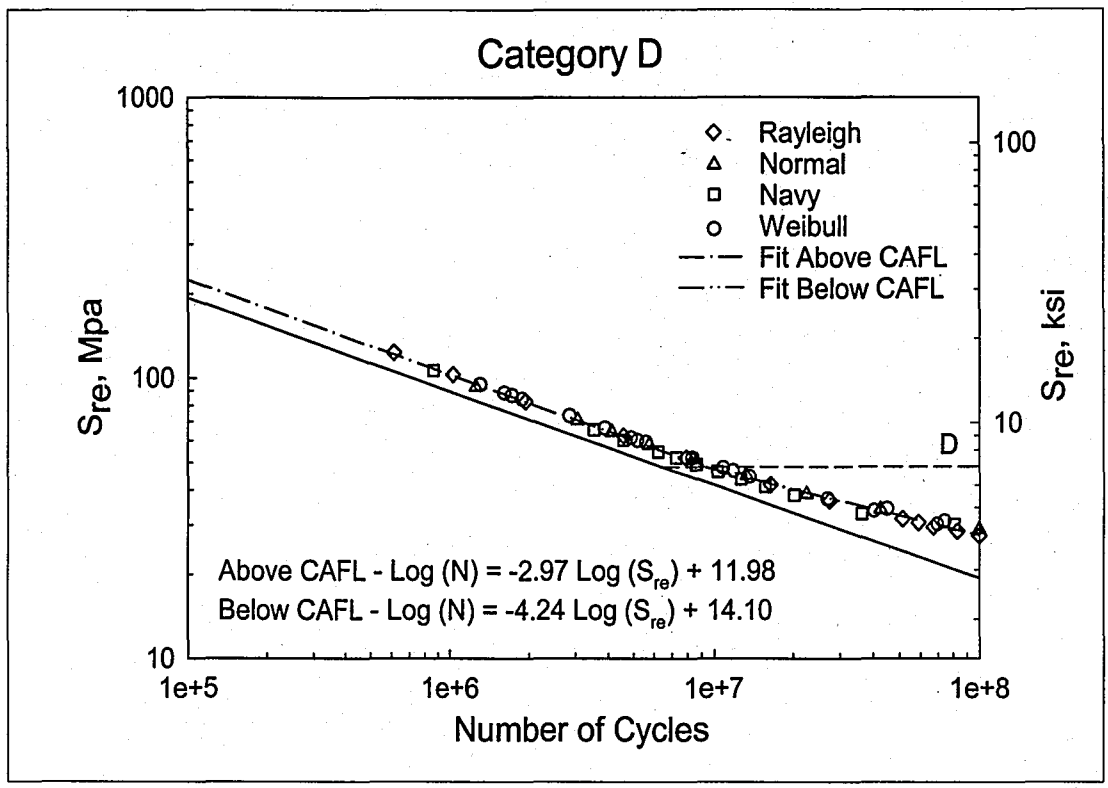

Figure 6.5.12 - Analytical Data Plotted with AASHTO
Category D Fatigue Curve and Linear Regression Results

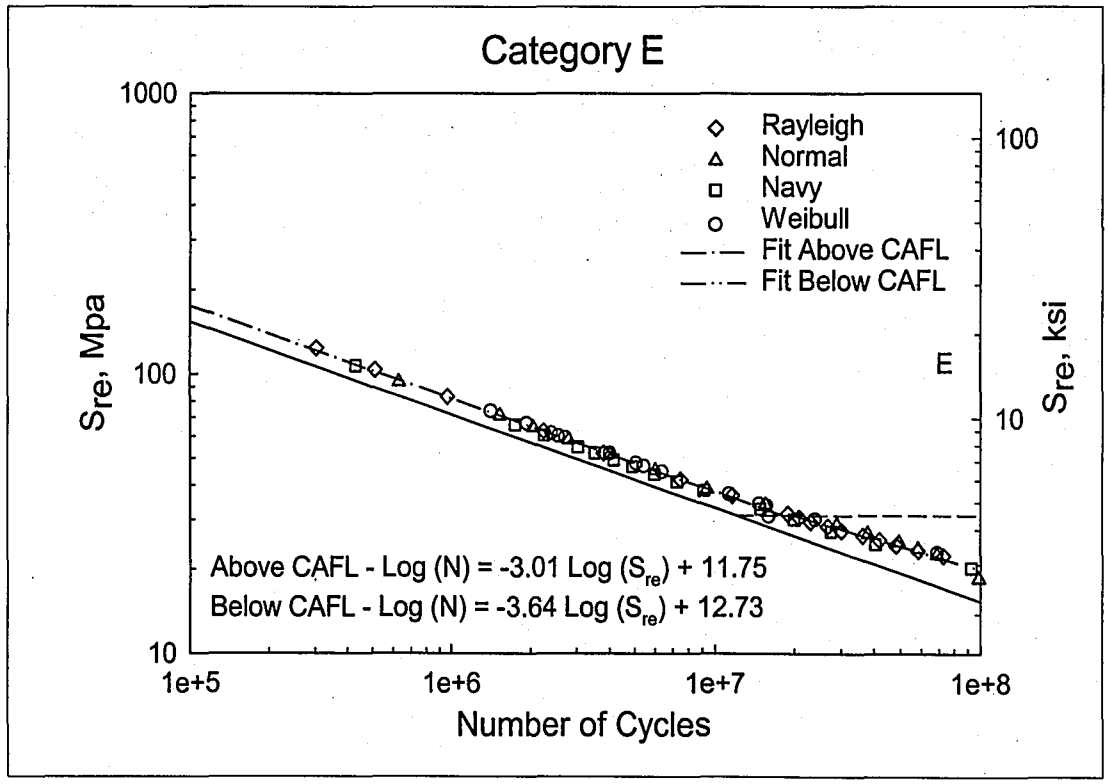

Figure 6.5.13 - Analytical Data Plotted with AASHTO
Category E Fatigue Curve and Linear Regression Results

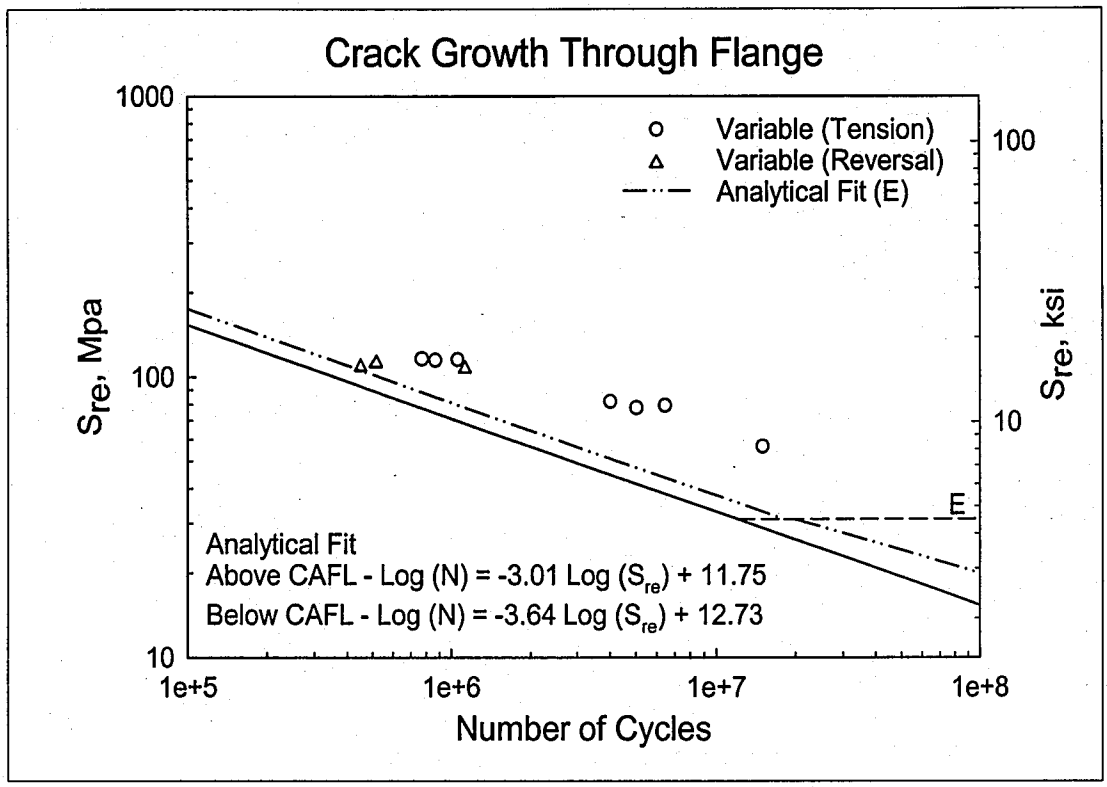

Figure 7.1.1 - Experimental Data Plotted with Linear Regression Results for Analytical Data for Category E

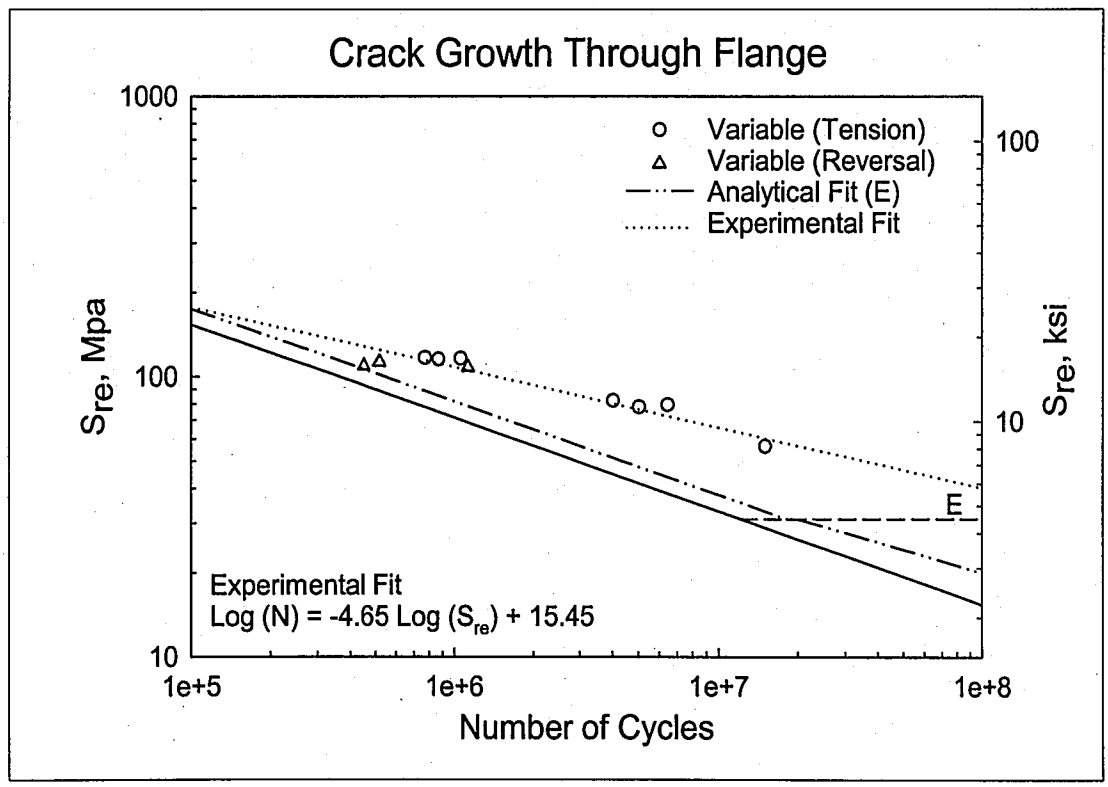

Figure 7.1.2 - Linear Regression Results for Experimental and Analytical Data

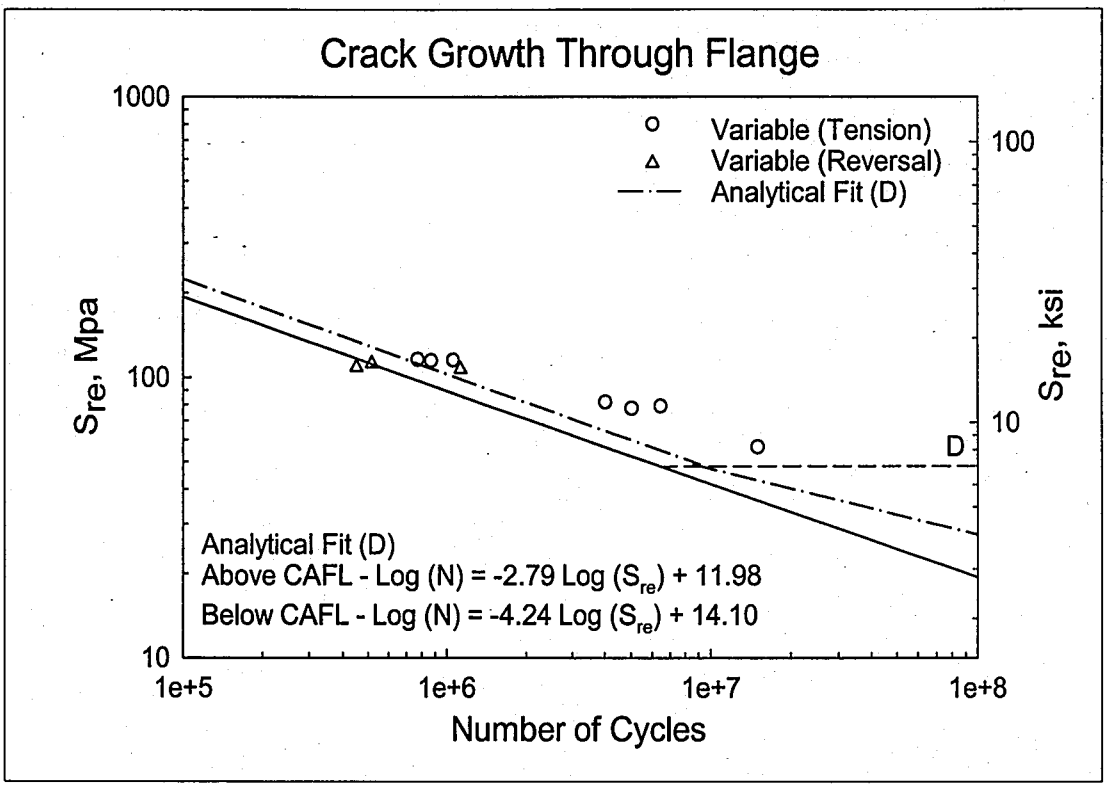

Figure 7.1.3 - Experimental Data Plotted with Linear Regression Results for Analytical Data for Category D

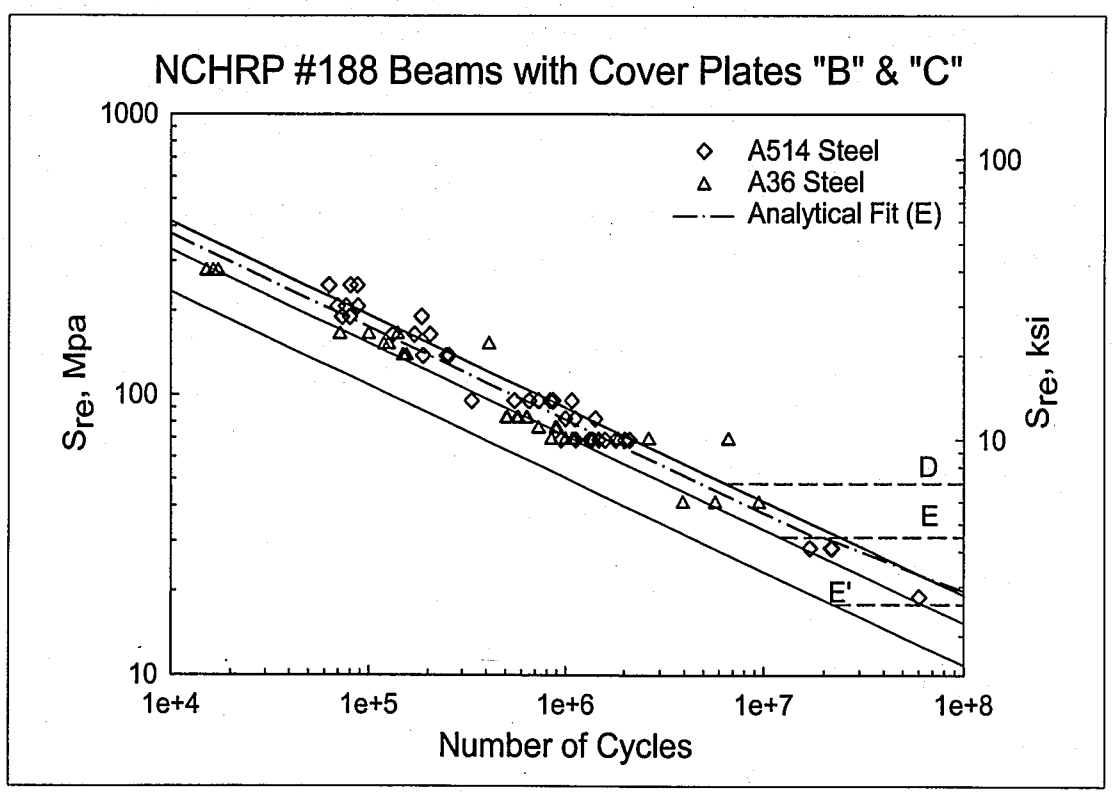

Figure 7.1.4 - Comparison of Analytical Variable Amplitude Fatigue Regression Lines with Test Data from NCHRP Report #188

Vita

Brenda Marie was born to the parents of James and Peggy Brownell and Brother Jimmy on May 2nd, 1978 in Utica, New York. The family lived in Inlet, New York, a small town in the Adirondack Park.

Brenda graduated from the Town of Webb High School as Valedictorian in 1996. Interested in mathematics and science, Brenda attended college at Clarkson University in Potsdam, New York enrolled in the Department of Civil and Environmental Engineering. While in college she attained many academic achievements including:

- John J. Bero Memorial Scholarship
- Department of Civil and Environmental Engineering Outstanding Senior Award
- Induction into Tau Beta Pi, The Engineering Honor Society
- Induction into Chi Epsilon, This Civil Engineering Honor Society
- President's List – 6 semesters
- President's list – 2 semesters
- Graduated With Great Distinction, May 2000

After attending Clarkson University, Brenda was accepted into the Graduate School of Lehigh University for a Master's Degree in Civil Engineering. At Lehigh, she was employed as a Research Assistant in the Advanced Technology for Large Structural Systems Research Center (ATLSS).

END OF TITLE